

2013-01-31

Ultraviolet Degradation of BTX in Waste Gas: Effects of Photocatalysis and Ozone Premixing

Atyabi, Mahsasadat

Atyabi, M. (2013). Ultraviolet Degradation of BTX in Waste Gas: Effects of Photocatalysis and Ozone Premixing (Master's thesis, University of Calgary, Calgary, Canada). Retrieved from <https://prism.ucalgary.ca>. doi:10.11575/PRISM/28547

<http://hdl.handle.net/11023/537>

Downloaded from PRISM Repository, University of Calgary

UNIVERSITY OF CALGARY

Ultraviolet Degradation of BTX in Waste Gas:
Effects of Photocatalysis and Ozone Premixing

by

MahsasadatAtyabi

A THESIS

SUBMITTED TO THE FACULTY OF GRADUATE STUDIES
IN PARTIAL FULFILMENT OF THE REQUIREMENTS FOR THE
DEGREE OF MASTER OF SCIENCE

DEPARTMENT OF CHEMICAL AND PETROLEUM ENGINEERING
CALGARY, ALBERTA

JANUARY, 2013

© MAHSASADAT ATYABI2013

Abstract

The focus of this study is on potential modifications of ultraviolet degradation of BTX (Benzene, Toluene and Xylene) in waste gas. A considerable amount of such pollutants is emitted from glycol dehydrators in the natural gas sector. The Photolytic technique has been recognized as a promising technique to control BTX emissions to the environment. In this work the effectiveness of other alternatives such as photocatalytic technology and photolysis in the presence of ozone are studied. A simulation model developed for benzene photolysis in waste gas by Mahmoudkhani (2012) was extended to include photocatalysis on the reactor wall. The model was applied to a cylindrical reactor containing a 40 W amalgam UV lamp in the axis. The model predictions of photodegradation with 254 nm and 185 nm light irradiation was compared with a combination of photolytic and photocatalytic degradation. At air flow rates of 1 L/min and benzene mass flow rates ranging from 0.5 to 10 mg/min, a degradation efficiency of 77%-23% is predicted for the catalytic process. In comparison, the model of Mahmoudkhani (2012) predicted an efficiency of 95%-20% for the noncatalytic process. However, a maximum quantum yield (ϕ) of 6.67×10^{-4} was predicted for the photocatalytic process. This low value explains the lack of benefit predicted when a photocatalytic coating is applied. It is concluded that the photolytic approach is a feasible alternative to the photocatalytic approach, especially for low concentrations of benzene emissions from waste gas. Furthermore, adding ozone greatly improves the efficiency of the process. Modeling of photolytic degradation with ozone confirms the experimental results; however, the modeling slightly overestimates the efficiency. Based on energy requirement calculations, it is concluded that the lowest energy is consumed when combination of ozone premixing and condensation pretreatment along with UV photolysis is used.

Acknowledgements

I would like to express my sincere gratitude to my supervisor, **Dr. Alex De Visscher**. His unsparing help, wide knowledge and logical way of thinking were of great value for me. I am thankful to Elena Vaisman who helped and supported me while doing experimental work.

I would like to thank my parents for their unconditional support, both financially and emotionally throughout my degree.

I also would like to thank my official referees, Dr. Abedi, Dr. Langford and Dr. Maini for their constructive criticism and excellent advice.

Dedication

Dedicated to

my beloved parents

Table of Contents

Abstract	ii
Acknowledgements	iii
Dedication	iv
Table of Contents	v
List of Tables	vii
List of Figures	viii
List of Symbols	xi
CHAPTER 1. INTRODUCTION	1
CHAPTER 2. LITERATURE REVIEW	4
2.1. Introduction to Photolysis and Photocatalysis	4
2.1.1. Photolysis	4
2.1.2. Photocatalysis	9
2.2. Photolysis in Waste Gas Treatment	11
2.3. Photocatalysis in Waste Gas Treatment	13
2.4. Photocatalysis with Ozone in Wastewater Treatment	16
2.5. Photocatalysis with Ozone in Waste Gas Treatment	17
CHAPTER 3. EXPERIMENTAL PROCEDURES	19
3.1. Basic System configuration	19
3.2. Equations used in experimental work	22
3.3. Improvements to the experimental results	25
CHAPTER 4. PHOTOCHEMICAL AND PHOTOCATALYTICAL MODEL DESCRIPTION	27
4.1. Flow Pattern Model	27
4.2. Material Balance	30
4.3. Chemical Model	33
4.4. Radiation Field Model	35
4.4.1. First Guess	35
4.4.2. Iterative Solution	38
4.4.3. Implementation	39
4.5. Extension of the Model to Include Photocatalysis	40
4.5.1. Sensitivity Analyses	47
CHAPTER 5. EXPERIMENTAL RESULTS	51
5.1. Ultraviolet degradation of m-xylene	51
5.2. BTEX Degradation by Photolysis and Ozone	57
CHAPTER 6. MODEL PREDICTIONS	61
6.1. Photolytic versus Photocatalytic Degradation of Benzene in Waste Gas	61
6.2. Effect of Adding Ozone on the Photolytic Degradation of Benzene in Waste Gas	70

CHAPTER 7. PROCESS DESIGN AND FEASIBILITY STUDY	79
7.1. Condensation Pre-treatment.....	79
Total amount of BTEX treated: 0.462 ton/year or 462 kg/year.	81
CHAPTER 8. CONCLUSIONS AND RECOMMENDATIONS	84
REFERENCES	86
APPENDIX A: BLANK RUN FOR M-XYLENE EXPERIMENTS	91
APPENDIX B: DEVELOPED CODE.....	92

List of Tables

Table 2.1. Some photochemical reactions and their properties (Sander et al., 2006).....	9
Table 3.1. Coefficients of the Antoine equation (3.2) (Poling et al., 2001)	23
Table 3.2. Coefficients of the Wanger equation (3.3) (Poling et al., 2001).....	23
Table 4.1. Experimental conditions and kinetic parameters presented by Ma et al. (2007).....	44
Table 6.1. Benzene photolysis quantum yields at 185 nm measured, predicted by Shindo and Lipsky (1966) and new predictions.....	68
Table 7.1. Condensation results	80

List of Figures

Figure 2.1. Energy balance	7
Figure 2.2. Laboratory scale-up for photocatalysis ozonation (Agustina et al., 2005).....	17
Figure 3.1. Photoreactor.....	20
Figure 3.2. Schematic diagram of the photoreactor system used in this study. 1. Pump, 2. Rotameter, 3. Contaminant wash-bottle, 4. Water wash-bottle, 5. T-valve, 6. Mixing bottle, 7. Inlet sample port, 8. Photoreactor, 9. Outlet sample port, 10. Flow meter.....	21
Figure 3.3. Calibration curve for m-xylene photodegradation experiments (sample size 500 μL).....	24
Figure 3.4. Calibration curve for benzene photodegradation experiments (sample size 500 μL).....	25
Figure 3.5. Ozone production rate versus volumetric air flow rate of the ozone generator	26
Figure 3.6. Schematic diagram of the photoreactor system used in this study with ozone pre-mixing process. 1. pump, 2. Rotameter, 3. Contaminant wash-bottle, 4. Ozone generator, 5. Water wash-bottle, 6. T-valve, 7. Mixing bottle, 8. Inlet sample port, 9. Photoreactor, 10. Outlet sample port, 11. Flow meter.....	26
Figure 4.1. Force balance on an annular element	29
Figure 4.2. Material balance on an annular element.....	31
Figure 4.3. Light rays in the simple model (dashed lines) and in the detailed model (solid lines).....	35
Figure 4.4. Photon balance.....	36
Figure 4.5. The effect of UV light intensity on the decomposition and the mineralization rate of benzene by the UV/TiO ₂ process: 10 ppm benzene, 100 ml min ⁻¹ flow rate, (Ma et al., 2007)	41
Figure 4.6. The effect of initial benzene concentration on the decomposition of benzene UV/TiO ₂ process at a light intensity of 2.1 mW/cm ² (Wang et al., 2003).....	45
Figure 4.7. The effect of UV light intensity on the decomposition of benzene by UV/TiO ₂ process at a benzene concentration of 70 ppm (Wang et al., 2003).....	46

Figure 4.8. Model predictions of photocatalytic degradation of benzene: 400 mL/min volumetric flow rate and different reaction rate constants ($k_0+20\%$, k_0 and $k_0-20\%$). Values of k_0 in legend are in molecules/(cm ² .s.(W/cm ²) ⁿ)	48
Figure 4.9. Model predictions of photocatalytic degradation of benzene: 400 mL/min volumetric flow rate and different adsorption equilibrium constants ($K+20\%$, K and $K-20\%$). Values of K in legend are in cm ³ /molecules.	48
Figure 4.10. Model predictions of photocatalytic degradation of benzene: 400 mL/min volumetric flow rate and different reaction orders ($n+20\%$, n and $n-20\%$).....	49
Figure 4.11. Model predictions of photocatalytic degradation of benzene based on equation (4.40): 400 mL/min volumetric flow rate and different reaction orders ($n+20\%$, n and $n-20\%$).....	50
Figure 5.1. M-xylene outlet concentration versus inlet concentration at volumetric flow rate 1 L/min.....	51
Figure 5.2. The effect of mass flow rate on the degradation efficiency of m-xylene by photochemical process	52
Figure 5.3. Comparison between m-xylene (current study) and toluene (De Visscher et al., 2010) on degradation efficiency versus mass flow rate.....	53
Figure 5.4. Irradiance at the reactor wall during the m-xylene degradation experiments versus m-xylene mass flow rate, at 1 L/min volumetric flow rate.....	54
Figure 5.5. Comparison between m-xylene (current work) and toluene (De Visscher et al., 2010) on irradiance at the reactor wall versus mass flow rate; 1 L/min volumetric flow rate.....	55
Figure 5.6. Light intensity changes over time.....	56
Figure 5.7. Benzene degrading efficiency of the ultraviolet reactor versus benzene mass flow rate at a volumetric flow rate of 2.2 L/min and an ozone mass flow rate of 17.6 mg/min (initial concentration 8 g/m ³); comparison with benzene degradation in the absence ozone	58
Figure 5.8. Benzene degradation rate in the ultraviolet reactor versus benzene mass flow rate at a volumetric flow rate of 2.2 L/min and an ozone mass flow rate of 17.6 mg/min (initial concentration 8 g/m ³); comparison with benzene degradation in the absence of ozone	59
Figure 5.9. Irradiance at the reactor wall during the benzene degradation experiments versus benzene mass flow rate, at a volumetric flow rate of 2.2 L/min, in the presence of ozone (inlet concentration 8 g/m ³).....	60

Figure 6.1. Model predictions of photolytic and mixed photolytic-photocatalytic degradation of benzene at 1 L/min volumetric flow rate.....	62
Figure 6.2. Model predictions of photolytic and mixed photolytic-photocatalytic degradation of benzene: 1 L/min volumetric flow rate and different values of k_0 (1.2×10^{14} , 2.5×10^{14} and 4.5×10^{14} molecules/cm ² .s.(W/cm ²) ⁿ)	63
Figure 6.3. Model predictions of photolytic and mixed photolytic-photocatalytic degradation of benzene versus external radius at 1 L/min volumetric flow rate and 1.2 g/m ³ benzene initial concentration	64
Figure 6.4. Benzene quantum yield profile for photocatalytic process	67
Figure 6.5. Benzene quantum yield profile for photolytic process.....	69
Figure 6.6. Comparison between processes including modeling of photolytic degradation with ozone (Mahmoudkhani, 2012), experiments of photolytic degradation with ozone (current study) and experiments of photolytic degradation alone (De Visscher et al., 2010) for benzene in waste gas.....	72
Figure 6.7. Model predictions of photolytic with ozone degradation of benzene versus external radius at 2.2 L/min volumetric flow rate and 8 g/m ³ ozone initial concentration, at four different benzene initial concentrations.....	73
Figure 6.8. Model predictions of photolytic with ozone degradation of benzene versus ozone initial concentration: 2.2 L/min volumetric flow rate and four different benzene initial concentrations	75
Figure 6.9. Model predictions of photolytic with ozone degradation of benzene versus volumetric flow rate: 8 g/m ³ ozone initial concentration and four different benzene initial concentrations.....	76
Figure 6.10. Model predictions of photolytic with ozone degradation of benzene versus mass flow rate: 8 g/m ³ ozone initial concentration and 2.2 L/min volumetric flow rate at three different lamp efficiencies (15 % 185 nm & 23 % 254 nm, 8 % 185 nm & 30 % 254 nm and 2 % 185 nm & 36 % 254 nm)	78
Figure 6.11. Model predictions of photolytic without ozone degradation of benzene versus mass flow rate: 1 L/min volumetric flow rate at three different lamp efficiencies (15 % 185 nm & 23 % 254 nm, 8 % 185 nm & 30 % 254 nm and 2 % 185 nm & 36 % 254 nm). 78	

List of Symbols

Symbol	Definition
A	absorbance, cm^2 area, cm^2
a	absorption coefficient, l/cm
c	speed of light, m/s
C	concentration, $molecules/cm^3$
d	pipe diameter, m
D	diffusion coefficient, cm^2/s
E	irradiance, W/m^2 efficiency, W/m^2
E _P	fluence rate, $photons/cm^2.s$
E _{Pλ}	energy per photon, $\frac{photon}{s.cm^2.nm}$
h	Planck's constant, $J.s$
k ₀	reaction rate constant, $\frac{molecules}{cm^2.s.(w/cm^2)^n}, ppmv^{-1} cm^{-2} s^{-1}$
K	adsorption equilibrium constant, $cm^3/molecules, ppmv^{-1}$
L	radiance, $\frac{W}{m^2.sr}$ length, cm
l	optical pathlength, cm
n	reaction order of applied UV light intensity
P	pressure, Pa
P _λ ⁰	incident spectral radiant power, $W, \frac{J}{s.cm^2.nm}$

P_λ	transmitted spectral radiant power, $W, \frac{J}{s.cm^2.nm}$
r	radial coordinate
r_i	photochemical reaction, $molecules/cm^3.s$
R	ideal gas constant, $J/mol.K$
	radius, m
R_{wall}	reflectivity
Q	volumetric flow rate, cm^3/s
S	area, m^2
t	reaction time, s
T	absolute temperature, K
U	mean velocity, cm/s
V	local velocity of gas, cm/s
z	length coordinate

Greek letters

α	absorption coefficient, l/cm
θ	angle
λ	wavelength, nm
μ	dynamic viscosity, $Pa.s$
ν	kinematic viscosity, m^2/s
σ	absorption cross-section, cm^2
τ	sheer stress, Pa
Φ	quantum yield, $molecules/photon$
Ω	solid angle

CHAPTER 1. INTRODUCTION

Benzene, toluene, and xylene (BTX) emissions from glycol dehydration units are typical pollutants by the oil and gas industry. In particular, benzene emissions have attracted some environmental concern because of the carcinogenic nature of benzene. Canadian glycol dehydration units emit more than 2000 tonnes of benzene per year (CAPP Status Report, 2008). Significant progress in the reduction of benzene emissions has been achieved; however, to achieve further emission reductions, the major issue is to find a technique which is relatively cheap and simple to operate for a wide use in industry. Photolysis and photocatalysis are two promising techniques that could fall into this category. The purpose of this study is to find a feasible and efficient technique for benzene degradation from waste gas based on ultraviolet light. Application of UV photolysis depends on wavelength. It is categorized as near UV, middle UV and far UV. The typical wavelength for near UV is 350 nm. Near UV light requires a catalyst to be effective. A common catalyst used is titanium dioxide (Demeestere et al., 2007). For middle UV, the typical wavelength is 254 nm and it can break ozone and some organic molecules, but not oxygen, water or benzene. The representative wavelength for far UV is 185 nm. It breaks oxygen (producing ozone), water (producing OH radicals), and benzene molecules.

Hg lamps emit UV light at two wavelengths, 185 nm and 254 nm, in narrow bands (<1nm). In the application of photolysis for BTX treatment, the 185 nm line is used to directly break benzene molecules. Also, it is used to produce OH radicals to attack benzene and reaction products. It is

also used to produce ozone. In this technique, the 254 nm line directly breaks reaction products and also breaks ozone into reactive species degrading benzene.

The feasibility of the photolysis technique versus photocatalysis for BTEX degradation from waste gas emitted by the oil and gas industry has been explored in this work. Prior to this research, Mahmoudkhani (2012) developed a photochemical reactor model with 59 reactions involving 47 species. In the current thesis, the model was extended to include photocatalytical reactions. Simulation results of photolysis have been compared with the ones from photocatalysis in a 0.5 L cylindrical reactor with a 40 W UV lamp at the centre. Furthermore, effects of pre-mixing ozone and of condensation as a pre-treatment stage on the economy of the process have been evaluated.

This thesis is part of a larger project aimed at developing an effective treatment system for benzene, toluene and xylene from waste gas based on ultraviolet light. In the preceding research, experimental data on photolysis of benzene and toluene was obtained. It was shown that the system worked but not as efficient as expected. Xylenes are also emitted by glycol dehydration units, but their degradation had not yet been studied in the preceding research. Hence, the first objective of this thesis is to determine the ultraviolet degradation rate of a representative xylene through experiments.

The second objective of this thesis is to find technologies to improve the efficiency of the process. Two technologies that were evaluated are photocatalysis and ozone premixing. For ozone premixing, which was formed to be the most promising option of the two, the modeling study was complemented with an experimental study.

This thesis is structured as follows: a brief introduction and literature review are introduced firstly. Then the experimental method for the investigation of m-xylene photodegradation is

described. Chapter 4 deals with the model development of the system. As the main part of the thesis, the results of m-xylene photodegradation experiments followed by the model predictions of photocatalysis are discussed. Moreover, the experimental results of the most promising method, photolysis accompanied by ozonation, are presented followed by some considerations needed for the scale-up. The significant points of this study are eventually highlighted in the conclusion chapter.

CHAPTER 2. LITERATURE REVIEW

2.1. Introduction to Photolysis and Photocatalysis

2.1.1. Photolysis

The sub-discipline of chemistry in which the chemical effects of light radiation is studied is called photochemistry (Braslavsky, 2007).

In order to estimate efficiency in photochemistry, the quantum yield is defined as the ratio of the total amount of converted molecules over the total amount of absorbed photons. The integral quantum yield is: (Shindo&Lipsky, 1966)

$$\Phi(\lambda) = \frac{\text{amount of reactant consumed or product formed}}{\text{amount of photons absorbed}} \quad (2.1)$$

Quantum yield is a function of wavelength (λ) and it has a value between 0 (no reaction) and 1 (all photons lead to reaction) (De Visscher, 2013).

The absorption coefficient (a) relates the absorbance (A) to the optical pathlength (l): (Braslavsky, 2007)

$$a(\lambda) = \frac{A(\lambda)}{l} = \left(\frac{1}{l}\right) \log\left(\frac{P_{\lambda}^0}{P_{\lambda}}\right) \quad (2.2)$$

P_{λ}^0 and P_{λ} are the incident and transmitted spectral power, respectively. Equation (2.2) also defines the absorbance. Using the napierian logarithms (the logarithm to the base e) results in the linear napierian absorption coefficient (α):

$$\alpha(\lambda) = a(\lambda) \ln 10 = \left(\frac{1}{l}\right) \ln\left(\frac{P_{\lambda}^0}{P_{\lambda}}\right) \quad (2.3)$$

The common unit for a and α is $\frac{1}{cm}$.

The absorption cross section of a component is its linear napierian absorption coefficient divided by its concentration:

$$\sigma(\lambda) = \frac{\alpha(\lambda)}{C} = \frac{1}{Cl} \ln\left(\frac{P_{\lambda}^0}{P_{\lambda}}\right) \quad (2.4)$$

The common unit for concentration in photochemistry is: $\frac{\text{molecules}}{\text{cm}^3}$

σ is in $\frac{cm^2}{\text{molecules}}$, or simply cm^2 for a component.

The total incoming radiant power from all directions onto a small sphere divided by the cross-sectional area of that sphere is the fluence rate. It is the main variable that drives homogeneous photochemical reaction rates. Its unit in SI is $\frac{W}{m^2}$ (Braslavsky, 2007).

The mathematical definition of fluence rate (E_0) is:

$$E_0 = \frac{dP}{dS} \quad (2.5)$$

where P is the incoming radiant power, and S is the area. With constant radiant power over the area, S , it can be expressed as:

$$E_0 = \frac{P}{S} \quad (2.6)$$

The integral definition is:

$$E_0 = \int_{4\pi} L.d\Omega \quad (2.7)$$

Here, L is the radiance (W/m².sr) of the beam at the given point and Ω is the solid angle of every passing beam at that point.

In contrast, the irradiance is the total incoming radiant power from all directions towards a small element of planar surface divided by the area of the element. It is the main variable that drives heterogeneous photocatalytical reaction rates. Its SI unit is $\frac{W}{m^2}$.

The mathematical definition is:

$$E = \frac{dP}{dS} \quad (2.8)$$

The difference between equation (2.8) and equation(2.5) is the geometry of the surface considered: spherical in the case of fluence rate and planar in the case of irradiance. The distinction is important because photolysis rates are driven by the fluence rate whereas photocatalysis on a surface is driven by the irradiance.

In case of constant radiant power over the surface area considered:

$$E = \frac{P}{S} \quad (2.9)$$

With the integral definition:

$$E = \int_{2\pi} L.\cos\theta.d\Omega \quad (2.10)$$

where θ is the angle between any beams and the normal to the surface at the given point(Braslavsky, 2007).

Fluence rate is identical to irradiance when the light field consists of parallel beams hitting the surface perpendicularly, without scattering by the target or the surroundings.

According to the previous concepts, the photochemical reaction rate can be derived as follows.

Based on the equation (2.3):

$$l.\alpha(\lambda) = \ln\left(\frac{P_{\lambda}^0}{P_{\lambda}}\right) \quad (2.11)$$

Therefore:

$$\exp(l.\alpha(\lambda)) = \frac{P_{\lambda}^0}{P_{\lambda}} \quad (2.12)$$

Or:

$$P_{\lambda} = P_{\lambda}^0 \cdot \exp(-l.\alpha(\lambda)) \quad (2.13)$$

By differentiating we obtain:

$$\frac{dP_{\lambda}}{dl} = P_{\lambda}^0 \cdot (-\alpha(\lambda)) \cdot \exp(-l.\alpha(\lambda)) \quad (2.14)$$

Substituting equation (2.13) into equation (2.14) yields:

$$\frac{dP_{\lambda}}{dl} = -\alpha(\lambda) \cdot P_{\lambda} \quad (2.15)$$

Applying the energy balance over a cylindrical element in the reactor, we get:

$$\text{Energy rate consumed} = \text{Incoming energy rate} - \text{Outgoing energy rate} \quad (2.16)$$

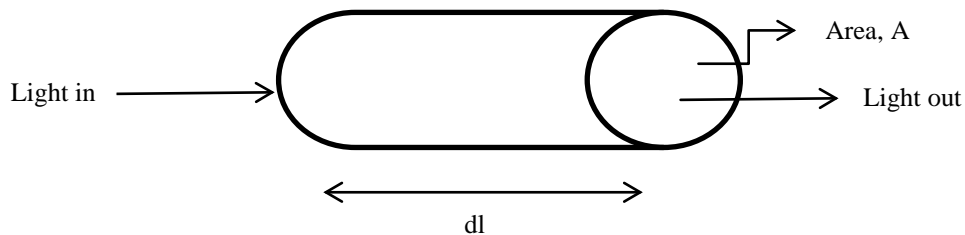


Figure 2.1. Energy balance

$$\text{Energy consumed} = A \cdot P_\lambda - A \cdot (P_\lambda + dP_\lambda) \quad (2.17)$$

As an assumption, all light energy is dissipated as heat or consumed in energy of reaction.

Dividing equation (2.17) by the volume of the element and substituting equation (2.15), we obtain:

$$\frac{\text{Energy consumed}}{\text{Volume}} = \frac{-A \cdot dP_\lambda}{A \cdot dl} = -\frac{dP_\lambda}{dl} = \alpha(\lambda) \cdot P_\lambda \quad (2.18)$$

Based on the definition of irradiance for each wavelength:

$$E_{P\lambda} = \frac{P_\lambda}{E_{\text{photon},\lambda}} \quad (2.19)$$

P_λ : spectral radiant power, $\frac{J}{s \cdot cm^2 \cdot nm}$

$E_{\text{photon},\lambda}$: energy per photon in the wavelength of λ , $\frac{J}{\text{photon}}$

Thus, the unit of $E_{P\lambda}$ is $\frac{\text{photon}}{s \cdot cm^2 \cdot nm}$. Integration removes the term nm from the unit.

Combination of equation (2.18) and (2.19) results in:

$$\frac{\text{Photons consumed}}{\text{Volume}} = \alpha(\lambda) \cdot \frac{P_\lambda}{E_{\text{photon}}} = \alpha(\lambda) \cdot E_p \quad (2.20)$$

The absorption coefficient of a component is the absorption cross-section times its concentration:

$$\alpha = \sigma \cdot C \quad (2.21)$$

Substituting this inequation (2.20), we get:

$$\frac{\text{Photons consumed}}{\text{Volume}} = C \cdot \sigma \cdot E_p \quad (2.22)$$

Reviewing the definition of quantum yield we have:

$$r = \phi \cdot \frac{\text{Photons consumed}}{\text{Volume}} \quad (2.23)$$

In brief, we achieve:

$$r = \phi \cdot C \cdot \sigma \cdot E_p \quad (2.24)$$

For each reactant compound:

$$r_i = -\phi_i \cdot C_i \cdot \sigma_i \cdot E_p \quad (2.25)$$

The photochemical reaction rate of component i can be achieved by determining the value of quantum yield, the concentration of component i, the absorption cross section and the fluence rate. Some of the key photochemical reactions and their absorption cross-section (σ) and quantum yield (ϕ) values are presented in Table 2.1.

Table 2.1. Some photochemical reactions and their properties (Sander et al., 2006)

Reaction	ϕ (185 nm)	σ (185 nm) cm ²	ϕ (254 nm)	σ (254 nm) cm ²
H ₂ O + hv → H + ·OH	1	5.5 × 10 ⁻²⁰		
O ₃ + hv → O(· ¹ D) + O ₂	0.9	66.1 × 10 ⁻²⁰	0.9	1148 × 10 ⁻²⁰
O ₃ + hv → O(· ³ P) + O ₂	0.1	66.1 × 10 ⁻²⁰	0.1	1148 × 10 ⁻²⁰

2.1.2. Photocatalysis

Photocatalysis is the application of photolysis in the presence of a substance, a photocatalyst, which absorbs light and participates in the chemical conversion of reactants. When

photocatalytic activity is defined for a certain wavelength, the quantum yield can be defined as in photolysis (Braslavsky et al., 2011).

Oxidation of contaminants by the action of ultraviolet radiation and a catalyst is named photocatalytic oxidation. This term is widely applied to the oxidation of organic contaminants at low concentration by UV light irradiation of titanium dioxide or UV/TiO₂ (Braslavsky et al., 2011).

Titanium dioxide is highly active and chemically stable to light illumination. Also, it has low toxicity and price (Kaneko & Okura, 2002).

The Langmuir-Hinshelwood kinetic model approximates the reaction rate depending on the reactant concentration in the bulk solution or bulk gas occurring at a solid-liquid or solid-gas interface. The equation is expressed as: (Parmon et al., 2002)

$$-r_{LH} = -\frac{dC}{dt} = \frac{k_0 \cdot K \cdot C}{(1 + K \cdot C)} \quad (2.26)$$

Here, k_0 is the apparent reaction rate constant and its SI unit is m³/mol.s. K is the assumed adsorption/desorption equilibrium constant. Based on the Langmuir isotherm, a fast adsorption/desorption equilibrium step takes place while the subsequent surface reaction step is slow. So, this model assumes a constant number of surface adsorption sites at equilibrium. That the adjacent adsorbed molecules have no interaction is another assumption in this model (Fox & Dulay, 1993).

2.2. Photolysis in Waste Gas Treatment

It is expected that photolysis in waste gas treatment, as in the case of water treatment, can be engineered to efficiently achieve total pollutant mineralization. The removal of airbornecontaminants, in particular BTX, is an area of promising applications for photolysis. Several unique photochemical methods for degradation of benzene have emerged in the scientific literature. Shindo and Lipsky have characterized the photochemical behaviour of gaseous benzene in 1966. However, more research is needed on the efficiency of the reactions to design a technology. Tsai et al. (2001) studied H atom elimination of photo-dissociation of benzene at 193 nm and 248 nm. Since benzene has a very stable molecular structure because of its aromatic ring, it requires extremely large energy to break the ring and produce two fragments. The kinetics of gas phase photo-oxidation of VOCs such as benzene and toluene in different conditions are evaluated by Wang and Ray (2000). This treatment method is applied to the waste gas originating from an air stripper with usually low VOC concentration in the effluent and highly saturated moisture in the air. The irradiation source was a low-pressure mercury UV lamp with low intensity which is capable of destroying various types of organic pollutants. They pointed out that the presence of moisture and chloride radicals improve the rate of oxidation of benzene and toluene significantly. Mohseni and Zhao (2006) suggested that coupling UV photolysis and biofiltration has the potential to either eliminate organic compounds from contaminated air streams or transform them into more biodegradable compounds. Such compounds are then readily treated by biofiltration. They concluded that the UV photolysis-biofiltration process

increased the removal of o-xylene by about 100 % compared with the control biofiltration process.

The photodegradation of other air pollutants has been investigated as well. Cheng et al. (2011) investigated the photodegradation of gaseous α -pinene using a vacuum UV (VUV) light at 242 nm in a spiral quartz reactor. They reported that hydroxyl radical, direct photolysis and ozone played a dominant role in α -pinene conversion. They eventually found that at low initial concentrations of α -pinene the conversion follows first order and at high initial concentrations the second order kinetic model applies to the α -pinene conversion. Thus, VUV photo-oxidation is a promising technology for conversion of α -pinene.

Domeno et al. (2010) have compared the efficiency of photo-oxidation with chemical oxidation by sodium hypochlorite and ozonization for the removal of VOCs and odors from industrial gaseous emissions. Ozonization, with an efficiency of 98%, and absorption, with an efficiency of 75%, were the most efficient methods, while photo-oxidation, with an efficiency of 59%, was the least effective one.

The investigation of Chou and Chang (2007) evaluated the feasibility of the UV (185 + 254 nm) and UV (254 nm)/O₃ processes for the destruction of gaseous hexamethyldisiazane (HMDS). They indicated that for all conditions, the decomposition rates for the UV (185 + 254 nm) irradiation is higher (>90 %) than that of the UV (254 nm)/O₃ with the maximum degradation rate of 77 %. This is because of 'OH radicals produced from photolysis of water or O(¹D) produced from photolysis of oxygen.

Robert et al. (2006) reported the combined dielectric barrier discharge (DBD) plasma and UV irradiation on destruction of toluene. They figured out that the combined system works more effectively than single treatment, either barrier discharge or UV irradiation. The decomposition rate of toluene by UV assisted BDB was at least 3 times higher than by the BDB only, and 2 times higher than the sum of decomposition rates by the BDB and UV light made separately.

Jeong et al. (2004) compared the feasibility of the use of short wavelength UV (254 + 185 nm) irradiation and TiO₂ catalyst for photochemical degradation of gaseous toluene. They stated that high conversions ($\approx 90\%$) were achieved at high initial concentration of toluene when 254 + 185 nm light is used. Catalyst deactivation as a result is a disadvantage of this technique.

Chen et al. (2002) have developed a reactor model for the photolytic degradation of chloroform (CHCl₃) and carbon tetrachloride (CCl₄) in gas phase. The photochemical reactor model of Mahmoudkhani (2012), which formed the basis of the current research, will be discussed in Chapter 4.

2.3. Photocatalysis in Waste Gas Treatment

A number of studies have been reported in literature on the photocatalytic treatment of waste gas. It is well understood that the photocatalytic technique has been successful for the removal of dissolved organic matter in wastewater and for some cases in waste gas depending on the reactor configuration type.

Cunningham and Hondnett (1981), Jacoby et al. (1996) and Yue(1993) reviewed heterogeneous photocatalytic mechanisms. The first step in the case of a porous catalyst is the mass transfer mechanism from the fluid bulk to the catalyst surface which involves the adsorption of reactants on the active catalyst sites. However, Jacoby et al. (1996) pointed out that the initial phenomenon is negligible in a photocatalytic reactor. This might be true for mass transfer around the catalyst but the transfer inside catalyst pores is independent of the fluid flow. They stated that electron-hole pairs occur once TiO_2 is irradiated and subsequently radicals are produced. These radicals take part in surface reactions and eventually lead to desorption and mass transfer of products from catalyst surface to fluid bulk.

In order to describe the behaviour of the oxidation of organic compounds over a titanium dioxide catalyst, several mathematical models have been developed by researchers. Peral and Ollis (1992) found that the Langmuir-Hinshelwood equation (see section 2.1.2) describes the reaction between adsorbed oxygen and adsorbed reactant molecules.

Ma et al. (2007) investigated the effects of humidity, UV light intensity and benzene initial concentration on the performance of a differential-type optical fiber photoreactor for benzene decomposition. Based on this type of reactor, they reported that the apparent quantum yields of benzene decomposition and CO_2 production by the UV/ TiO_2 process were found to increase with UV intensity. They also came to the conclusion that an appropriately designed optical fiber reactor could be a feasible alternative for the photocatalytic decomposition of gas phase organic compounds.

For the photocatalytic degradation of toluene, acetone, methanol and trichloroethylene, Kim and Hong (2002) reported that at low UV intensity, below 2 mW/cm^2 , the conversion follows first order kinetics with respect to UV light intensity while at high UV light intensity, above 2 mW/cm^2 , the order is lower than unity.

Wang et al.(2003) stated that the deactivation of the catalyst during the reaction is the major disadvantage of the photocatalytic technology. The more decrease in active catalyst sites, the more decrease in catalyst activity. This is because of the production of reaction intermediates. Phenol, maloinic acid, hydroquinone, benzoic acid and benzoquinone are some typical intermediates adsorbed on TiO_2 for the photocatalytic decomposition of benzene (Wang et al., 2003). They reported that the catalyst purging with ozone containing air removed organic residues adhered on catalyst surface, which led to catalyst regeneration within 30 min.

Jeong et al. (2004) studied the application of short wavelength UV (254 + 185 nm) irradiation accompanied with a TiO_2 catalyst in the photodegradation of gaseous toluene. They found out that this technique is more efficient than UV alone for removing a wide range of VOCs in polluted air, especially when $\cdot\text{OH}$ radicals and ozone molecules are highly active. Even at high initial concentrations of toluene, high conversions were achieved.

Wang and Ku (2003) carried out their experiments for the photocatalytic oxidation of gaseous benzene in a batch-type photoreactor with a TiO_2 coated quartz fiber bundle. In similar operational conditions, the maximum quantum yield of the experiments with the optical fiber photoreactor was 0.5 while this was 3.5×10^{-3} for those conducted in an annular fixed film

photoreactor. Furthermore, the deactivation of photocatalyst in an annular photoreactor is more noticeable than in an optical fiber photoreactor.

2.4. Photocatalysis with Ozone in Wastewater Treatment

UV photocatalysis for wastewater treatment has been investigated far more than waste gas photocatalysis. However, photocatalytic oxidation and ozonation appear to be the most promising pre-treatment technologies compared with other advanced oxidation processes as shown by a large amount of information available in the literature. In fact, photocatalytic oxidation in the presence of ozone is a process that is qualitatively and quantitatively different from the well-known photocatalytic oxidation and ozonation without photocatalyst, according to Agustina et al. (2005).

Sanchez et al. (1998) studied the ozonation pretreatment followed by TiO₂ photocatalysis in the degradation of aniline in aqueous solution. Their results demonstrate that this combined process dramatically enhances the yield of TOC removal in comparison to either ozonation or photocatalysis when carried out separately. Interestingly enough, the opposite sequence, photocatalysis pre-treatment followed by ozonation, is not as efficient as the first sequence. They claimed that formation of ozone anion radicals prior to the generation of OH radicals explains the synergistic effect between ozone and TiO₂ under illumination. Other oxygen containing radicals are formed during photocatalysis with ozone, such as the superoxide radical anion and the hydroperoxide radical.

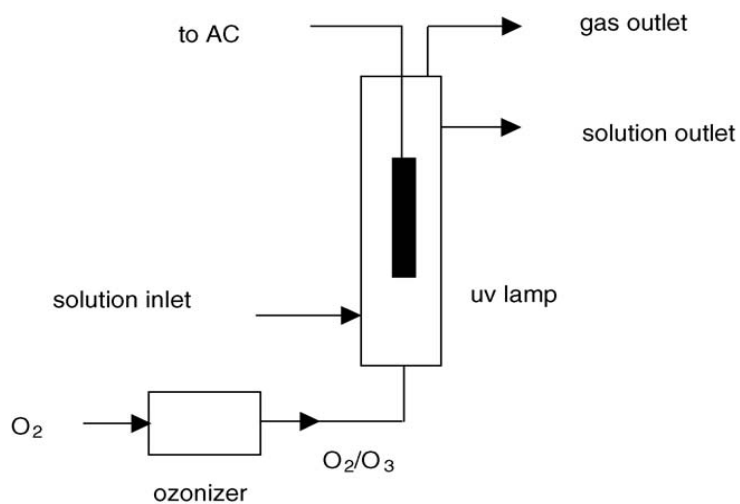


Figure 2.2. Laboratory scale-up for photocatalysis ozonation (Agustina et al., 2005)

2.5. Photocatalysis with Ozone in Waste Gas Treatment

As discussed earlier, photocatalytic oxidation (PCO) is one of the most widely investigated technologies to control BTX emissions. However, its application is greatly prevented by the deactivation of photocatalyst. In order to improve the PCO rate, the ozone-enhanced photocatalytic oxidation process (O_3 -PCO) has received some attention for its strong ability to degrade BTX pollutants from waste gas.

Zhang and Liu (2004) reported that ozone has a positive effect on activity enhancement and regeneration of TiO_2 photocatalyst. They also investigated the effect of ozone concentration and velocity on degradation efficiency of gaseous acetaldehyde.

Huang and Li (2011) focused on the removal efficiency of gaseous toluene in the O_3 -PCO process. They claimed that this process is much more complicated than the ordinary PCO process. PCO mostly deals with the strong oxidant of $\cdot OH$ while O_3 -PCO process involves not only $\cdot OH$ but also active oxygen $\cdot O$. Although O_3 -PCO has not yet been studied in detail, they

investigated the mechanism of toluene destruction based on the intermediates and main oxidants in the O₃-PCO process. According to Huang and Li (2011), the oxidation of toluene not only happens on the surface of photocatalyst as in the UV/TiO₂ and O₃/TiO₂ but also occurs in the bulk of gas phase as in the UV/O₃ which confirms the supremacy of O₃-PCO over the other discussed methods.

CHAPTER 3. EXPERIMENTAL PROCEDURES

3.1. Basic System configuration

A system was built to test the effectiveness of the ultraviolet degradation of benzene, toluene, and m-xylene in reducing BTX emissions. All the ultraviolet degradation experiments were run in a continuous flow set-up. The set-up is centered around a photoreactor which is the most important component of the system. The UV reactor used in this set-up is an HRCS-T-1 water purification system from UV Sciences (San Diego, CA). The photoreactor uses a high intensity but low pressure 40 W amalgam UV lamp. The amalgam lamp emits 8% of its electrical energy consumption as 185 nm light, and 30% as 254 nm light (data provided by the supplier). The reactor is cylindrical, with the lamp in the axis. It has a length of 56 cm, and the gap between the lamp and reactor wall is 8.5 mm (from radius 12.5 mm to 21 mm). Hence, the reactor volume is approximately 500 cm³. What distinguishes this reactor from similar reactors from other suppliers is that the cylinder wall reflects ultraviolet light, whereas reactors from other suppliers have absorbing walls. A sensor measuring the UV light intensity and tracking the lamp life is also placed in the middle of the reactor wall. The sensor is equipped with a digital display control unit to access lamp history data, such as the total hours of operation, the current output and the maximum output during the current cycle. The reactor is shown in Figure 3.1



Figure 3.1. Photoreactor

Two individual air streams as inlets were generated in parallel using air pumps. Contaminants (BTX), as well as near-saturation water vapour were added by bubbling the parallel air streams through washing bottles containing the contaminant and water. The air flows were controlled with needle valves and measured with rotameters. The flow of each stream can be individually manipulated to achieve various contaminant concentrations, as well as different total mass flow rates. The air stream containing water and the one containing organic vapour were then combined in different ratios, creating varying conditions at the reactor inlet. The desired BTX concentration was always achieved with a contaminant flow that was less than 10 % of the total air flow. Hence, the humidity was nearly constant at about 80 % relative humidity in all experiments which is the relative humidity generated in the water washing bottle. Two sampling ports, one at the inlet, and the other at the outlet of the reactor, allow for sampling and analysis of the inlet and outlet streams. The samples are then analyzed using a gas chromatography (GC) unit. The set-up configuration is demonstrated in Figure 3.2.

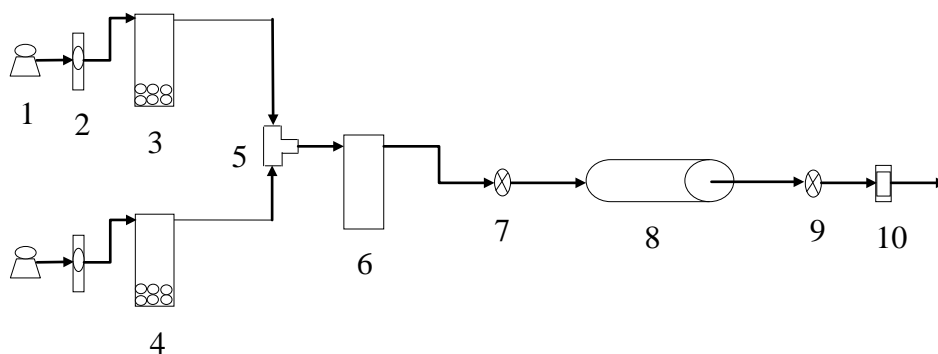


Figure 3.2. Schematic diagram of the photoreactor system used in this study. 1. Pump, 2. Rotameter, 3. Contaminant wash-bottle, 4. Water wash-bottle, 5. T-valve, 6. Mixing bottle, 7. Inlet sample port, 8. Photoreactor, 9. Outlet sample port, 10. Flow meter

Based on inlet concentration, C_{in} , and outlet concentration, C_{out} , the degradation efficiency, E , was calculated as follows:

$$E = \frac{C_{in} - C_{out}}{C_{in}} \quad (3.1)$$

The first set of experiments was carried out with m-xylene 99% as a BTX representative at volumetric flow rate 1 L/min. The results are shown in chapter 5.

Since UV lamp performance decays over time, it is essential to keep track of it during the course of experiments. Before starting a set of experiments, a blank run, with only humid air and no m-xylene going through the reactor, was performed. Parameters such as date, reactor hours, maximum intensity output, as well as total flow rate and relative humidity of the air stream were recorded in each blank run (Appendix A).

It typically took about an hour for the experimental conditions to reach steady state conditions, and the time to steady state was mainly dependent on the inlet concentration or flow rate. When the inlet concentration was low, steady state conditions were reached within 15 minutes, the time needed for the lamp to generate a steady light output. However, at high inlet concentrations, the

efficiency of the reactor decreased with time, went through a minimum, and increased again to reach a steady state. Concurrent with this trend, the measured light intensity first decreased, went through a minimum, and increased to reach a steady value. It was hypothesized that a layer of condensed reaction products was formed on the lamp, absorbing part of the ultraviolet light. As the lamp heats up over time, the layer of reaction products evaporates again. Steady state can only be reached when the lamp is sufficiently hot to prevent reaction product condensation.

Condensation of reaction products was observed on the outlet line of the reactor, confirming that condensation can be an issue. The condensate was a brown viscous liquid, partially soluble in water. Based on the chemistry of the process (Mahmoudkhani, 2012), it can be assumed that the nature of the condensate is mainly phenolic.

3.2. Equations used in experimental work

The vapour generation system is based on evaporation. So vapour pressure gives a good indication of the concentration produced. This calculation was used to set the conditions of the experiment. However, there are some deviations due to under-saturation. Hence, the actual inlet concentration was measured by sampling the gas stream at the inlet sample port, and then analyzing the sample by GC.

The most frequently used equation for correlating temperature dependence of vapour pressure is the Antoine equation which is employed in this study (Poling et al., 2001).

$$\log_{10} P_v = A - \frac{B}{C + T} \quad (3.2)$$

Where P_v is vapour pressure in bar, T is temperature in °C. A , B and C are component specific constants. Table 3.1 shows the coefficients of the Antoine equation for benzene and m-xylene.

Table 3.1. Coefficients of the Antoine equation (3.2) (Poling et al., 2001)

Compound	A	B	C+273.15
benzene	3.98523	1184.240	217.572
m-xylene	4.14051	1468.703	216.120

Another correlation used in this study to achieve temperature dependence of vapour pressure is defined by the Wanger equation as follows (Poling et al., 2001):

$$\ln P_v = \ln P_c + \frac{T_c}{T} \left[a.t_{au} + b.t_{au}^{(1.5)} + c.t_{au}^{(2.5)} + d.t_{au}^{(5)} \right] \quad (3.3)$$

T_c and P_c are the critical temperature and pressure in Kelvin and bar respectively and T is the actual temperature in Kelvin. a , b , c and d are component specific constants and t_{au} is defined as:

$$t_{au} = 1 - \frac{T}{T_c} \quad (3.4)$$

Table 3.2 shows the coefficients of the Wanger equation.

Table 3.2. Coefficients of the Wanger equation (3.3) (Poling et al., 2001)

Compound	T_c (K)	P_c (bar)	a	b	c	d
benzene	562.16	48.98	-7.01433	1.55256	-1.8479	-3.7130
m-xylene	617.05	35.38	-7.67717	1.80240	-2.47745	-3.66068

Under normal conditions, dry ambient air contains approximately 78.08% nitrogen, 20.94% oxygen and traces of other gases (Lide, 2008). As ambient air always approximates an ideal gas, the concentration of the contaminant satisfies the ideal gas law:

$$C = \frac{P}{RT} \quad (3.5)$$

where,

C = contaminant concentration, mol/m³

P = partial pressure, Pa

R = ideal gas constant, 8.3144621 J/mol.K

T = absolute temperature, K

Bearing in mind that molar mass of m-xylene is 106.16 g/mol and the proper syringe used for GC is 500 µl (according to the supplier), the calibration curve for m-xylene can be plotted as in Figure 3.3.

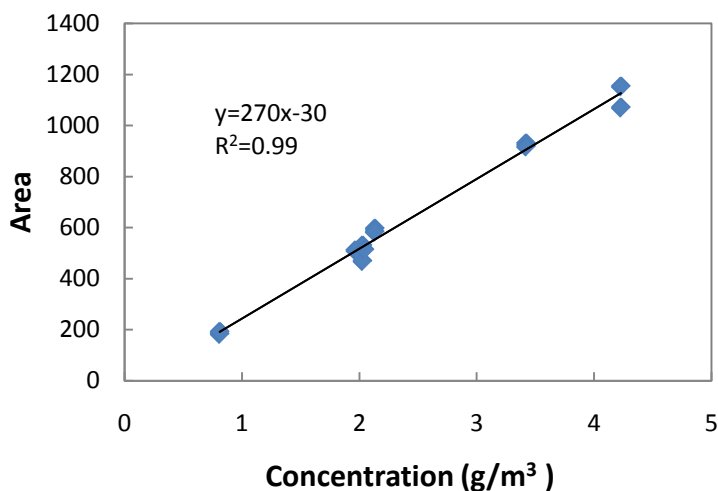


Figure 3.3. Calibration curve for m-xylene photodegradation experiments (sample size 500 µL)

The calibration curve of m-xylene was obtained by incubating flasks containing liquid m-xylene sealed with Teflon lined rubber stoppers at a known temperature until the headspace is saturated with m-xylene vapour. Samples with known volumes were taken from the headspace, and analyzed by the GC.

For benzene, this procedure would have required sample volumes that are too small to be reproducible. Hence, after equilibration, headspace samples were injected into empty flasks with known volumes to dilute the benzene, and samples from this flask were injected in the GC. The calibration curve of benzene is presented in Figure 3.4.

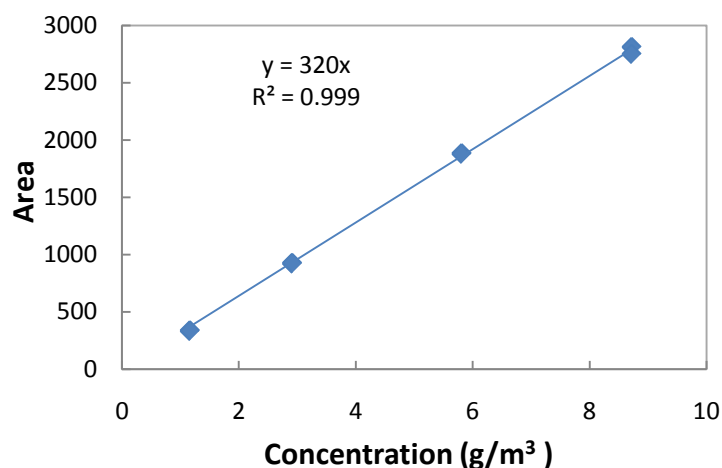


Figure 3.4. Calibration curve for benzene photodegradation experiments (sample size 500 μ L)

3.3. Improvements to the experimental results

Since this work is one part of a larger project, a couple of improvements in the experimental study of benzene photodegradation, which is the main product of interest, are considered. Adding ozone in a pre-mixing system is recognized as an improvement in this regard. An additional set of experiments was carried out where the air flow was passed through an OZ-4AD ozone

generator (Ozone Solutions, Inc.). The ozone production rate of the ozone generator depends on the volumetric air flow rate, as shown in Figure 3.5.

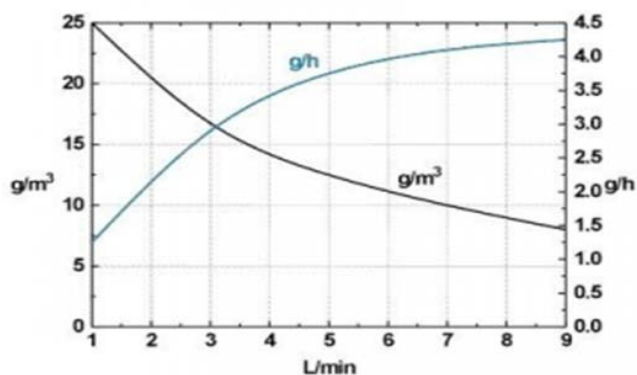


Figure 3.5. Ozone production rate versus volumetric air flow rate of the ozone generator

The flow rate sent through the ozone generator was 8 L/min, which led to an ozone concentration of 8 g/m³. Of this stream, 2.2 L/min was sent to the water washing bottle, and the rest was purged. Hence, an ozone mass flow rate of 17.6 mg/min was sent to the reactor.

The experimental set-up when ozone is pre-mixed is shown in Figure 3.6

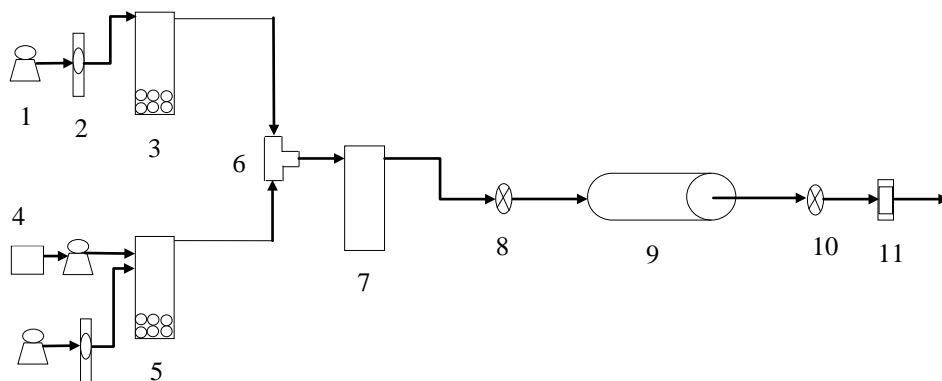


Figure 3.6. Schematic diagram of the photoreactor system used in this study with ozone pre-mixing process. 1. Pump, 2. Rotameter, 3. Contaminant wash-bottle, 4. Ozone generator, 5. Water wash-bottle, 6. T-valve, 7. Mixing bottle, 8. Inlet sample port, 9. Photoreactor, 10. Outlet sample port, 11. Flow meter

CHAPTER 4. PHOTOCHEMICAL AND PHOTOCATALYTICAL MODEL DESCRIPTION

A simulation model was developed to obtain a better understanding of the ultraviolet degradation process. To that effect, the model developed in this project consists of four modules: a waste gas velocity profile, a material balance, a chemical (kinetic) model, and a radiation field model.

Combining the four modules is a significant challenge, because of the mutual interactions that exist between the processes. In particular, combining a light field model with the other modules is difficult. The material balance is calculated from the entrance to the exit of the reactor. The light field, however, consists of photons that move in all directions, some with the flow and some against the flow. To calculate the absorption of the photons moving in both directions, the concentration profile in the reactor must be known in advance. However, the concentration depends on the photolysis rates, which requires knowledge of the photon fluxes. Hence, the problem can only be solved iteratively.

The purpose of this chapter is to describe the photolytic reactor model of Mahmoudkhani (2012), (section 4.1 – 4.4), and to extend the model to include photocatalytic reactions (section 4.5).

4.1. Flow Pattern Model

The gas flows between the lamp and the reactor, which can be imagined as a gas flow between two concentric pipes. Based on the volumetric flow rate and the geometry, the model assumes that the air flow in the reactor is laminar. This will be demonstrated with an example calculation.

Gas flow through a pipe is laminar when the Reynolds number is less than 2100. The Reynolds number is defined as:

$$\text{Re} = \frac{dv\rho}{\mu} = \frac{dv}{\nu} \quad (4.1)$$

Where d is the pipe diameter, v is the flow velocity, ρ is the fluid density, and μ is the dynamic viscosity. Kinematic viscosity, ν , is defined as μ/ρ . This value for air is $\nu = 1.5 \times 10^{-5} \text{ m}^2 / \text{ s}$.

In case of pipes that do not have a circular cross-section, the diameter can be replaced by hydraulic diameter d_h , defined by:

$$d_h = \frac{4A}{L} \quad (4.2)$$

Where A is the cross-sectional area and L is the wet perimeter. As an example for an annular space between cylinders with radii $R_1=1.25$ cm and $R_2=2.1$ cm, the hydraulic diameter is 1.7 cm.

Based on the above numbers and assuming a volumetric flow rate of $2200 \text{ cm}^3/\text{min}$, the highest flow rate used in the experiments, a Reynolds number of 46.5 is obtained, far below the threshold for turbulent flow. Even when the flow velocity and the hydraulic diameter are both increased fivefold, as an up-scaling perspective, a Reynolds number of 1160 is found, well into the laminar range. Hence, a laminar flow velocity profile is a wise assumption in this regard.

Although a parabolic velocity profile applies to flow in pipes with a circular cross-section and flow between parallel plates, this is not the case in an annular space. The laminar velocity profile in an annular space is based on a force balance and Newton's viscosity law. Since the gas mixture contains over 99% air and water vapour, the rest being organic vapours, this assumption of Newtonian fluids is justified.

In order to derive an equation for the velocity profile, a force balance is applied on a thin cylindrical element (Figure 4.1). Negative velocity gradient corresponds with momentum transfer in the direction of increasing r .

$$\text{Force} = (\text{Pressure or stress}) \times \text{Area} \quad (4.3)$$

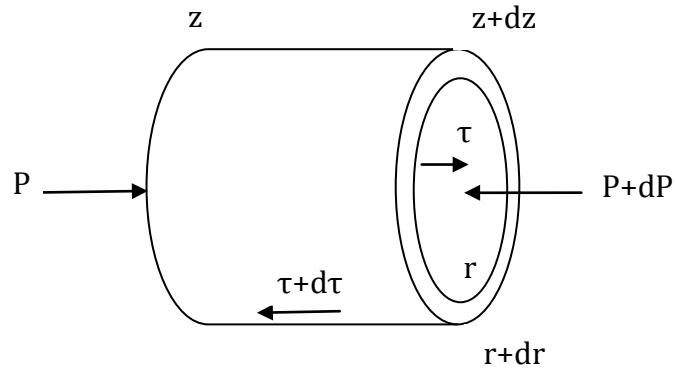


Figure 4.1. Force balance on an annular element

Writing the force balance:

$$\text{Pressure} + \text{Shear stress forward} = \text{Pressure} + \text{Shear stress backward} \quad (4.4)$$

The proper expressions of pressure and shear stress were substituted in the force balance equation by Mahmoudkhani (2012). A first-order differential equation was solved by integration between the radius of the lamp (R_1) and the inside radius of the reactor (R_2). The result is as follows:

$$V = \frac{\frac{2U(R_2^2 - R_1^2)}{\ln \frac{R_2}{R_1}} \ln \frac{r}{R_1} - 2U(r^2 - R_1^2)}{R_2^2 + R_1^2 - \frac{R_2^2 - R_1^2}{\ln \frac{R_2}{R_1}}} \quad (4.5)$$

Where R_1 and R_2 are the internal and external radii, respectively, U is the mean flow velocity defined as the volumetric flow rate divided by the cross-sectional area, and r is the radial coordinate, which has a value between R_1 and R_2 in the annular space.

This equation was used to calculate local gas velocity in the model. Mahmoudkhani (2012) compared model predictions with the plug flow velocity profile, $V=U$, with predictions using the laminar flow velocity profile. The results differed by only a few percents. Although the choice of velocity does not seem critical in the calculation, the laminar velocity profile was used in all calculations reported in this study.

4.2. Material Balance

The material balance is defined on an annular element in the reactor. As an assumption, advection is the dominant mass transfer mechanism in the direction of the flow. When the Peclet

number $Pe_L = \frac{L \cdot u}{D}$ is greater than 40, the dominant mass transfer mechanism in the flow

direction is advection (Froment & Bischoff, 1993). Here L is the length of the reactor, u is the

mean gas velocity, $u = \frac{Q}{\pi(R_2^2 - R_1^2)}$, and D is diffusivity. At the lowest flow rate investigated in

this study (0.5 L/min), $Pe_L=521.64$ with $L=56$ cm, $u=0.9315$ cm/s, $D=0.1$ cm²/s. Hence, it is

justified to assume advection is the dominant mass transfer mechanism in the flow direction in

this study. However, as the flow is laminar, as discussed in section 4.1, diffusion is dominant in

the radial direction. To that effect, radial diffusion of all species is included. Species are

produced or consumed through reactions occurring in the element. All these phenomena are

depicted in Figure 4.2.

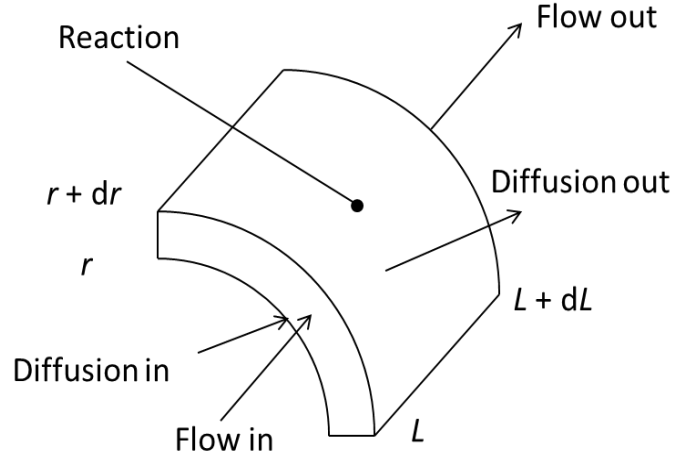


Figure 4.2. Material balance on an annular element

The material balance is as follows:

$$\text{Flow in} + \text{Diffusion in} + \text{Reaction} = \text{Flow out} + \text{Diffusion out} \quad (4.6)$$

These terms are defined as follows:

$$\text{Flow in} = C_i \cdot v \cdot 2\pi r \cdot dr \quad (4.7)$$

$$\text{Flow out} = (C_i + \frac{\partial C_i}{\partial L} dL) \cdot v \cdot 2\pi r \cdot dr \quad (4.8)$$

$$\text{Diffusion in} = -D_i \frac{\partial C_i}{\partial r} \cdot 2\pi r \cdot dL \quad (4.9)$$

$$\text{Diffusion out} = -D_i \frac{\partial(C_i + \frac{\partial C_i}{\partial r} dr)}{\partial r} \cdot 2\pi(r + dr) \cdot dL \quad (4.10)$$

$$\text{Reaction} = r_i \cdot 2\pi r \cdot dr \cdot dL \quad (4.11)$$

In these terms C_i is the concentration of compound i (molecules/cm³), D_i is the molecular diffusivity of compound i (cm²/s), r_i is the reaction rate of i (molecules/cm³.s) and v is the local gas velocity (cm/s).

Substitution into the material balance leads to:

$$\begin{aligned}
 & C_i.v.2\pi r.dr - D_i \frac{\partial C_i}{\partial r}.2\pi r.dL + r_i.2\pi r.dr.dL \\
 & = C_i.v.2\pi r.dr + \frac{\partial C_i}{\partial L}dL.v.2\pi r.dr \\
 & - D_i \frac{\partial C_i}{\partial r}.2\pi r.dL - D_i \frac{\partial C_i}{\partial r}.2\pi.dr.dL \\
 & - D_i \frac{\partial^2 C_i}{\partial r^2}.2\pi r.dr.dL - D_i \frac{\partial^2 C_i}{\partial r^2}.2\pi.(dr)^2.dL
 \end{aligned} \tag{4.12}$$

Where r_i in the third term is reaction rate, which is dependent on radius.

Dividing all of the terms by $2\pi r.dr.dL$ results in:

$$r_i = v.\frac{\partial C_i}{\partial L} - \frac{D_i}{r}.\frac{\partial C_i}{\partial r} - D_i.\frac{\partial^2 C_i}{\partial r^2} - \frac{D_i}{r}.\frac{\partial^2 C_i}{\partial r^2}.dr \tag{4.13}$$

In which the last term approaches zero at the limit to $dC_i \rightarrow 0$ and $dr \rightarrow 0$. So:

$$v.\frac{\partial C_i}{\partial L} = D_i.\frac{\partial^2 C_i}{\partial r^2} + \frac{D_i}{r}.\frac{\partial C_i}{\partial r} + r_i \tag{4.13}$$

There is one material balance partial differential equation per compound. In principle, a different value of D_i should be used for all chemical species. To simplify, the value of benzene ($D = 0.1$ cm²/s) was used for all species. This is a conservative estimate as most species considered in this model have a diffusivity greater than 0.1 cm²/s.

The boundary condition of the concentration at the reactor inlet is assumed to be a known concentration of the feed stream. For the radial derivatives, boundary conditions at $r = R_1$ (lamp) and $r = R_2$ (wall) are needed. The no-flux condition is assumed, i.e.:

$$\frac{\partial C_i}{\partial r} = 0 \quad r = R_1, r = R_2 \quad (4.14)$$

Finding the value of the reaction rate (r_i) is the purpose of the next section.

4.3. Chemical Model

According to Mahmoudkhani (2012), 59 chemical and photochemical reactions involving 47 chemical species were included in the chemical model. This includes the main degradation pathways and all the relevant chemical and radical reactions, involving oxygen, water, ozone, benzene and reaction products.

For the description of the kinetics, a distinction is made between chemical kinetics (reactions not involving photons) and photochemical kinetics (reactions caused by the absorption of a photon).

The rate of a photochemical reaction can be described as:

$$r_i = -\phi_i \cdot C_i \cdot \sigma_i \cdot E_p \quad (4.15)$$

In which:

ϕ_i is the quantum yield of molecule i in molecules/photon, the fraction of absorbed photons causing a reaction.

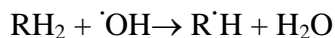
C_i is the number concentration of the compound involved in moles/cm³.

σ_i is the absorption cross-section of molecule i in cm²/molecule or simply cm², a measure of the ability of the molecule to absorb photons.

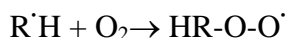
E_p is the fluence rate in photons/cm².s or simply 1/cm².s.

For the chemical reactions, second-order kinetics is assumed. Most of the chemical reactions are groupings of reactions based on the concept of the rate limiting step.

As an example, the oxidation of a hydrocarbon RH_2 initiated by an OH radical is considered. Assuming that the initial, rate limiting step is the abstraction of a hydrogen atom, the result is an alkyl radical.

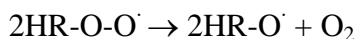


The alkyl radical reacts with oxygen to form a peroxyalkyl radical:



This reaction is very fast (typical reaction rate constant $>10^{12}$ $\text{cm}^2/\text{molecule}\cdot\text{s}$ (Atkinson, 1997)), and completes in a fraction of a microsecond.

Peroxy radicals can produce alkoxy radicals ($\text{HR-O}\cdot$) and oxygen by the Russell reaction when there is no NO in the system:

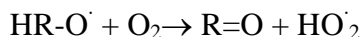


In the presence of NO the conversion is oxidation of NO to NO_2 :

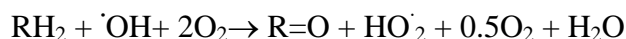


Since these radicals will accumulate until the rate of reaction equals the rate of formation of these species, these reactions are assumed instantaneous.

If the alkyl group has hydrogen on the last carbon, then the next reaction is usually hydrogen abstraction by oxygen:



The overall reaction is as follows:

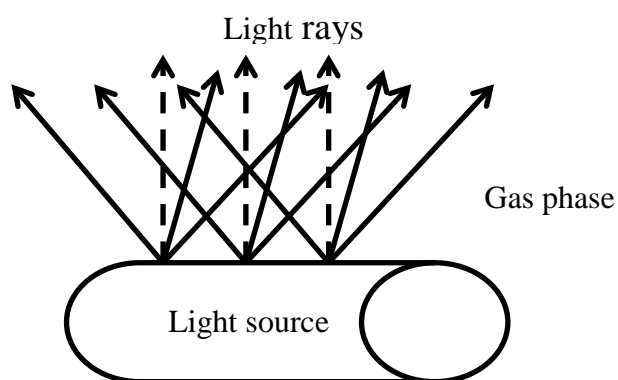


with a reaction rate determined by the rate of the first reaction. The guiding principles of the development of the chemical mechanism are from De Visscher et al. (2008).

4.4. Radiation Field Model

4.4.1. First Guess

This model is an approximation that assumes that the lamp is a line source of light that sends out light rays perpendicular to the lamp. This underestimates the real light absorption since it considers only the light with the shortest path length. In reality, the situation is more



complicated, as shown in Figure 4.3.

Figure 4.3. Light rays in the simple model (dashed lines) and in the detailed model (solid lines)

Because of the extent of reflection of the light back and forth between the lamp and the outside cylinder, it is likely that path length does not play a significant role in the system, which means that the approximate model and the detailed model are in close agreement. This is unlike photochemistry in the water phase, where absorption is much stronger, and the reaction is more confined to a zone close to the lamp.

Based on Mahmoudkhani's radiation field model (2012), two versions of light field model were developed. The first version formed an initial estimate of the light intensity in the reactor, whereas the second version calculates light rays moving at different angles and within a plane

that contains the lamp axis, in an iterative procedure in cylindrical symmetry. The summation of the irradiance of the outgoing light and the reflected light is assumed to be equal to the fluence rate in the simplified model.

In order to calculate the values of the light intensity at each location in the reactor, an annular element of the reactor is considered for the photon balance, Figure 4.4

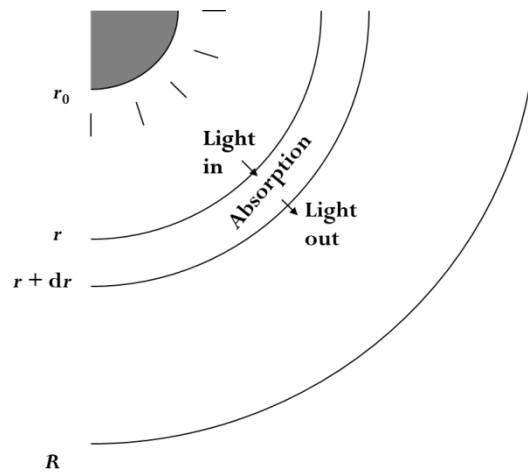


Figure 4.4. Photon balance

The photon balance is as follows:

$$\text{Light out} = \text{Light in} - \text{Absorption} \quad (4.16)$$

where the terms are as follows:

$$\text{Light in} = E_p \cdot 2\pi r \cdot L \quad (4.17)$$

$$\text{Light out} = (E_p + dE_p) \cdot 2\pi \cdot (r + dr) \cdot L \quad (4.18)$$

$$Absorption = \sum_i \alpha_i E_p \cdot 2\pi r \cdot dr \cdot L \quad (4.19)$$

where the extinction coefficient α_i is given by:

$$\alpha_i = C_i \cdot \sigma_i \quad (4.20)$$

Here:

E_p is irradiance in photons/cm².s

C_i is the concentration of compound i in molecules/cm³

σ_i is the absorption cross-section of compound i in cm²

Substitution in equation (4.16) leads to the following equation:

$$(E_p + dE_p) \cdot 2\pi \cdot (r + dr) \cdot L = E_p \cdot 2\pi r \cdot L - \sum_i \alpha_i E_p \cdot 2\pi r \cdot dr \cdot L \quad (4.21)$$

where the summation is over all chemical species i. Expanding the terms between brackets, and dividing by $2\pi L$ leads to:

$$E_p \cdot r + dE_p \cdot r + E_p \cdot dr + dE_p \cdot dr = E_p \cdot r - \sum_i \alpha_i E_p \cdot r \cdot dr \quad (4.22)$$

The last term in the left-hand side has two differentials, and is negligible in comparison with the other terms. The first term on both sides cancels out. Hence:

$$dE_p \cdot r + E_p \cdot dr = - \sum_i \alpha_i E_p \cdot r \cdot dr \quad (4.23)$$

Dividing by $r \cdot dr$ and rearranging leads to the following differential equation:

$$\frac{dE_p}{dr} = - \frac{E_p}{r} - \sum_i C_i \cdot \sigma_i E_p \quad (4.24)$$

There is one differential equation for each wavelength, at each location in the reactor. As a boundary condition, the emitted light power of the lamp is divided by the surface area of the lamp, to obtain irradiance, and divided by the energy of one photon, to obtain photon irradiance.

The supplier of the UV reactor indicated that 99% of the photons reaching the reactor outer wall is reflected but no information was available on the fraction of the photons reaching the lamp that are re-emitted. This fraction can be determined by comparing the light irradiance at the wall by model predictions with experimental measurements. For pure air, good agreement was found (55 mW/cm^2) when it was assumed that 64% of the light returning to the lamp is re-emitted, (Mahmoudkhani, 2012). The mechanism of the re-emission is the excitation of Hg molecules by the photons, followed by return of the Hg molecules to the ground states with emission of a photon.

4.4.2. Iterative Solution

Calculating the light field resulting from light rays moving at different angles was much more challenging than the first guess light field model (Mahmoudkhani, 2012).

For the iterative solution, emission points were defined at 1 mm intervals on the lamp radiating light at 39 different angles θ at each source; from $\frac{2\pi}{40}$ to $39 \cdot \frac{2\pi}{40}$. The reactor space was divided by a two-dimensional grid consisting of 9 concentric cylinders and 560 cross-sectional planes. The intersection of the light rays with each grid plane was calculated, and the local concentration was calculated in order to calculate the light absorption. All reflections of the light ray are accounted for until the light ray returns to the lamp. The fluence rate of each grid point is calculated based on its definition (Section 2.1.1), using the intensity of each light ray approaching the grid point to within 1 mm.

The calculations are first made with a unit emission at each emission point of the lamp. Based on the locations and intensities of the light rays returning to the lamp, and the 64 % re-emission rate,

an updated emission is calculated at each emission point. The update is made iteratively until the light intensity no longer changes. The resulting light fluence distribution is multiplied with the actual emission rate of the lamp to obtain the real fluence distribution. Based on the fluence distribution the material balance is recalculated, and with the new concentration profile the entire calculation is repeated. Further iterations did not improve the accuracy of the calculation.

4.4.3. Implementation

Based on Mahmoudkhani's thesis (2012), the space between the lamp and the outside reactor wall was divided equally into 9 concentric cylinders. This model was also tested with 19 concentric cylinders, and the results were about 1 % apart.

The material balance was defined on each cylinder, and converted to a set of ordinary differential equations by finite differences.

In the case of the approximate model (i.e., the first guess light field), the light irradiance was calculated based on the local concentrations by integrating the photon balance from the lamp to the outside wall. Reflection at the outside wall was assumed to be 99 % effective, and the photon balance was integrated back to the lamp. Further passes were calculated until the light ray had negligible irradiance. Because of the geometry assumed in this model, the fluence rate is the sum of the irradiances coming from both sides. These fluence rates were used to calculate the photochemical reactions in the model.

The ordinary differential equations describing the material balance were integrated numerically in MATLAB using the function ode15s, a variable order solver for stiff sets of differential equations.

After completing the first guess light field and concentration profile, the final solution is calculated along the lines explained in Section 4.4.2.

The predicted benzene degradation rates of the final solution differed from the first guess model by less than 2%, but took more than 20 times as long to calculate. For that reason, it was opted to use the first guess model for further model extensions. A photocatalytic extension is discussed in the next section.

4.5. Extension of the Model to Include Photocatalysis

The ultraviolet light reaching the outer wall of the reactor and then reflecting back into the reactor towards the lamp is considered as the configuration in photolysis. An alternative configuration would be to coat the outer wall of the photolytic reactor with a catalyst, creating a hybrid photolytic-photocatalytic system. The potential advantage of such a system is a better utilization of the light, as less light would be absorbed in the lamp, and a potentially higher efficiency of the catalytic reaction versus the direct photolytic reaction. However, catalyst deactivation is considered as a disadvantage of the hybrid system, leading to photon absorption that does not lead to reaction. Another disadvantage is increased mass transfer limitation, leading to a low benzene concentration at the catalyst surface, where most of the reaction is meant to take place.

Photocatalysis of benzene has been studied before in the literature. The results from experiments in the literature in a system similar to the current photoreactor can be applied to develop a photocatalytic module that can be added to the photochemical model. Hence, the kinetic parameters can be calculated from the literature.

The basis of the photocatalytic model is the photolytic model with a simple light field model. Because of the small difference between the simple (first guess) light field model and the refined (iterative) model, it is assumed that there is no need to use the refined model for this evaluation. This was the subject of Section 4.4.

The catalytic reaction kinetics used in the chemical model is based on the following equation:

$$r_A = \frac{k_0 I^n K C_A}{1 + K C_A} \quad (4.25)$$

where, r_A is the reaction rate of compound A (benzene) in molecules/cm².s, k_0 and K are kinetic constants, I is the irradiance in W/cm² and C_A is the number concentration in molecules/cm³.

In order to find the kinetic parameters, a set of calculations were applied to literature data of Ma et al. (2007) and Wang et al. (2003) whose experimental conditions were almost the same as the current study. Ma et al. (2007) estimated the values of the kinetic constants based on the data presented in Figure 4.5.

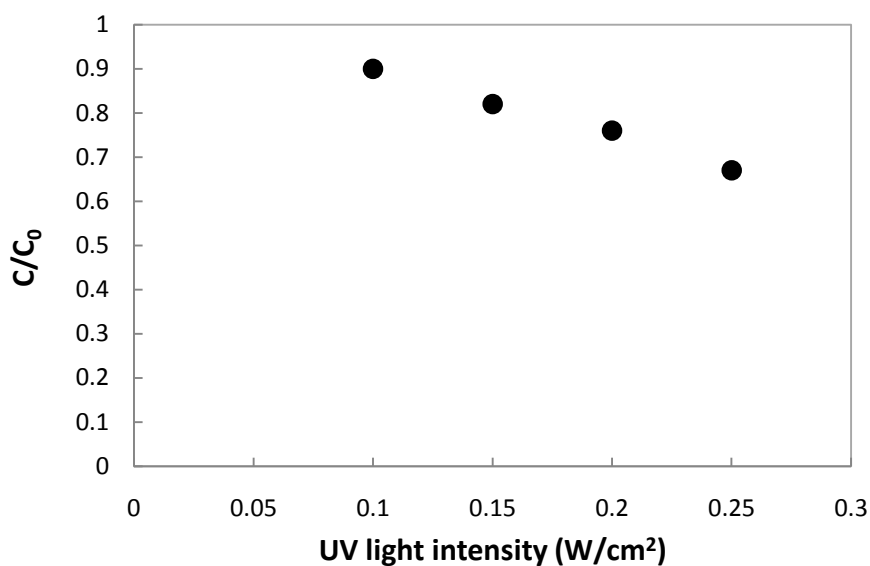


Figure 4.5. The effect of UV light intensity on the decomposition and the mineralization rate of benzene by the UV/TiO₂ process: 10 ppm benzene, 100 ml min⁻¹ flow rate, (Ma et al., 2007)

The K value was determined to be 0.0885 ppm^{-1} ; the value of n was determined to be 0.8832 (Ma et al, 2007). However, the parameter estimation of Ma et al. (2007) assumes that no mass transfer limitations take place, which is inconsistent with the current model, where mass transfer limitations are simulated explicitly. Hence, the parameters must be re-estimated before the catalytic model can be incorporated in the photolytic model. This is the objective of the current section.

First, an initial guess of the parameters is made as indicated below. Then, the simulation model is run with the initial guess of the parameters, and with alternative combinations of the parameters. The optimal parameters were obtained by a trial and error.

As an initial guess for the parameter estimation, the values of n and K of Ma et al. (2007) are used, with the units of K converted to include molecules/cm³ instead of ppm, based on Avogadro's Number = 6.02×10^{23} . A first guess of k_0 is obtained by fitting a simplified model to the data of Wang et al. (2003).

Under normal conditions, dry ambient air contains approximately 78% nitrogen and 21% oxygen and the rest is traces of other gases (Lide, 2008). Percentages are basically expressed as percent by volume for gas. Volume percent is the same as mole percent for an ideal gas. Ambient air approximates an ideal gas that always satisfies the ideal gas law:

$$PV = nRT \quad (4.26)$$

Where, P is absolute pressure in Pa, V is volume in m³, n is the number of moles, R is the ideal gas constant in m³.Pa/mol.K, T is the absolute temperature in K. In air pollution work, the reference conditions are usually chosen as 25 °C (298K) and 1 atm (10^5 Pa).

The concentration measure ppm is simply 10^{-6} mole fraction of the pollutant in the gas mixture.

Solving equation (4.26) for 1 ppm leads to:

$$C = \frac{n}{V} = \frac{P}{RT} (10^{-6}) = \frac{10^5}{8.314 \times 298} (10^{-6}) = 4.09 \times 10^{-5} \text{ mol} / \text{m}^3 = 2.46 \times 10^{13} \text{ molecules} / \text{cm}^3 \quad (4.27)$$

In the same way, 1 ppm⁻¹ equals to 4.1 × 10⁻¹⁴ cm³/molecule. So, the K value is:

$$K = 0.0885 \text{ ppm}^{-1} \times \frac{4.1 \times 10^{-14} \text{ cm}^3 / \text{molecule}}{1 \text{ ppm}^{-1}} = 3.64 \times 10^{-15} \text{ cm}^3 / \text{molecule} \quad (4.28)$$

The initial guess of k₀ is derived by writing a molar mass balance over the photochemical reactor along the direction of the flow:

$$\text{Flow in} - \text{Flow out} = \text{Reaction} \quad (4.29)$$

$$\text{Flow in} = Q.C \quad (4.30)$$

$$\text{Flow out} = Q.(C + dC) \quad (4.31)$$

$$\text{Reaction} = r.dA \quad (4.32)$$

Substituting the above expressions in equation (4.29) leads to equation (4.33):

$$-Q.dC = r.dA \quad (4.33)$$

Rate of reaction (r) can be replaced with equation (4.25):

$$-Q.dC = \frac{k_0 \cdot I^n \cdot K \cdot C}{1 + KC} .dA \quad (4.34)$$

$$\frac{dC \cdot (1 + KC)}{C} = -\frac{k_0 \cdot I^n \cdot K}{Q} .dA \quad (4.35)$$

$$\frac{dC}{C} + K.dC = -\frac{k_0 \cdot I^n \cdot K}{Q} .dA \quad (4.36)$$

Integrating equation (4.36) from C₀ to C and 0 to A results in:

$$\int_{C_0}^C \frac{dC}{C} + K \int_{C_0}^C dC = -\int_0^A \frac{k_0 \cdot I^n \cdot K}{Q} .dA \quad (4.37)$$

$$\ln \frac{C}{C_0} + K(C - C_0) = \frac{-k_0 \cdot I^n \cdot K}{Q} \cdot A \quad (4.38)$$

Or

$$\ln \frac{C}{C_0} + K(C - C_0) + \frac{k_0 \cdot I^n \cdot K}{Q} \cdot A = 0 \quad (4.39)$$

Equation (4.39) is solved to determine the value for k_0 in $\text{molecules/cm}^2 \cdot \text{s} \cdot (\text{W/cm}^2)^n$. C/C_0 and I are known from Figure 4.5. A value of k_0 was determined for each data point, and the average value was taken. Other values were taken from Ma et al.'s paper (2007) presented in Table 4.1:

Table 4.1. Experimental conditions and kinetic parameters presented by Ma et al. (2007)

Parameters	Values
Volumetric flow rate, Q	1.67 cm^3/s
Benzene initial concentration, C_0	2.46×10^{14} molecules/ cm^3
TiO ₂ -coated area in the optical fiber reactor, A	1.57 cm^2
Reaction order of applied UV light intensity, n	0.8832
Adsorption equilibrium constant of benzene on TiO ₂ particles, K	3.64×10^{-15} $\text{cm}^3/\text{molecules}$

The initial guess of the reaction rate constant, k_0 , was found to be equal to 5.66×10^{14} $\text{molecules/cm}^2 \cdot \text{s} \cdot (\text{W/cm}^2)^n$.

Photocatalytic decomposition of gaseous benzene at room temperature with an annular reactor has been studied by Wang et al. (2003). Figure 4.6 shows the effect of different initial benzene

concentration on the decomposition rate of benzene found by Wang et al. (2003) when a constant value of UV intensity, 2.1 mW/cm^2 is used.

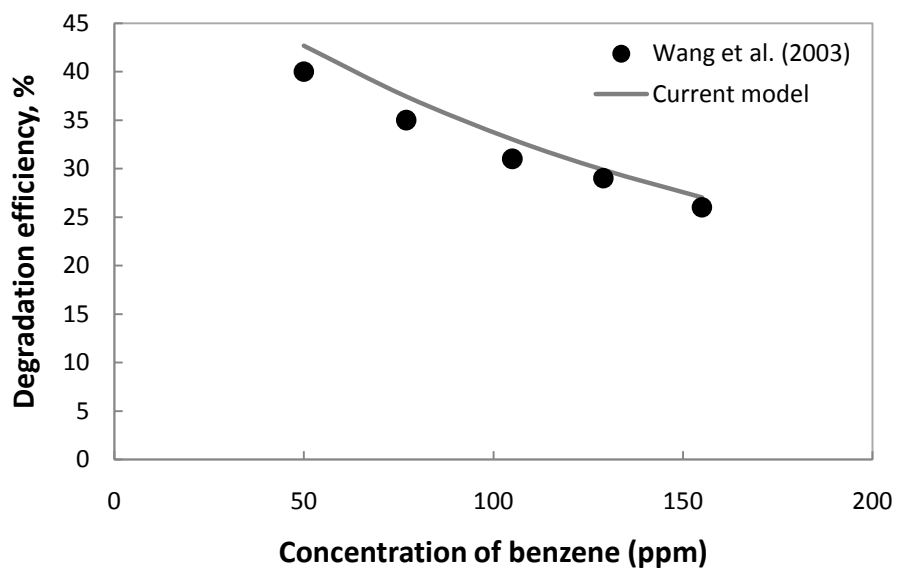


Figure 4.6. The effect of initial benzene concentration on the decomposition of benzene UV/TiO₂ process at a light intensity of 2.1 mW/cm^2 (Wang et al., 2003)

Figure 4.7 presents the effect of UV light intensity on the decomposition rate of benzene found by Wang et al. (2003) at initial benzene concentration of 70 ppm.

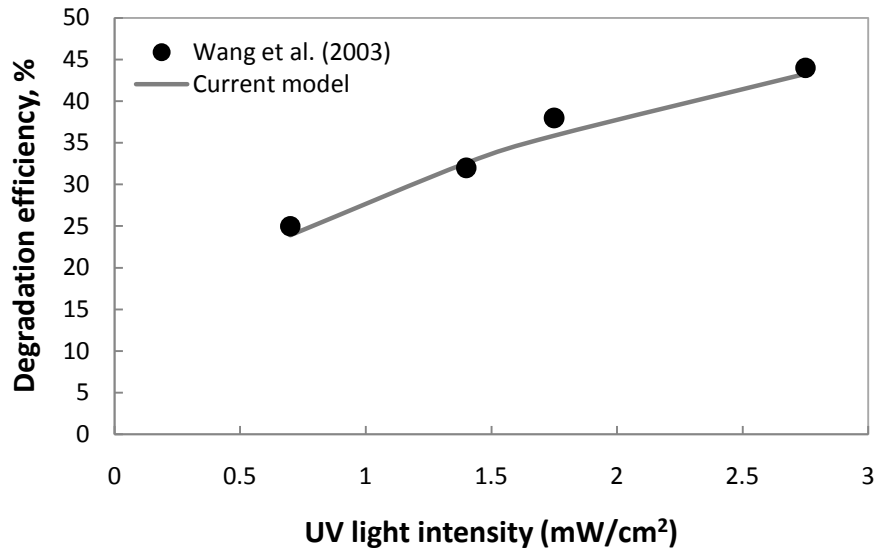


Figure 4.7. The effect of UV light intensity on the decomposition of benzene by UV/TiO₂ process at a benzene concentration of 70 ppm (Wang et al., 2003)

Starting from the initial estimates of n , k_0 and K , the model was run for different combinations of parameter values and predictions of the data of Wang et al. (2003) were obtained. For each parameter combination, the sum of squares of the deviations between the model and the data was calculated. The parameter combination with the smallest sum of squares was kept.

The following kinetic parameters were obtained:

$$k_0 = 1.2 \times 10^{14} \frac{\text{molecules}}{\text{cm}^2 \cdot \text{s} \cdot \left(\frac{\text{W}}{\text{cm}^2}\right)^n}$$

$$n = 0.5$$

$$K = 5 \times 10^{-16} \frac{\text{cm}^3}{\text{molecule}}$$

As can be seen from Figure 4.6 and 4.7 that the fit between the model and the data is satisfactory. The model overestimates the data in Figure 4.6, but this data set appears to be lower than the data set in Figure 4.7. This may be the result of catalyst deactivation. For that reason, an accurate fit with the data in Figure 4.7 was preferred.

4.5.1. Sensitivity Analyses

To investigate the accuracy of the parameter estimates, a sensitivity analysis was carried out. One by one, each parameter was changed by 20 % in both directions, and the model predictions were compared with the model predictions based on the optimal parameter values. The results are shown in Figures 4.8-4.10. The parameter, k_0 , affects the reaction rate similarly in all conditions, whereas K affects only the concentration dependence of the reaction rate, and n affects only the light intensity dependence of the reaction rate. For that reason, the effect of k_0 and K was tested on the data at different benzene concentrations, whereas the effect of n was tested on the data at different light intensities.

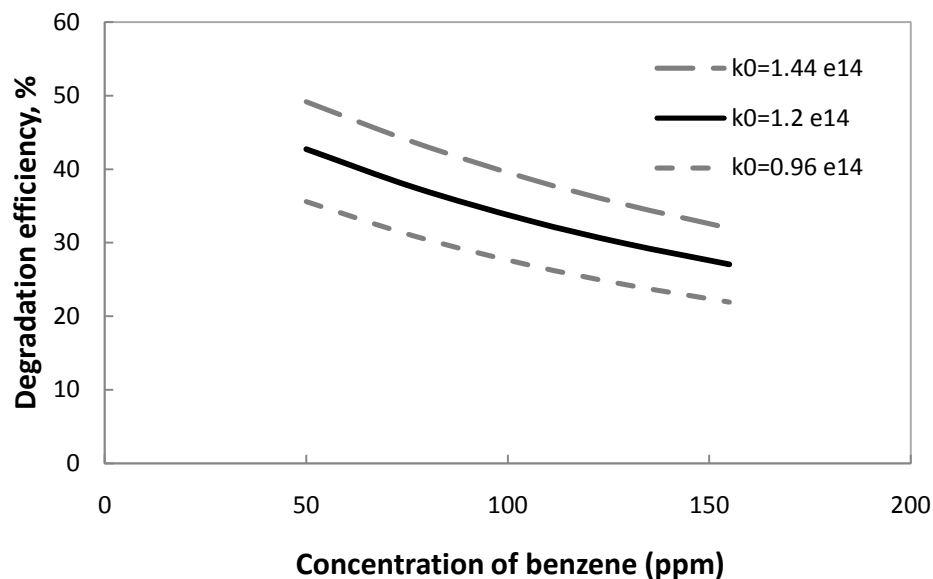


Figure 4.8. Model predictions of photocatalytic degradation of benzene: 400 mL/min volumetric flow rate and different reaction rate constants ($k_0+20\%$, k_0 and $k_0-20\%$). Values of k_0 in legend are in molecules/($\text{cm}^2 \cdot \text{s} \cdot (\text{W}/\text{cm}^2)^n$)

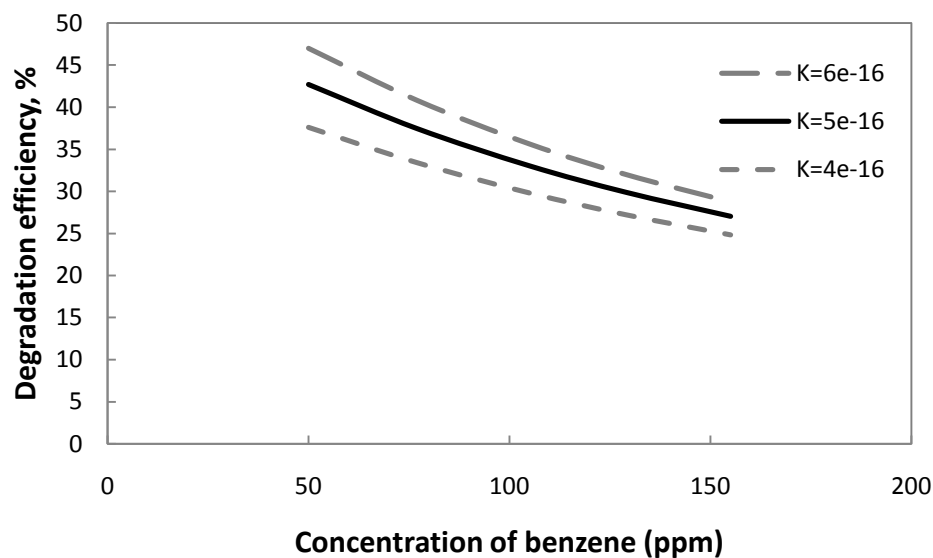


Figure 4.9. Model predictions of photocatalytic degradation of benzene: 400 mL/min volumetric flow rate and different adsorption equilibrium constants ($K+20\%$, K and $K-20\%$). Values of K in legend are in $\text{cm}^3/\text{molecules}$.

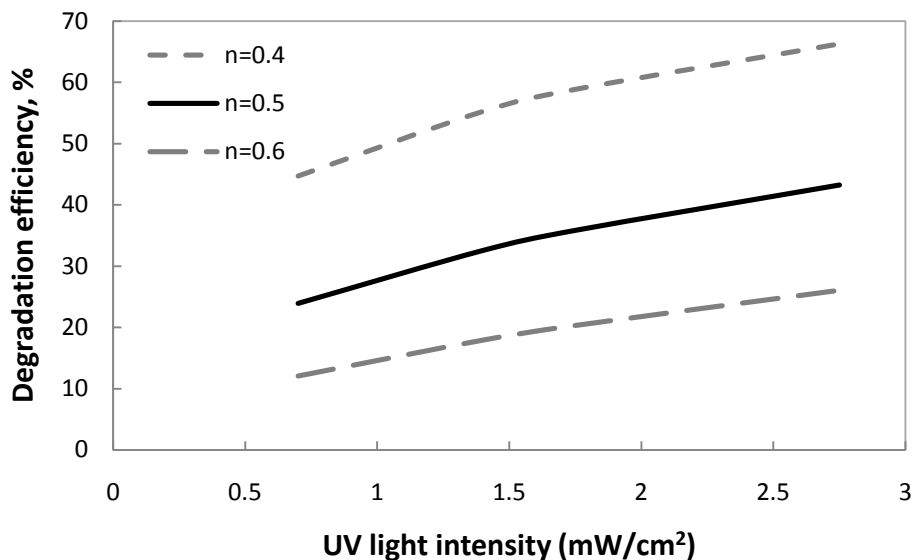


Figure 4.10. Model predictions of photocatalytic degradation of benzene: 400 mL/min volumetric flow rate and different reaction orders ($n+20\%$, n and $n-20\%$)

As expected, k_0 affected all degradation rates similarly, whereas K affected mostly the slope of the curve. K also affects the overall activity to some extent, which could, in principal, be compensated by an increase of k_0 accompanying a decrease of K .

By comparing Figure 4.9 with Figure 4.6, it may be inferred that K might be slightly overestimated, as the optimal K value leads to a concentration dependence that is stronger than the concentration dependence of the experimental data of Wang et al. (2003). The reason why the parameter optimization favored a higher value of K is because a good fit with the data in Figure 4.7 was given preference in the parameter estimation. These data were obtained at 70 ppm benzene, which is below the average of the data in Figure 4.6. Hence, an overestimated concentration dependence lowered the sum of squares of the residuals in parameter estimation. Because of the satisfactory fit between the data and the model, no attempt was made to correct for this deviation.

From Figure 4.10 it is clear that parameter n affects the overall activity very strongly, making it difficult to compare slopes. This is because n is a power exponent of a variable with an order of magnitude of 10^{-3} . For that reason, the kinetic equation (equation (4.25)) was rewritten as follows:

$$r_A = k_0 \left(\frac{I}{I_{av}} \right)^n I_{av}^{0.5} \frac{KC_A}{1 + KC_A} \quad (4.40)$$

Where $I_{av} = 1.75 \times 10^{-3} \text{ W/cm}^2$, the average of the light intensities in Figure 4.7. This equation forces the predictions for different values of n to be the same when $I = I_{av}$. The result is shown in Figure 4.11.

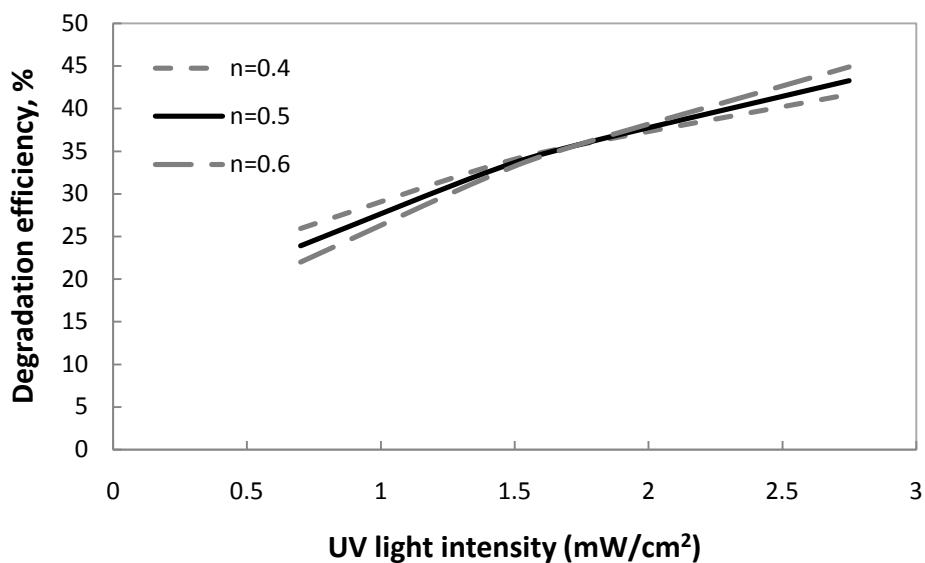


Figure 4.11. Model predictions of photocatalytic degradation of benzene based on equation (4.40): 400 mL/min volumetric flow rate and different reaction orders ($n+20\%$, n and $n-20\%$)

As expected, n affects the slope in Figure 4.11. Comparing the model fits in Figure 4.6 and 4.7 with the parameter sensitivities in Figures 4.8-4.11, it is concluded that all three parameters were estimated to within 20%, at least when equation (4.40) is used.

CHAPTER 5. EXPERIMENTAL RESULTS

5.1. Ultraviolet Degradation of m-Xylene

In previous studies the ultraviolet degradation of benzene and toluene were investigated (De Visscher et al., 2010; 2012). However, glycol dehydration units emit xylene, along with benzene and toluene. For that reason, the ultraviolet degradation of m-xylene was investigated in this study.

Photolysis experiments were carried out with m-xylene at volumetric flow rate 1 L/min. The results are shown in Figure 5.1.

The data shows that m-xylene degradation is nearly complete for concentrations up to 1-1.5 g/m³ at a volumetric flow rate of 1 L/min.

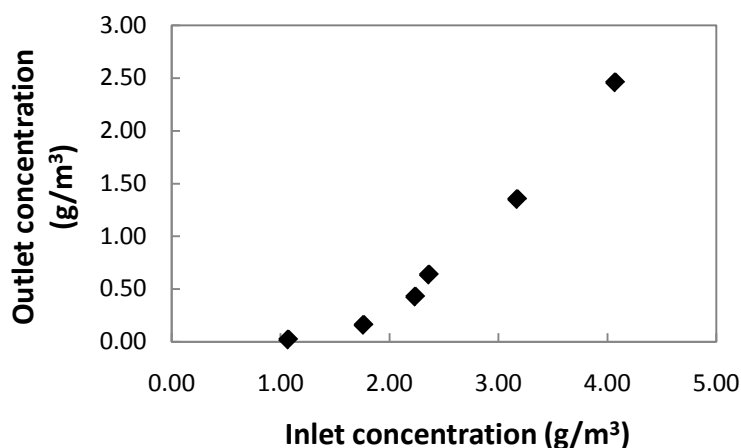


Figure 5.1.m-xylene outlet concentration versus inlet concentration at volumetric flow rate 1 L/min

According to the experimental results conducted for toluene degradation by De Visscher et al. (2010; 2012), it was found that the degradation efficiency of BTX was mainly dependent on the mass flow rate, and relatively independent of the volumetric flow rate. In other words, the degradation rate was relatively insensitive to the concentration as long as the mass flow rate of the pollutant was kept constant. Because of this observation, experiments were only carried out at 1 L/min volumetric flow rate in this study. Figure 5.2 depicts the effect of mass flow rate on the degradation efficiencies of m-xylene by the photochemical process. It is observed that high efficiencies (>90%) can be maintained for mass flow rates up to 1.8 mg/min.

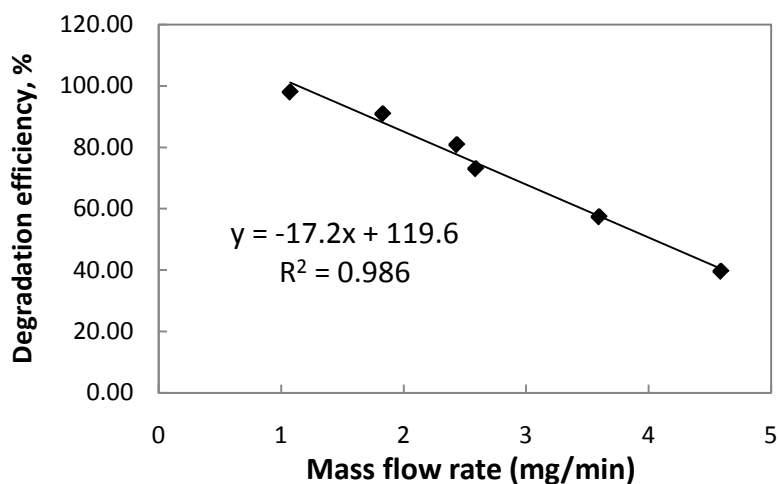


Figure 5.2. The effect of mass flow rate on the degradation efficiency of m-xylene by photochemical process

The overall m-xylene degradation rate is highest at an inlet mass flow rate of about 3 mg/min. At this flow rate about 2 mg/min of m-xylene was degraded. At lower mass flow rates not all the photons emitted by the lamp are absorbed by the pollutant, and a substantial fraction of the photons are re-absorbed by the lamp, leading to a reduced reaction rate. The measured light intensity of the reactor is discussed further down.

On the other hand, at high concentrations there is more opportunity for condensation to occur. In particular, a combination of high concentration and high flow rate should be avoided because the incoming flow of air will cool the lamp, preventing the reaction products from evaporating. Alternatively, a reduced degradation rate may be the result of a reduced quantum yield of the direct photolysis of m-xylene at high concentration. A similar phenomenon was observed for benzene (Shindo and Lipsky, 1966).

Within the range tested, the removal efficiency of m-xylene versus mass flow rate was found to form a linear equation with a coefficient of determination (R^2) of 98.6%, which is acceptable enough.

Experiments were also carried out with toluene as pollutant (De Visscher et al., 2012). The results for toluene are shown in Figure 5.3. The toluene trend is generally the same as for the m-xylene experiments and toluene degradation rate is slightly higher, but very close to the rates observed with m-xylene.

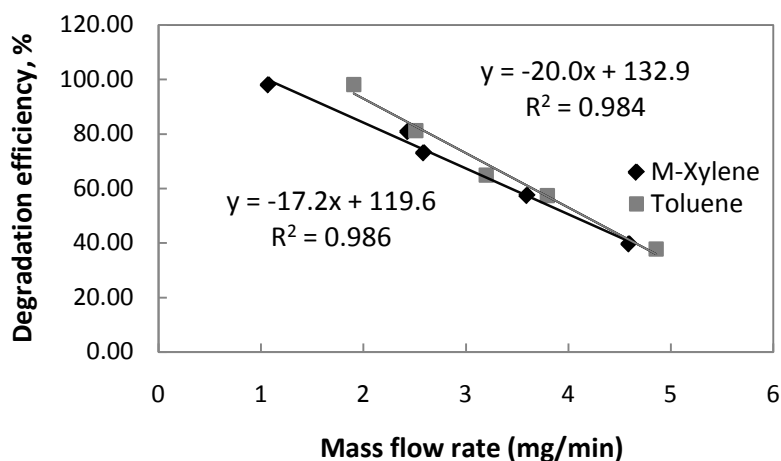


Figure 5.3. Comparison between m-xylene (current study) and toluene (De Visscher et al., 2010) on degradation efficiency versus mass flow rate

It was found that a 40 W ultraviolet reactor emitting light at 185 nm and 254 nm is capable of treating 2 mg/min of toluene or m-xylene with an efficiency > 80%. A volumetric flow rate of 1 L/min was found to be optimal in these experiments, so the pollutant concentration was 1-1.5 g/m³ in the case of m-xylene and toluene.

The experimental reactor has a built-in detector that measures the UV irradiance at the reactor wall. This measurement can be used as a diagnostic for the optimal functioning of the reactor. The steady state irradiance measurements of the m-xylene degradation experiments are shown in Figure 5.4.

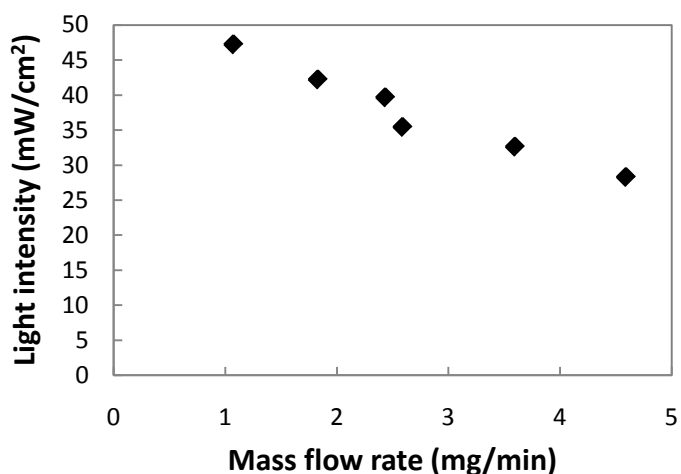


Figure 5.4. Irradiance at the reactor wall during the m-xylene degradation experiments versus m-xylene mass flow rate, at 1L/min volumetric flow rate

From Figure 5.4 it can be seen that the UV irradiance decreases with increasing mass flow rate, and with decreasing volumetric flow rate. This means that the m-xylene concentration is the main driver of the light intensity in the reactor. This is not surprising, as the light intensity is determined by the amount of light absorption occurring in the reactor. In the absence of m-xylene (blank run), an irradiance of about 48 mW/cm² was observed. The fairly high irradiance

values measured indicate that a fairly large portion of the photons remain unutilized. This indicates that there must be room for optimizing the process, by increasing the diameter of the reactor.

Figure 5.5 shows the comparison of the irradiance measurements for the m-xylene and toluene experiments. The result is very similar as for m-xylene, and the conclusions are also the same.

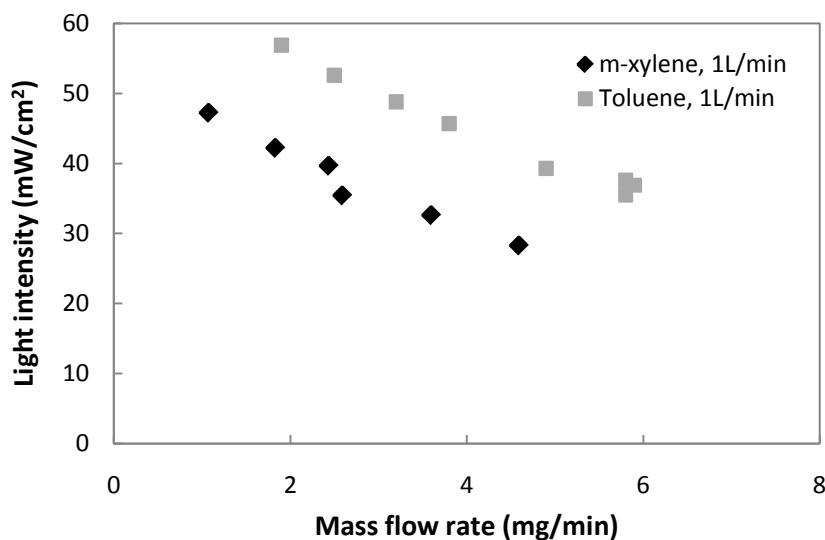


Figure 5.5. Comparison between m-xylene (current work) and toluene (De Visscher et al., 2010) on irradiance at the reactor wall versus mass flow rate; 1L/min volumetric flow rate

To put the irradiance values in perspective, it is useful to calculate the expected irradiance generated by the lamp in the absence of absorption or reflection. To that effect the electrical power is multiplied by the lamp efficiency (8 % at 185 nm, 30 % at 254 nm, totalling 38 %), leading to a value of $15.2 \text{ W} = 15,200 \text{ mW}$ of light energy. This light is divided over a cylinder mantle area of $2\pi \times 2.1 \text{ cm} \times 56 \text{ cm} = 739 \text{ cm}^2$. Hence, an irradiance of $15,200/739 = 20.6 \text{ mW/cm}^2$ is expected. The actual irradiance in the absence of pollutant, 48 mW/cm^2 , is about two times as large. It follows that multiple reflections on the reactor wall intensify the light field. It

can be assumed that less than half of the light is absorbed in the lamp with every pass. Even in the presence of high m-xylene concentrations, the light irradiance at the reactor wall exceeds the theoretically expected value.

It can be expected that increasing the reactor radius will increase the efficiency. This is because increasing the light path length will increase the light absorption by m-xylene molecules, leaving less light to be absorbed in the lamp itself.

Figure 5.6 shows the effect of run of time on light intensity. The whole experiment takes a long time to reach a steady state. In the beginning, the light intensity has the maximum value during the blank run. When contaminants enter the reactor, light intensity decreases and reaches its minimum. After passing the minimum, it again increases somewhat.

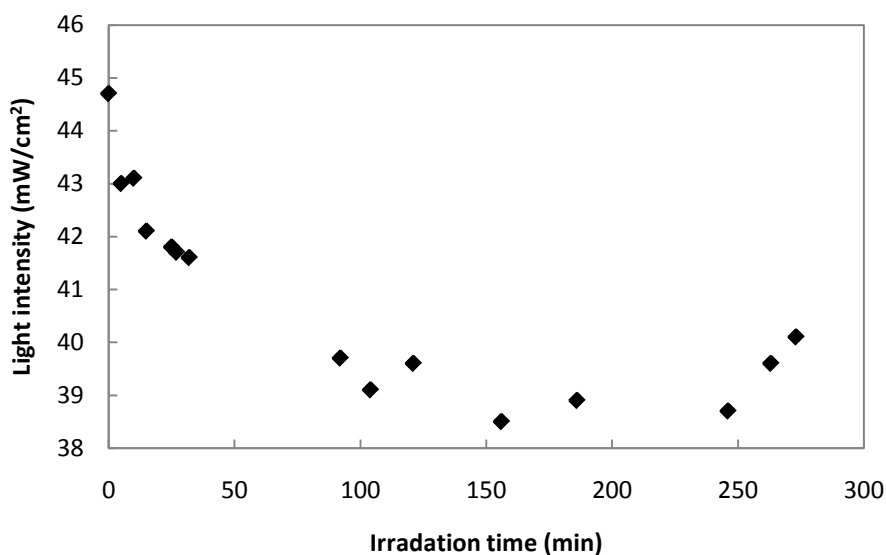


Figure 5.6. Light intensity changes over time

It is hypothesised that the minimum in the light intensity is caused by condensation of reaction products in the reactor. As the lamp heats up, the reaction products evaporate, leading to the steady state light intensity.

5.2. BTEX Degradation by Photolysis and Ozone

Ozone can be produced inexpensively by a corona discharge. The photolysis of ozone is easy and generates highly reactive oxidizing species which can accelerate the degradation of BTEX. Experiments with added ozone were conducted at a flow rate of 2.2 L/min. This higher flow rate was chosen because the observed efficiency was markedly higher in the presence of ozone. Considering the earlier observations of the effect of condensation products, a higher volumetric flow rate was chosen to avoid overly high concentrations. The ozone mass flow rate in these experiments was 17.6 mg/min.

Experimental results of benzene degradation with added ozone are shown in Figure 5.7, and compared with the results in the absence of ozone. Degradation rates 3-4 times as high as in the absence of ozone were observed. Figure 5.7 shows an efficiency of 70 % at a mass flow rate as high as 5 mg/min. The results were negatively affected due to a number of high-concentration preliminary experiments that fouled the reactor walls, and it is anticipated that the results would have been better after cleaning the reactor.

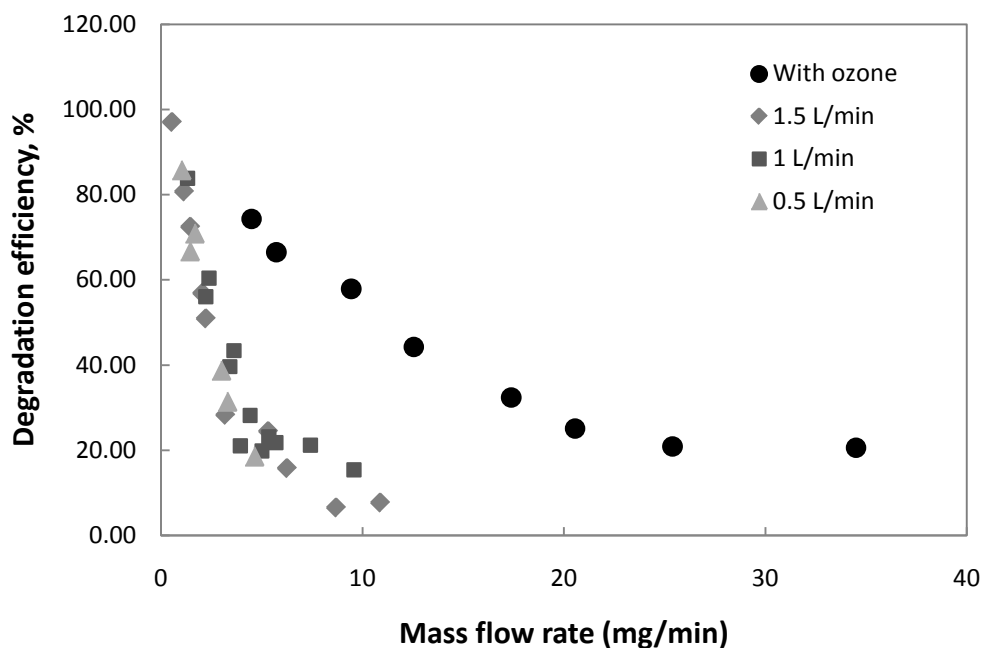


Figure 5.7. Benzene degrading efficiency of the ultraviolet reactor versus benzene mass flow rate at a volumetric flow rate of 2.2 L/min and an ozone mass flow rate of 17.6 mg/min (initial concentration 8 g/m³); comparison with benzene degradation in the absence of ozone

Figure 5.8 compares degradation rates of benzene with and without added ozone. There is no clear optimum in the data as the degradation rates keep increasing with increasing mass flow rate. However, the data point at a mass flow rate of 35 mg/min has a large measurement uncertainty, so it is assumed that it does not point at an increase of the degradation rate. It follows that the highest degradation rates are achieved at relatively low degradation efficiencies.

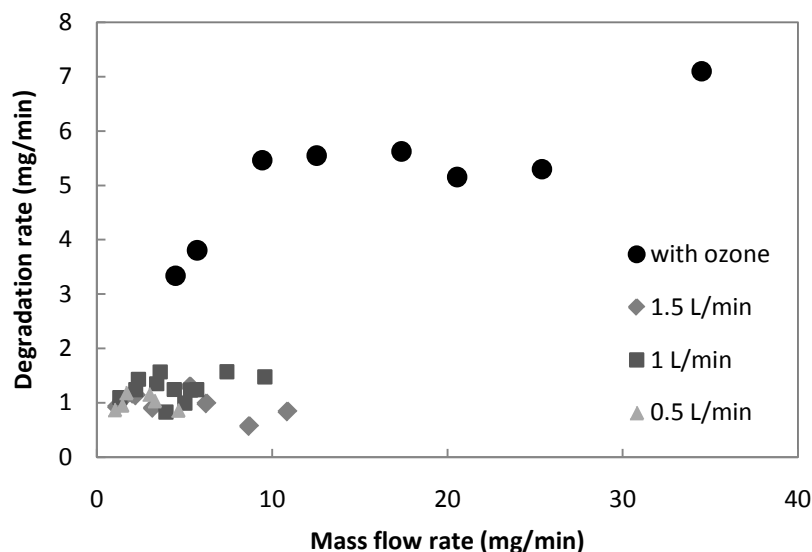


Figure 5.8. Benzene degradation rate in the ultraviolet reactor versus benzene mass flow rate at a volumetric flow rate of 2.2 L/min and an ozone mass flow rate of 17.6 mg/min (initial concentration 8 g/m³); comparison with benzene degradation in the absence of ozone

The light irradiance at the reactor wall was also determined in the experiments in the presence of ozone. The results are shown in Figure 5.9. The light intensities are about a factor 4 lower in these experiments than in the absence of ozone. This is partly due to the effect that the experiments in the presence of ozone were conducted at much higher benzene concentrations and partly due to the strong absorption of ultraviolet light by ozone. Photolysis of ozone, followed by pollutant degradation by the reactive species produced in the ozone degradation, is the main mechanism of pollutant degradation in these experiments.

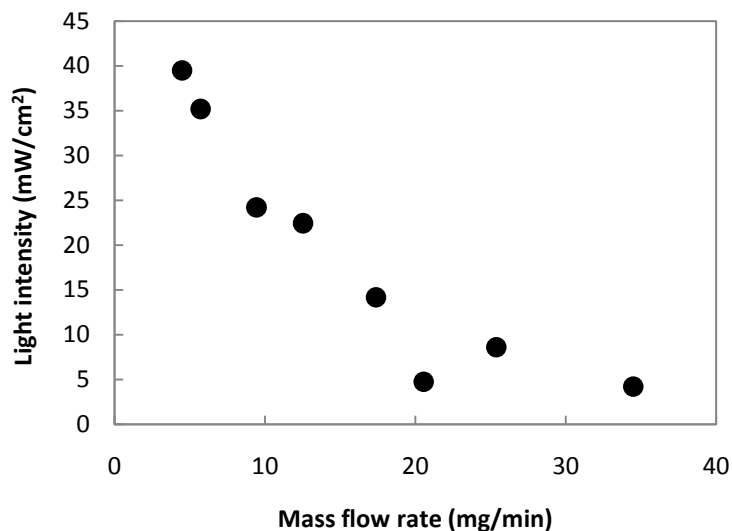
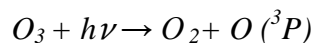
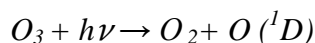


Figure 5.9. Irradiance at the reactor wall during the benzene degradation experiments versus benzene mass flow rate, at a volumetric flow rate of 2.2 L/min, in the presence of ozone (inlet concentration 8 g/m³)

Ozone produces oxygen atoms upon photolysis by ultraviolet light:



O (³P) is the oxygen atom in its most stable state. O (¹D) is the oxygen atom in a more reactive state. At wavelengths below 305 nm, the photolysis of ozone has an O (¹D) quantum yield of 90 %, and an O (³P) quantum yield of 10 % (Atkinson et al., 2004).

The oxygen atoms can react with benzene or toluene directly, but this is probably not the dominant degradation mechanism. The majority of oxygen atoms react with water, forming hydroxyl radicals:



These radicals are the main oxidizing species in organic pollutant degradation.

CHAPTER 6. MODEL PREDICTIONS

6.1. Photolytic versus Photocatalytic Degradation of Benzene in Waste Gas

The simulation model of Mahmoudkhani (2012) for the photolysis of benzene in waste gas was extended to include a photocatalytic reaction on the reactor wall. The kinetic parameters of the photocatalytic reactions were derived from literature experimental data in section 4.5. The model was applied to a cylindrical reactor containing a 40 W amalgam UV lamp in the axis. The model predictions of photodegradation with 254 nm and 185 nm light irradiation (reactor with uncoated walls) was compared with a combination of photolytic and photocatalytic degradation (reactor with walls coated with TiO₂ catalyst).

At air flow rates of 1 L/min and benzene mass flow rates ranging from 0.5 to 10 mg/min, a degradation efficiency of 77%-23% is predicted for the catalytic process. In comparison, the model of Mahmoudkhani (2012) predicted an efficiency of 95%-20% for the noncatalytic process. For photochemical experiments conducted with an initial benzene concentration of 1.2 g/m³, about 80% of benzene was decomposed in the annular photoreactor in the presence of about 80% relative humidity.

The result is shown in Figure 6.1, and compared with non-catalytic model predictions (De Visscher et al., 2010).

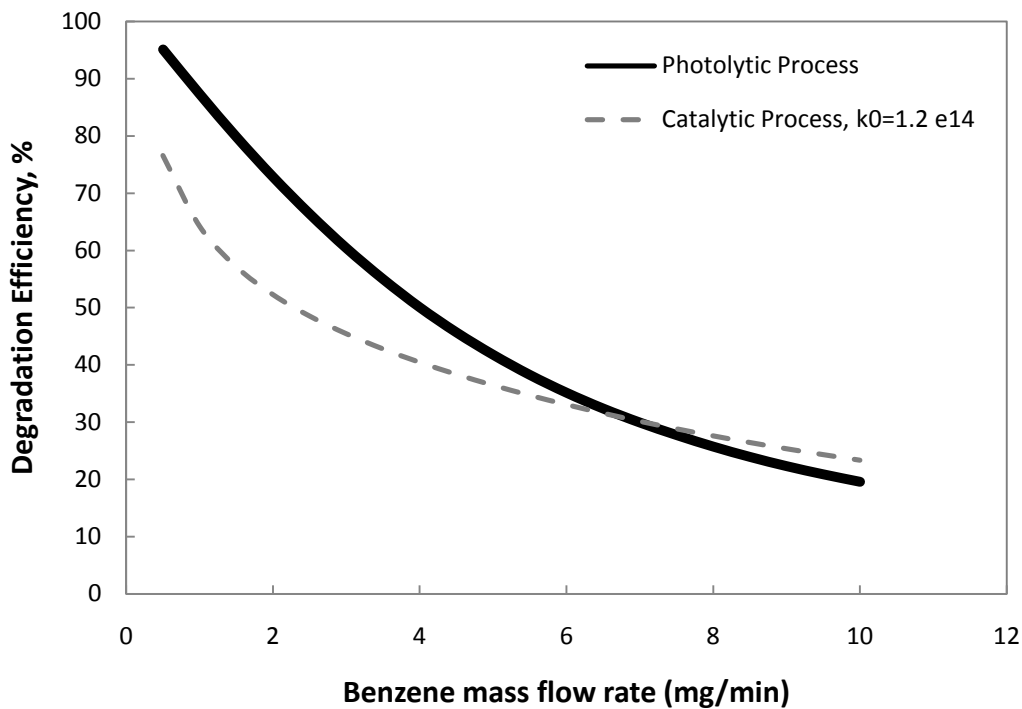


Figure 6.1. Model predictions of photolytic and mixed photolytic-photocatalytic degradation of benzene at 1 L/min volumetric flow rate

The photolytic and mixed photolytic-photocatalytic results are very similar, with neither performing systematically better. However, in conditions where the degradation efficiency is high, the non-catalytic process markedly outperforms the catalytic process. In practical situations a benzene degradation system will be used in conditions where the efficiency is high. Based on these calculations it appears that the catalytic process is a less promising avenue.

The influence of the reaction rate constant (k_0) on the degradation efficiency is demonstrated in Figure 6.2. Calculations were made at the k_0 values of 1.2×10^{14} , 2.5×10^{14} and 4.5×10^{14} molecules/cm².s.(w/cm²)ⁿ.

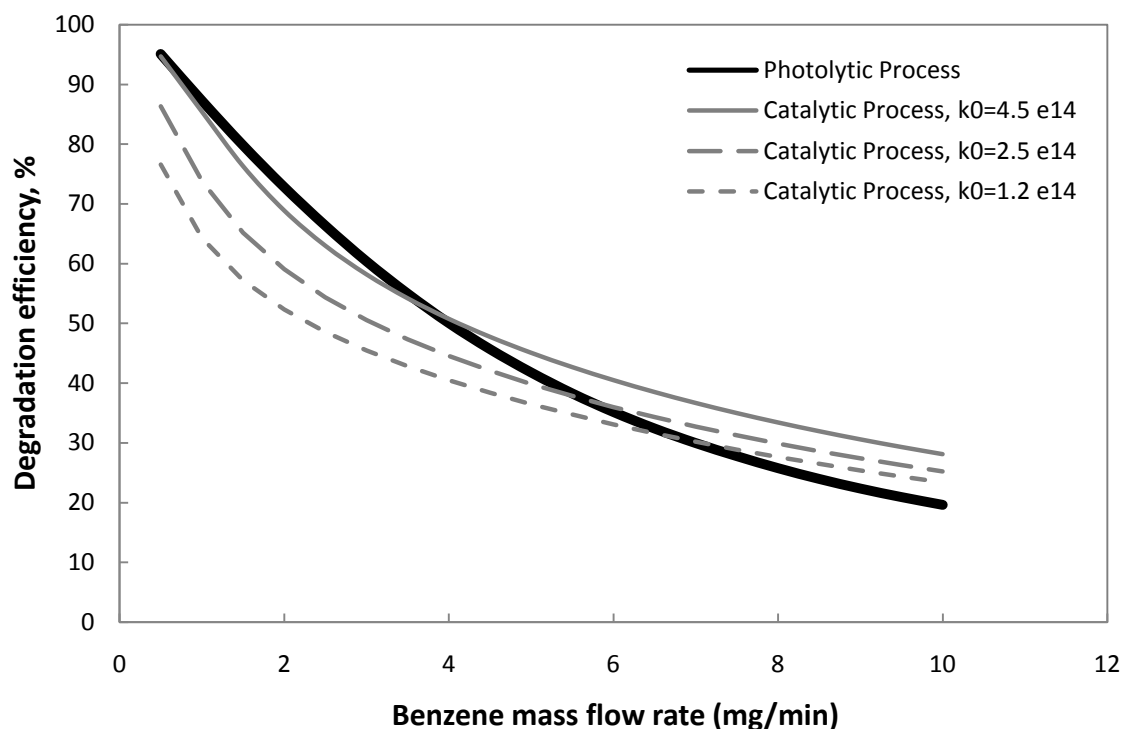


Figure 6.2. Model predictions of photolytic and mixed photolytic-photocatalytic degradation of benzene: 1 L/min volumetric flow rate and different values of k_0 (1.2×10^{14} , 2.5×10^{14} and 4.5×10^{14} molecules/cm².s.(W/cm²)ⁿ)

As is shown in Figure 6.2, the degradation efficiency increases with increasing reaction rate constant. However, even at $k_0 = 4.5 \times 10^{14}$ molecules/cm².s.(W/cm²)ⁿ, the photolytic process is predicted to be superior to the photolytic-photocatalytic process; with the efficiency of the photocatalytic process in the 55%-90% range. An increase of k_0 by a factor 4 is needed to obtain a process that is competitive with direct photolysis in a wide range of conditions.

In Figure 6.3 degradation efficiency of photolytic and photocatalytic processes are compared in terms of changing the reactor diameter. The degradation efficiency increases by increasing the reactor diameter.

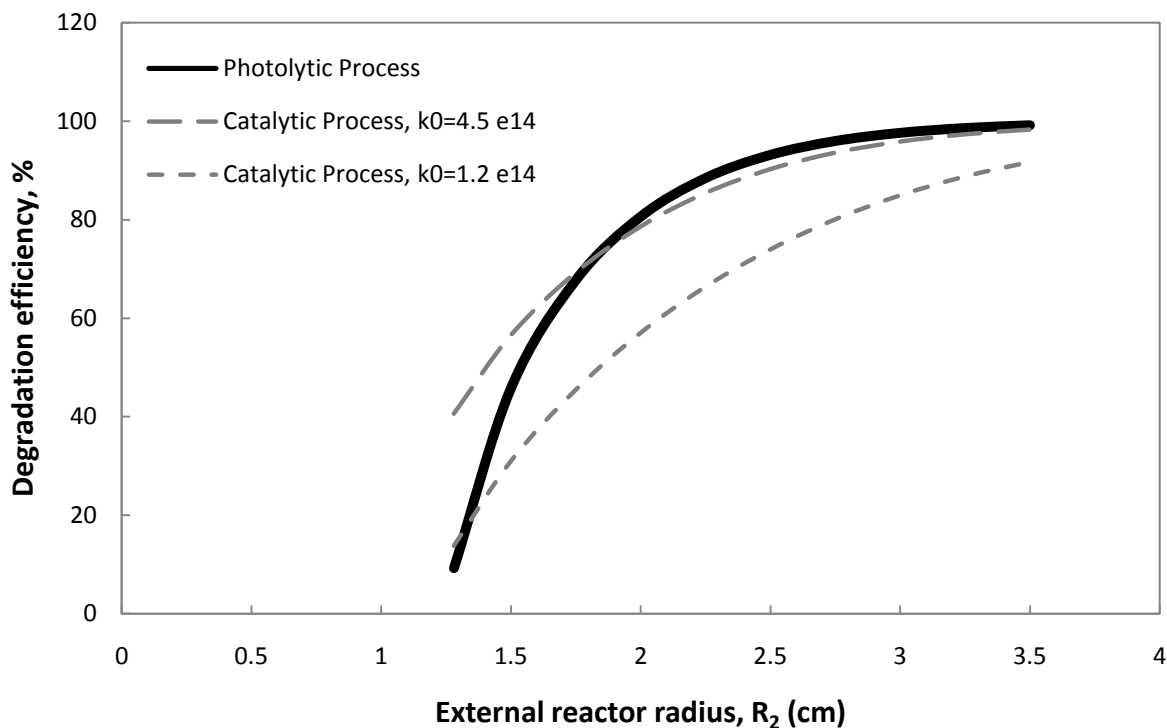


Figure 6.3. Model predictions of photolytic and mixed photolytic-photocatalytic degradation of benzene versus external radius at 1L/min volumetric flow rate and 1.2 g/m^3 benzene initial concentration

Larger diameter means more diffusion limitation, but also more space for the direct (non-catalytic) process. It follows that the catalyst becomes less important as the radius increases. However, increasing the diameter increases the efficiency of both the catalytic and the non-catalytic process. Again, the processes are most efficient in conditions where the non-catalytic process is superior. It is concluded that the catalytic process is not a promising avenue, and it was not pursued further in terms of experimental work.

To understand why the photocatalytic process is not competitive in the investigated conditions, the quantum yield of the photocatalytic process is calculated.

The quantum yield (ϕ) expresses the number of molecules undergoing a reaction relative to the number of photons absorbed by the photocatalyst.

$$\phi = \frac{\text{Number of molecules reacted}}{\text{Number of photons of light absorbed}} = \frac{r_A}{E_{Total}} \quad (6.1)$$

Here, r_A is the photocatalytic reaction rate in molecules/cm².s. It can be calculated as:

$$r_A = \frac{k_0 I^n K C_A}{1 + K C_A} \quad (6.2)$$

where

$$k_0 = 1.2 \times 10^{14} \text{ molecules/cm}^2 \cdot \text{s} \cdot (\text{W/cm}^2)^n$$

I is the irradiance in W/cm², which will be calculated below.

$$n = 0.5$$

$$K = 5 \times 10^{-16} \text{ cm}^3/\text{molecules}$$

C_A is the number concentration of benzene in molecules/cm³

E_{Total} , in photons/s.cm², is the photon irradiance defined as below:

$$E_{Total} = E_{\lambda=185nm} + E_{\lambda=254nm} \quad (6.3)$$

$$E_{\lambda=185nm} = \frac{P_{I,\lambda=185nm} / U_{\lambda=185nm}}{A} \quad (6.4)$$

$$E_{\lambda=254nm} = \frac{P_{I,\lambda=254nm} / U_{\lambda=254nm}}{A} \quad (6.5)$$

$P_{I,\lambda=185nm,254nm}$ and U are described separately as follows:

$P_{I,\lambda=185nm}$, UV light intensity power, is in W. Since the 40W UV lamp emits 8% of its electrical energy consumption as 185 nm light, and 30% as 254 nm light (data provided by the supplier),

$P_{I,\lambda=185nm}$ and $P_{I,\lambda=254nm}$ are:

$$P_{I,\lambda=185nm} = 40 \times 0.08 = 3.2 \text{ W} \quad (6.6)$$

$$P_{I,\lambda=254nm} = 40 \times 0.3 = 12 \text{ W} \quad (6.7)$$

A, the area of the reactor wall, is in cm^2 and defined as:

$$a = 2\pi(R_2.L) = 2\pi(2.1 \times 56) = 738.528 \text{ cm}^2 \quad (6.8)$$

Therefore, the light irradiance (I) at the wall is calculated as:

$$I = \frac{P_{I,\lambda=185nm} + P_{I,\lambda=254nm}}{A} = \frac{3.2 + 12}{738.528} = 0.0206 \text{ W/cm}^2 \quad (6.9)$$

U, energy of a single photon at a specific wavelength, is in J/photon. It is defined as:

$$U = \frac{h.c}{\lambda} \quad (6.10)$$

where,

h is Planck`s constant, $6.626 \times 10^{-34} \text{ J.s} / \text{photon}$

c is the speed of light, $2.998 \times 10^8 \text{ m/s}$

λ is the wavelength, $1.85 \times 10^{-7} \text{ m}$ and $2.54 \times 10^{-7} \text{ m}$

Therefore,

$$U_{\lambda=185nm} = \frac{(6.626 \times 10^{-34}).(2.998 \times 10^8)}{1.85 \times 10^{-7}} = 1.07 \times 10^{-18} \text{ J / photon} \quad (6.11)$$

$$U_{\lambda=254nm} = \frac{(6.626 \times 10^{-34}).(2.998 \times 10^8)}{2.54 \times 10^{-7}} = 7.82 \times 10^{-19} \text{ J / photon} \quad (6.12)$$

Now that all the values are known, E_{Total} is achievable by substituting all the parameters in equations (6.3- 6.5):

$$E_{\lambda=185nm} = \frac{3.2 / 1.07 \times 10^{-18}}{738.528} = 4 \times 10^{15} \text{ photon} / s.cm^2 \quad (6.13)$$

$$E_{\lambda=254nm} = \frac{12 / 7.82 \times 10^{-19}}{738.528} = 2.1 \times 10^{16} \text{ photon} / s.cm^2 \quad (6.14)$$

$$E_{Total} = 4 \times 10^{15} + 2.1 \times 10^{16} = 2.5 \times 10^{16} \text{ photon} / s.cm^2 \quad (6.15)$$

Figure 6.4 presents the influence of different benzene concentrations on the quantum yield values. A maximum quantum yield (ϕ) of 6.67×10^{-4} was predicted for the photocatalytic process, according to Figure 6.4.

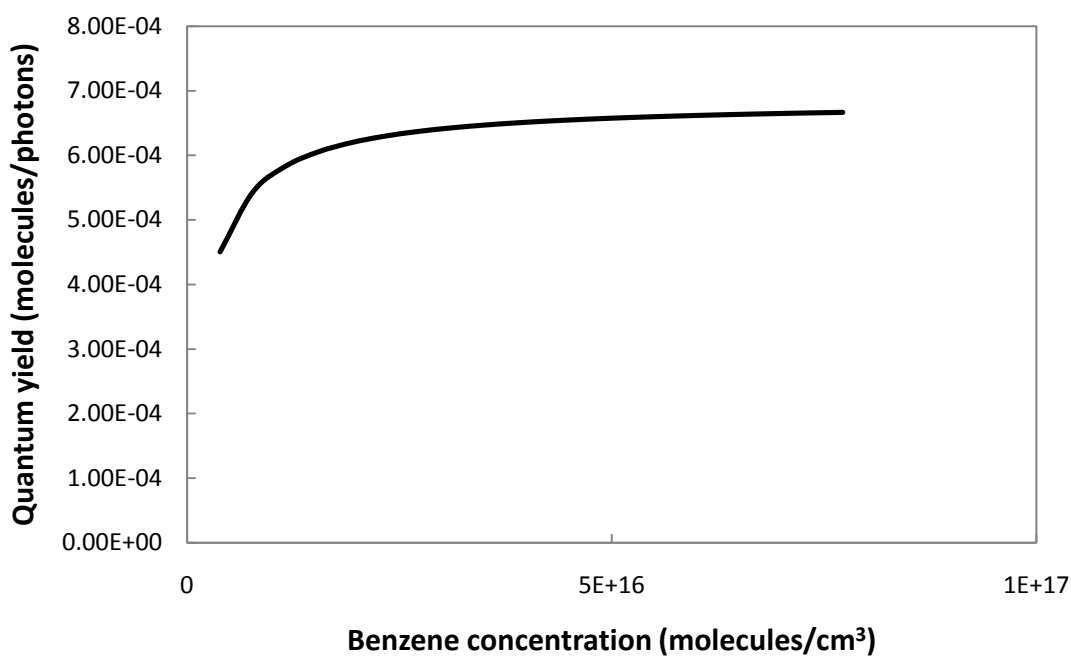


Figure 6.4. Benzene quantum yield profile for photocatalytic process

This low value explains the lack of benefit predicted when a photocatalytic coating is applied. Hence, it is concluded that photolytic approach is a feasible alternative to the photocatalytic approach, especially for low concentrations of benzene emissions from waste gas.

Just as an indication, 1 g/m³ benzene means 7.72×10^{15} molecules/cm³.

Shindo and Lipsky (1966) measured the quantum yield of benzene photolysis in nitrogen gas.

The results are shown in Table 6.1.

Table 6.1. Benzene photolysis quantum yields at 185 nm measured, predicted by Shindo and Lipsky (1966) and new predictions

P_{N_2} (atm)	$P_{C_6H_6}$ (atm)	Φ_{measured}	$\Phi_{\text{predicted}}$ (Shindo&Lipsky, 1966)	$\Phi_{\text{predicted}}$ (current study)
0	0.00132	0.25	0.2495	0.2494
0	0.00263	0.13	0.1430	0.1429
0	0.00395	0.10	0.1000	0.0999
0.1	0.00132	0.22	0.1965	0.2137
0.5	0.00132	0.16	0.1063	0.1358
1	0.00132	0.070	0.0675	0.0933
2	0.00132	0.042	0.0391	0.0574
10	0.00132	0.037	0.0089	0.0141
50	0.00132	0.020	0.0018	0.0029

Shindo and Lipsky(1966) proposed the following model to predict the quantum yield:

$$\phi = \frac{1}{10.8(P(N_2) + 211P(C_6H_6)) + 1} \quad (6.16)$$

where the pressures are expressed in atm.

Because of the large deviations between some of the data and the model fits, the data was re-analyzed with non-linear least squares regression. The result was as follows:

$$\phi = \frac{1}{6.71(P(N_2) + 340P(C_6H_6)) + 1} \quad (6.17)$$

This model was used to make quantum yield predictions for the direct photolytical process. In the calculation, it is assumed that the quantum yield at 254 nm is 0. Furthermore, it is assumed that 8% of the electrical power is emitted as 185 nm light, and 30% as 254 nm light.

Based on the energy of photons at 185 nm and 254 nm, it is calculated that 16.3% of photons are emitted at 185 nm, and 83.7% at 254 nm. This proportion is assumed in the calculation of ϕ . The result is shown in Figure 6.5. The value of ϕ is on the order of 0.01-0.02 when all the light is considered and on the order of 0.06-0.12 where only light at 185 nm is considered.

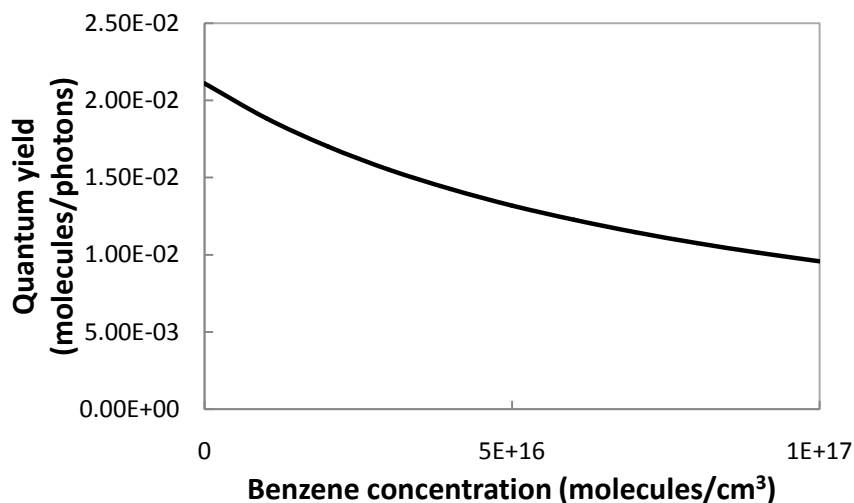


Figure 6.5. Benzene quantum yield profile for photolytic process

It is clear from comparing Figure 6.4 with Figure 6.5 that the quantum yield of the photocatalytic process is 15-60 times lower than the quantum yield of direct photolytic process. This explains why a photolytic process is generally more efficient. Adding a catalyst only improves the efficiency if most of the 185 nm UV light is used in direct photolysis, so only the 254 nm UV light reaches the catalyst. This is the case at high benzene concentration.

6.2. Effect of Adding Ozone on the Photolytic Degradation of Benzene in Waste Gas

The experimental determination of the impact of ozone on benzene degradation by ultraviolet light is discussed in section 5.2. The current section presents the model prediction of benzene photolysis in the presence of ozone.

Figure 6.6 shows the photochemical degradation efficiency of the reactor in the presence and absence of ozone. It also compares the experimental data of the photolytic process with ozone, along with its modelling results. It can be seen that when the photolytic process is accompanied with ozone pre-mixing, the degradation efficiency is much higher than when it is applied without ozone pre-mixing. Therefore, adding ozone greatly improves the efficiency of the process. Modeling of photolytic degradation with ozone confirms the experimental results; however, the model slightly overestimates the efficiency.

The original model was calibrated to be consistent with an actual irradiance in the absence of the pollutant of 55 mW/cm^2 (Mahmoudkhani, 2012). However, in the preparation of the experiments in the presence of ozone, a lower value was observed, 45 mW/cm^2 . Soot generation over time on the reactor surface probably is the main reason. In order to account for the difference between

the previous light intensity and the current one, the model of Mahmoudkhani (2012) was adjusted by incorporating a reflectivity of the reactor wall in the model.

The intensity of a light ray during the passage from the lamp to the reactor wall, as introduced in section 2.1.1 is given by the following equation based on a photon balance:

$$\frac{dE_p}{dr} = -\frac{E_p}{r} - E_p \sum_i C_i \cdot \sigma_i \quad (6.18)$$

which is calculated separately at 185 nm and 254 nm.

The boundary condition is based on the known properties of the lamp. In the absence of reflections, the boundary condition is as follows, also mentioned in equations (6.3-6.5):

$$\text{Photon Irradiance, } E_\lambda (\text{photon/cm}^2 \cdot \text{s}) = \frac{\text{Radiant Power, } P_{l,\lambda} (\text{W})}{\text{Area, } A (\text{cm}^2) \times \text{Photon Energy, } U_\lambda (\text{J/photon})} \quad (6.19)$$

The light intensity of the light ray back from the wall to the lamp is given by the following boundary condition:

$$E_{\text{out}} = R_{\text{wall}} \cdot E_{\text{in}} \quad (6.20)$$

Here, R_{wall} is the reflectivity on the reactor wall. The value of R_{wall} was determined by trial and error: the model was run in the absence of benzene or ozone, for different values of R_{wall} , and predictions of the light irradiance at the reactor wall at the center of the reactor (i.e., at 28 cm from the inlet and exit) were made. An irradiance of 45 mW/cm² was obtained for $R_{\text{wall}}=0.950$.

The predictions in Figure 6.6 were made with this corrected model.

Although experiments for photolysis alone could be conducted with very low mass flow rates with high efficiency (>80%), this result was not achievable for photolysis with ozone experiments because of some experimental limitations of the set-up devices. Achieving higher efficiencies requires lower mass flow rates. The flow of air to the water and contaminant wash-

bottles is controlled by rotameters. It was observed that a portion of ozone plus water enters back to the contaminant rotameter when the mass flow rate is less than 5 mg/min. This is considered as an example of experimental limitation.

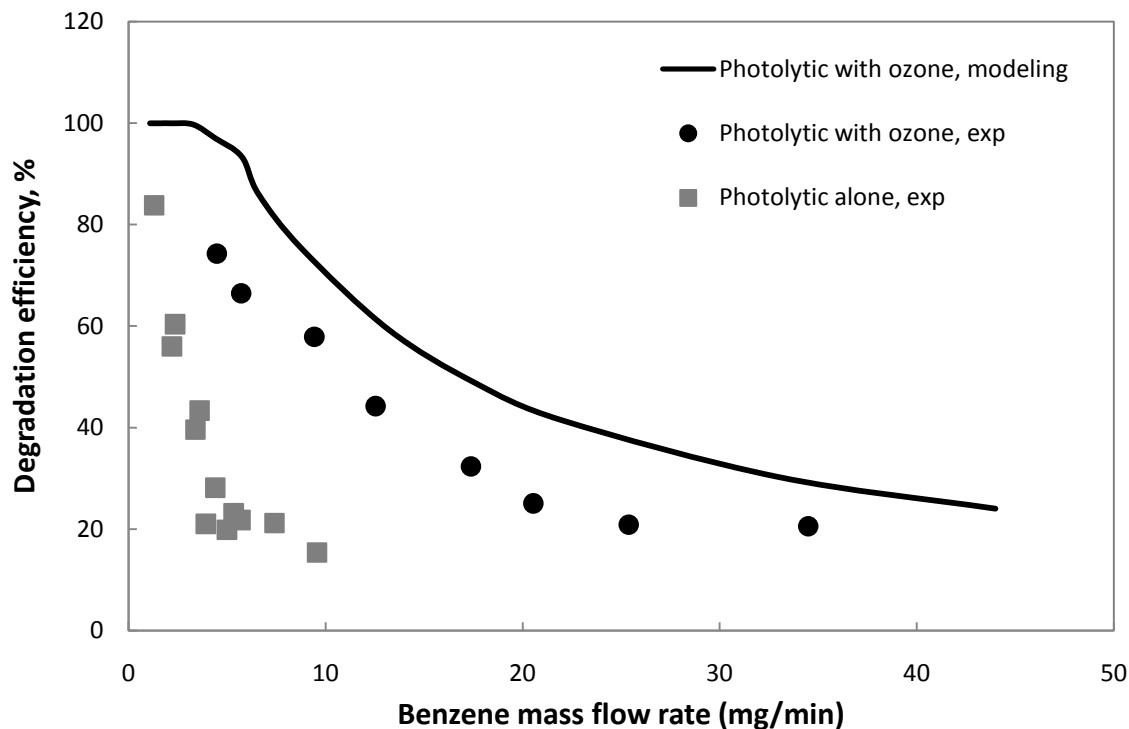


Figure 6.6. Comparison between processes including modeling of photolytic degradation with ozone (Mahmoudkhani, 2012), experiments of photolytic degradation with ozone (current study) and experiments of photolytic degradation alone (De Visscher et al., 2010) for benzene in waste gas

Figure 6.7 provides model predictions of the influence of external reactor radius changes on the degradation efficiency of benzene in the photolytic technique in the presence of ozone. The degradation efficiency is predicted to increase with increasing reactor diameter and reaches a constant value around 3 cm (gap width 1.75 cm). Larger radii do not lead to higher degradation

efficiencies because the absorption of ultraviolet light is nearly complete in 3.5 cm (i.e., across the gap and back). This will be demonstrated with a calculation below.

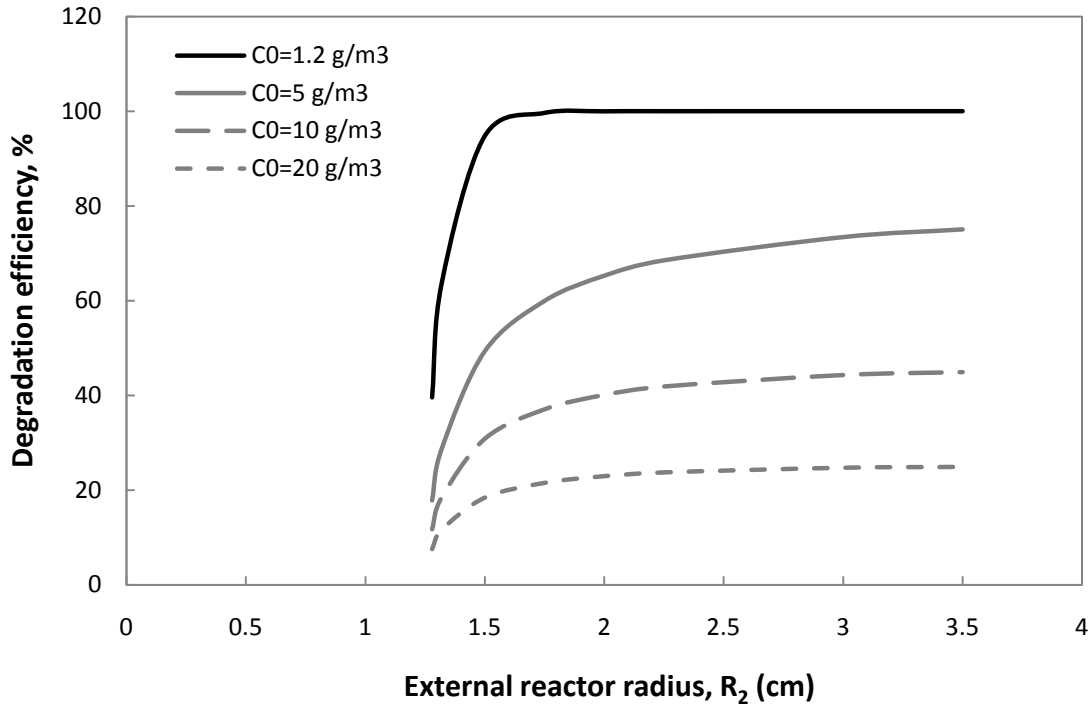


Figure 6.7. Model predictions of photolytic with ozone degradation of benzene versus external radius at 2.2 L/min volumetric flow rate and 8 g/m³ ozone initial concentration, at four different benzene initial concentrations

The purpose of this calculation is to determine the fraction of ultraviolet light absorbed by 8 g/m³ ozone over a distance of 3.5 cm.

Based on the Beer-Lambert's law of light absorption, equation (2.2), the absorbance of a system, $A(\lambda)$, is proportional to the path length, l :

$$A(\lambda) = \log\left(\frac{P_{\lambda}^0}{P_{\lambda}}\right) = \sigma(\lambda)Cl \quad (6.21)$$

With C , number concentration, in molecules/cm³. The variable, $\sigma(\lambda)$, is termed the absorption cross-section and must have units of cm²/molecules or simply cm². It is defined as a measure of the ability of a molecule to absorb photons and depends on the wavelength very strongly (De Visscher, 2013).

The absorption cross-section of ozone at 185 nm is $66.1 \times 10^{-20} \text{ cm}^2$ and at 254 nm is $1148 \times 10^{-20} \text{ cm}^2$. The calculation of the number concentration of ozone at 8 g/m^3 is as below:

$$8 \frac{\text{g}}{\text{m}^3} \times 1 \frac{\text{mol}}{48 \text{g}} \times 6.022 \times 10^{23} \frac{\text{molecules}}{1 \text{mol}} \times 1 \frac{\text{m}^3}{10^6 \text{cm}^3} = 1.004 \times 10^{17} \frac{\text{molecules}}{\text{cm}^3} \quad (6.22)$$

Therefore, the absorbances of ultraviolet light at two different wavelengths are derived as:

$$A(\lambda = 185 \text{ nm}) = 66.1 \times 10^{-20} \times 1.004 \times 10^{17} \times 3.5 = 0.2 \quad (6.23)$$

$$A(\lambda = 254 \text{ nm}) = 1148 \times 10^{-20} \times 1.004 \times 10^{17} \times 3.5 = 4 \quad (6.24)$$

Based on equation (6.21),

$$\exp(-\sigma_{185 \text{ nm}} \cdot Cl) = \frac{P}{P^0} = 0.793 \quad (6.25)$$

$$\exp(-\sigma_{254 \text{ nm}} \cdot Cl) = \frac{P}{P^0} = 0.0174 \quad (6.26)$$

Where P is the radiant power returning to the lamp and P^0 is the radiant power going out from the lamp; the lower the ratio, the more consumption during reaction. Comparing the ozone absorptivity in 185 nm and 254 nm proves that most of the ultraviolet light is absorbed by ozone at 254 nm.

Clearly, at 254 nm, nearly all the ultraviolet light is absorbed before returning to the lamp, and increasing the reactor diameter will not increase the absorption. The absorption at 185 nm is not

complete, but at this wavelength benzene is a much stronger absorber than ozone ($\sigma_{\text{benzene}, \lambda=185 \text{ nm}} = 1.24 \times 10^{-17} \text{ cm}^2$).

When a low benzene initial concentration is fed, the maximum degradation efficiency is higher. As an illustration, the highest degradation efficiency for 1.2 g/m^3 is near 100% while it is 25% for 20 g/m^3 as a benzene initial concentration.

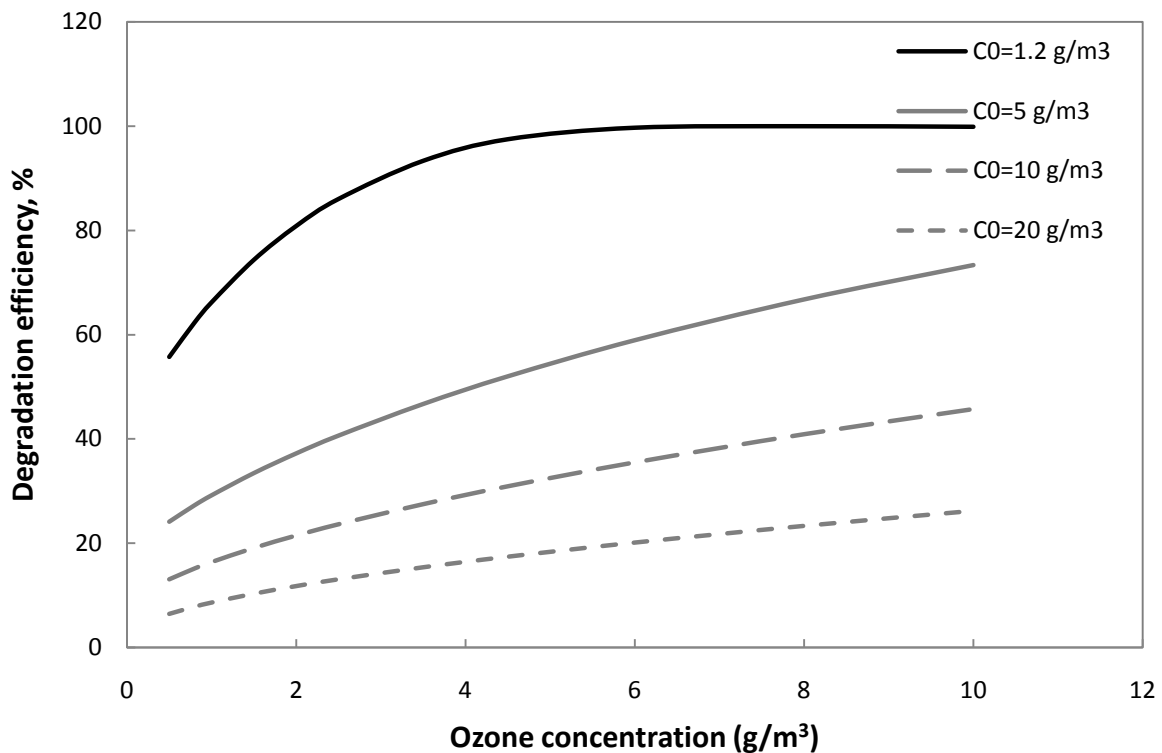
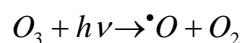


Figure 6.8. Model predictions of photolytic with ozone degradation of benzene versus ozone initial concentration: 2.2 L/min volumetric flow rate and four different benzene initial concentrations

Figure 6.8 indicates that increasing the ozone initial concentration leads to more decomposition of waste gas. This is because the production of radicals such as $\cdot\text{OH}$ and $\cdot\text{O}$ increases with ozone concentration, so the chance of the photolytic reaction increases.

The main reaction is:



The quantum yields of this photodegradation reaction for 185 nm and 254 nm are (Sander et al., 2006):

$$\phi(O(^1D)) = 0.9$$

$$\phi(O(^3P)) = 0.1$$

The oxygen atoms produced in the decomposition of ozone react with water, with a reaction rate constant of 2.2×10^{-10} (Atkinson et al., 1997):



As can be seen in Figure 6.9, an increase in volumetric flow rate causes a decrease in degradation efficiency.

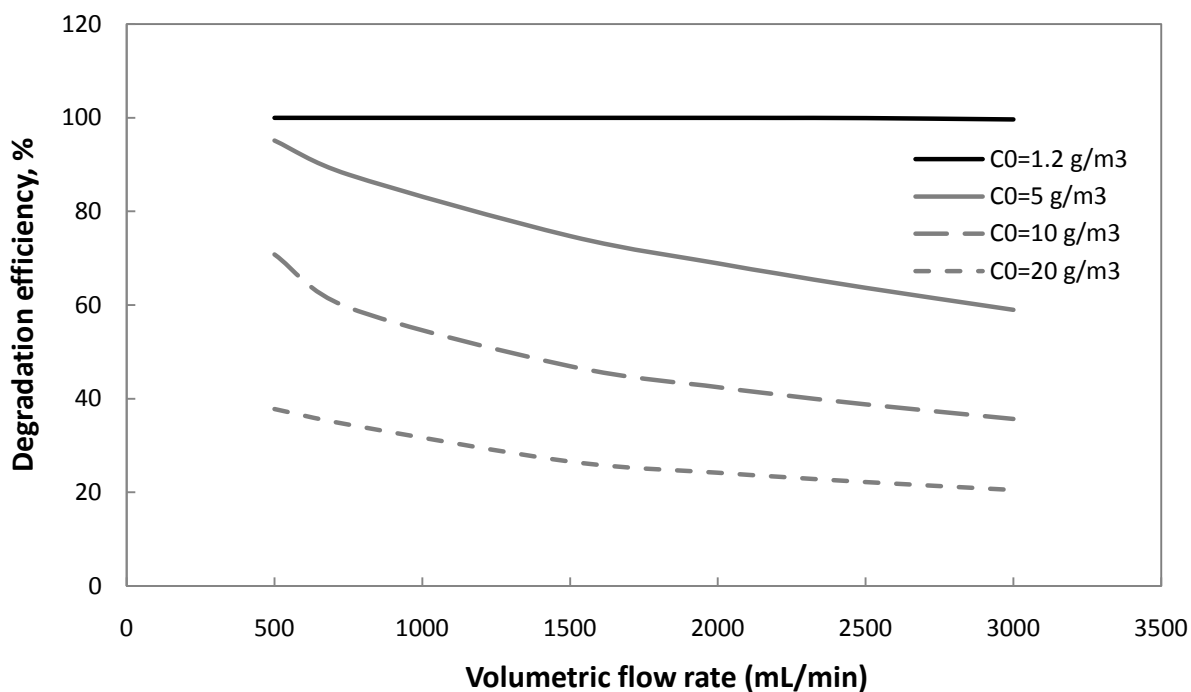


Figure 6.9. Model predictions of photolytic with ozone degradation of benzene versus volumetric flow rate: 8 g/m^3 ozone initial concentration and four different benzene initial concentrations

The dominant reaction mechanism of photolytic benzene degradation in the absence of ozone is direct photolysis mediated by 185 nm ultraviolet. Ozone adds the generation of $O(^1D)$ as a second mechanism, followed by OH generation in a reaction with water vapour, and benzene degradation by the generated OH radicals. The latter mechanism is mainly initiated by 254 nm ultraviolet light, due to the large absorption cross section of ozone at this wavelength. It follows that the optimal proportion of 185 nm and 254 nm light intensities may be very different for the processes in the absence and in the presence of ozone. For that reason, simulations were run at constant overall lamp efficiency, but at varying proportions of 185 nm and 254 nm light intensities.

The results are shown in Figure 6.10 in the presence of ozone and in Figure 6.11 in the absence of ozone. The base case is a lamp efficiency of 8 % at 185 nm and 30 % at 254 nm. A first alternative calculated is a lamp efficiency of 15 % at 185 nm and 23 % at 254 nm. A second alternative is a lamp efficiency of 2 % at 185 nm and 36 % at 254 nm.

Comparing Figure 6.10 with Figure 6.11 shows that wavelength has stronger effect on photolytic degradation in the absence of ozone. In the presence of ozone, the increasing proportion of 185 nm ultraviolet light is predicted to have a slight beneficial effect on the benzene degradation. This is because two parallel mechanisms lead to benzene degradation: one mediated by 185 nm ultraviolet light and one mediated predominantly by 254 nm ultraviolet light. In this case, maximizing the overall lamp efficiency is the main optimization strategy.

In the absence of ozone, an increase of the proportion of ultraviolet light emitted at 185 nm causes a pronounced increase of the benzene degradation efficiency. In this case, maximizing the conversion of electric power to 185 nm light is a better strategy than maximizing the overall lamp efficiency.

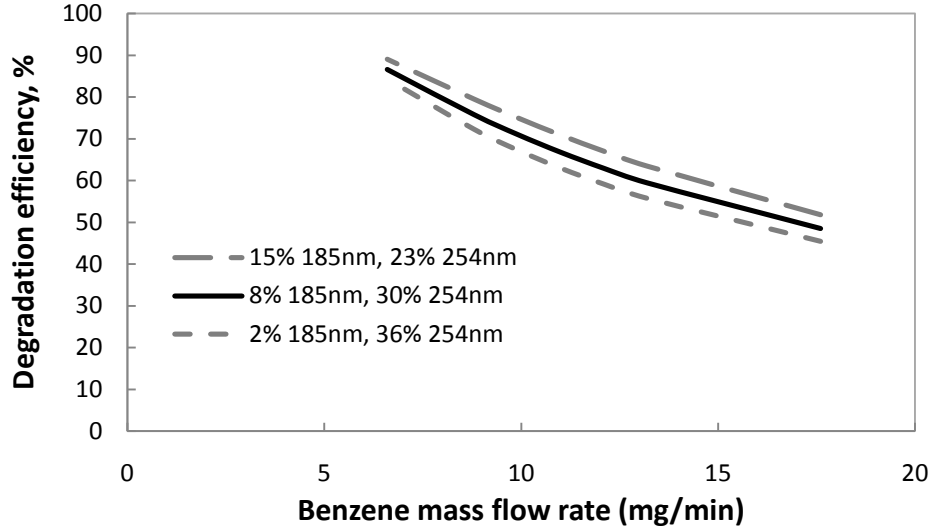


Figure 6.10. Model predictions of photolytic with ozone degradation of benzene versus mass flow rate: 8 g/m³ ozone initial concentration and 2.2 L/min volumetric flow rate at three different lamp efficiencies (15% 185 nm & 23% 254 nm, 8% 185 nm & 30% 254 nm and 2% 185 nm & 36% 254 nm)

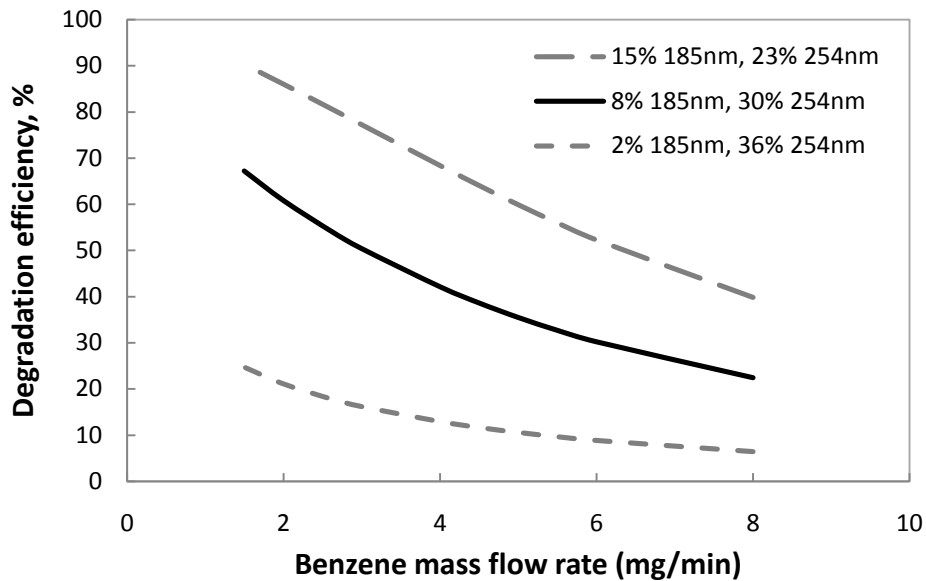


Figure 6.11. Model predictions of photolytic without ozone degradation of benzene versus mass flow rate: 1 L/min volumetric flow rate at three different lamp efficiencies (15% 185 nm & 23% 254 nm, 8% 185 nm & 30% 254 nm and 2% 185 nm & 36% 254 nm)

CHAPTER 7. PROCESS DESIGN AND FEASIBILITY STUDY

In order to evaluate the process cost in photolysis technology, energy cost is considered one of the dominant factors. Therefore, it is a proper parameter in the feasibility studies. The energy requirement of a system treating 3 tonnes per year of BTX, containing 1 tonne of benzene, 1 tonne of toluene and 1 tonne of xylene, was calculated. It is assumed that the photolytical degradation efficiency is the same for all BTX, which is a conservative estimate, because both toluene and xylene are degraded more efficiently by ultraviolet light than benzene.

7.1. Condensation Pre-treatment

Condensation is considered as a promising pre-treatment for photochemical degradation of BTEX. A simple model for condensation from a vapour mixture containing benzene, toluene, m-xylene, water and air was developed in VMG-Sim (Virtual Materials Group, Calgary). This condensation model is based on the Peng-Robinson equation of state and liquid-liquid-vapour phase equilibrium at 30 °C.

The feed is assumed to be from a typical glycol dehydrator of a natural gas plant, containing of water vapour, BTX and non-condensable. For instance, if, in addition to the above BTX flow rates, a flow rate of 10 mol/hr water vapour and 5 mol/hr methane is assumed, the benzene condensation efficiency is predicted to be 69.4 %. Details of the condensation predictions are given in Table 7.1.

After condensation, air would be mixed into the gas mixture to add oxygen and optimize the BTX concentration.

When targeting an overall benzene emission reduction efficiency of 90 %, we find that 0.462 tonne of BTEX remaining after condensation must be treated with 67.3 % efficiency.

Summary of calculations is as follows:

Table 7.1. Condensation results

	Condensation Efficiency	BTEX treated (ton/year)	BTEX removed (ton/year)	Not removed (ton/year)
Benzene	0.694	1	0.694	0.306
Toluene	0.883	1	0.883	0.117
Xylene	0.961	1	0.961	0.039
Total		3	2.538	0.462

$$\text{Total amount of benzene removed with 90 \% efficiency} = 1 \times 0.9 = 0.9 \frac{\text{ton}}{\text{year}}$$

$$\text{Total amount of benzene not removed} = 1 - 0.9 = 0.1 \frac{\text{ton}}{\text{year}}$$

$$\text{Benzene must be removed by photolysis} = 0.306 - 0.1 = 0.206 \frac{\text{ton}}{\text{year}}$$

$$\text{Photolysis efficiency required} = \frac{0.206}{0.306} = 0.673$$

Total amount of BTEX treated: 0.462 ton/year or 462 kg/year.

According to Figure 6.6 for the photolysis with ozone experimental data, the appropriate equation passing through those points is $y=0.0843^2-5.0713x+95.02$, where y is representative of degradation efficiency (in %) and x is benzene mass flow rate (in mg/min). Hence, BTEX mass

flow rate treated with 67.3 % efficiency per 40 W lamp is $6.08 \frac{mg}{min}$ or:

$$6.08 \frac{mg}{min} \cdot \frac{60 min}{1hr} \cdot \frac{24hr}{1day} \cdot \frac{365day}{1year} \cdot \frac{1kg}{10^6 mg} = 3.20 \frac{kg}{year}$$

$$\text{Number of the lamps required} = \frac{\text{Total BTEX treated}}{\text{BTEX mass flow rate per lamp}} = \frac{462}{3.20} = 145$$

This amounts to an annual energy consumption of:

$$145 \text{ lamps} \times \frac{40W}{1 \text{ lamp}} = 5800W = 5.8kW \times \frac{365day}{1year} \times \frac{24hr}{1day} = 50808 kWh$$

Or an annual electricity cost of \$5080 assuming \$0.1 per kWh.

Based on experimental data, ozone concentration at volumetric flow rate, 2200 mL/min was 8 g/m³. So, ozone mass flow rate is:

$$(8g / m^3) \times (2.2m^3 / min) \times (10^{-3} mg / g) = 17.6mg / min$$

The amount of ozone needed to be pre-mixed with 462 kg of benzene is:

$$462kg \text{ benzene} \times \frac{17.6 mg/min \text{ Ozone}}{6.08 mg/min \text{ benzene}} = 1337kg \text{ Ozone}$$

The generation of this amount of ozone requires a 29422 kWh for the ozone generator annually, assuming a 22 kWh electricity requirement for the production of 1 kg ozone. Hence, the ozone electricity cost is \$3000/year. Moreover, the total electricity cost is on the order of \$8000/year for benzene and ozone which is commercial beneficial.

According to Mahmoudkhani's thesis (2012) which is only focussed on photolysis process without ozone, BTEX mass flow rate treated with 67.3 % efficiency per 40 W lamp is 1.667

$$\text{mg/min or } 1.667 \frac{\text{mg}}{\text{min}} \cdot \frac{60 \text{ min}}{1 \text{ hr}} \cdot \frac{24 \text{ hr}}{1 \text{ day}} \cdot \frac{365 \text{ day}}{1 \text{ year}} \cdot \frac{1 \text{ kg}}{10^6 \text{ mg}} = 0.876 \frac{\text{kg}}{\text{year}}$$

$$\text{Number of the lamps required} = \frac{\text{Total BTEX treated}}{\text{BTEX mass flow rate per lamp}} = \frac{462}{0.876} = 528$$

This amounts to an annual energy consumption of:

$$528 \text{ lamps} \times \frac{40 \text{ W}}{1 \text{ lamp}} = 21120 \text{ W} = 21.1 \text{ kW} \times \frac{365 \text{ day}}{1 \text{ year}} \times \frac{24 \text{ hr}}{1 \text{ day}} = 185011 \text{ kWh}$$

Or an annual electricity cost of \$18500 assuming \$0.1 per kWh. Comparing photolysis cost with ozone pre-mixing cost concludes that ozone pre-mixing technique saves energy by more than 55 % relative to the photolysis process in the absence of ozone.

This estimate is conservative in two ways. First, the benzene degradation efficiency was assumed to apply to toluene and xylene as well, even though higher efficiencies were found experimentally for those compounds in comparison with benzene. Second, no attempt was made to incorporate process optimizations in the cost estimate. Simulations indicate that further improvements of the efficiency are possible by increasing the reactor diameter and pre-mixing more ozone. Given the fact that the ratio of the light intensities at 185 and 254 nm is not critical, it may be possible to use a more efficient light source.

As discussed, in order to increase the efficiency of the photochemical process, ozone is pre-mixed with the gas stream. This is effective in wastewater treatment, but has never applied as a treatment technique in waste gas.

CHAPTER 8. CONCLUSIONS

Experiments have shown that it is possible to degrade benzene, toluene and xylenes in a waste gas stream with 185 nm + 254 nm ultraviolet light. When m-xylene is the pollutant, up to 2 mg/min can be treated with 90% efficiency in a 40 W reactor. When ozone is added to the waste gas stream, the efficiency of the process is approximately tripled with benzene as the contaminant, in spite of the fact that the results were obtained in a reactor with sub-optimal efficiency due to fouling.

Computer simulations of the process were made, and the model predictions were in general agreement with the experimental results, although a slight overestimation of the results was observed.

Based on the simulation model, a number of alternatives were explored. First, an alternative configuration involving photolysis and photocatalysis of benzene was considered. A simulation model was developed that successfully describes ultraviolet degradation of benzene from waste gas accompanied by catalyst, TiO_2 , on the reactor wall. But it was found that the efficiency of this alternative did not exceed the efficiency of the original process (Mahmoudkhani, 2012). One reason for the lack of improvement is the increase of mass transfer limitations, as the reaction is more localized. A second reason is the low quantum yield of the catalytic process. Especially in the region of high efficiency, the photocatalytical option showed inferior results in comparison with the photochemical option.

A second alternative that was explored first with experiments and then confirmed by a computer simulation is the application of ozone pre-mixing technology. It was concluded that this process is highly efficient and leads to increased generation of radicals such as $\cdot\text{OH}$ and $\cdot\text{O}$.

Calculations based on the experimental data indicate that the electrical cost for treating 3 tonnes per year of BTX, containing 1 tonne of benzene, 1 tonne of toluene and 1 of tonne xylene in a photolysis process with added ozone that removes 90% of pollutants is about \$8000 per year if condensation is used as a pretreatment step.

As discussed before, the model tends to overestimate the actual efficiency, so the actual energy requirements may be higher than calculated here. On the other hand, toluene and xylene are degraded more efficiently, which will offset the possible overestimate.

According to the simulation results presented here, the overall consumed energy decreases when a combination of ozone pre-mixing and condensation pre-treatment is employed. Experiments confirm the model predictions. However, pilot scale studies are required to test the practical feasibility of the process.

REFERENCES

Agustina, T. E.; Ang, H. M.; Vareek, V. K., “A Review of synergistic effect of photocatalysis and ozonation on wastewater treatment.”, *J. Photochem. Photobiol.*, **2005**, 6, 264-273.

Atkinson, R.; Arey, “Atmospheric degradation of volatile organic compounds”, *J. Chem. Rev.*, **2004**, 103, 4605-4638.

Atkinson, R., “Atmospheric reactions of alkoxy and β -hydroxyalkoxy radicals.”, *Int. J. Chem. Kinet.*, **1997**, 29, 99-111.

Atkinson, R.; Baulch, D.L.; Cox, R.A.; Hampson, R.F.; Kerr, J.A.; Rossi, M.J.; Troe, J., “Evaluated kinetic, photochemical and heterogeneous data for atmospheric chemistry: Supplement V”, *J. Phys. Chem. Ref. Data*, **1997**, 26, 521-1011.

Braslavsky, S. E., “Glossary of terms used in photochemistry, 3rd edition.”, *Pure Appl. Chem.*, **2007**, 79, 293-465.

Braslavsky, S. E.; Braun, A. M.; Cassano, A. E.; Emeline, A.V.; Litter, M. I.; Palmisano, L.; Parmon, V. N.; Serpone, N., “Glossary of Terms Used in Photocatalysis and Radiation Catalysis”, *Pure Appl. Chem.*, **2011**, 83, 931-1014.

CAPP Website, “Upstream Petroleum Industry Benzene Emissions from Glycol Dehydrator Status 2006”, **2008**, 2008-1032.

Chen, F.; Yang, Q.; Pehkonen, S. O.; Ray, M. B., “Modeling of gas-phase photodegradation

of chloroform and carbon tetrachloride”, *J. Water Res.*, **2002**, 54, 1281-1292.

Cheng, Z.W.; Jiang, Y.F.; Zhang, L.L.; Chen, J.M.; Wei, Y.Y., “Conversion characteristics and kinetic analysis of gaseous alpha-pinene degraded by a VUV light in various reaction media”, *Separa. Purific. Techno.*, **2011** 26-32.

Chou, M. S.; Chang, K. L., “UV/ozone degradation of gaseous hexamethyldisilazane (HMDS)”, *Chemosphere*, **2007**, 69, 697-704.

Cunningham, J.; Hondnett, B., “Kinetic studies of secondary alcohol photo-oxidation on ZnO and TiO₂ at 348 K studied by gas chromatograph analysis”, *J. Chem. Soc.*, **1981**, 77, 2777-2802.

Demeestere, K.; Dewulf, J.; Van Langenhove, H., “Heterogeneous Photocatalysis as an Advanced Oxidation Process for the Abatement of Chlorinated, Monocyclic Aromatic and Sulfurous Volatile Organic Compounds in Air: State of Art”, *Crit. Rev. Environ. Sci. Technol.*, **2007**, 37, 489-538.

De Visscher, A., “Air Dispersion Modeling, Foundations and Applications”, *J. Wiley & Sons*, in preparation, **2013**.

De Visscher, A.; Dewulf, J.; Van Durme, J.; Leys, C.; Morent, R.; Van Langenhove, H., “Non-thermal plasma destruction of allyl alcohol in waste gas: kinetics and modeling”, *Plasma Sources Sci. Eng. 17*, **2008**, 015004 (11pp), doi:10.1088/0963-0252/17/1/015004.

De Visscher, A.; Rezaei, M.; Mahmoudkhani, F.; Langford, C. H.; Vaisman, E., “Photochemical Degradation of BTEX in Waste Gas: Experiments and Modeling”, *AWMA*, **2010-A-594**.

De Visscher, A.; Rezaei, M.; Mahmoudkhani, F.; Atyabi, M.; Asili, V.; Vaisman, E.;

Langford, C., "Photochemical Degradation of BTEX in Waste Gas; Experiments and Modeling" final report, **2012**.

Domeno, C.; Rodriguez-Lafuente, A.; Martos, J. M.; Bilbao, R.; Nerin, C., "VOC removal and deodorization of effluent gases from an industrial plant by photo-oxidation, chemical oxidation, and ozonization.", *J. Environ. Sci. Technol.*, **2010**, 44, 2585-2591.

Fox, M. A.; Dulay, M. T., "Heterogeneous Photocatalysis", *Chem. Rev.*, **1993**, 93, 341-357.

Froment, G. F.; Bischoff, K. B., "Chemical Reactor Analysis and Design" 2nd Ed., *J. Wiley & Sons*, New York, **1993**.

Huang, H.; Li, W., "Destruction of toluene by ozone-enhanced photocatalysis: performance and mechanism", *Appl. Catal. B: Environ.*, **2011**, 102, 449-543.

Jacoby, W.; Black, D.; Fennel, D.; Boutlet, J.; Vargo, L.; George, M.; Dolberg, S.; "Heterogeneous photocatalysis for control of volatile organic compounds in indoor air", *J. Air Waste Manage. Assoc.*, **1996**, 46, 691-898.

Jeong, J.; Sekiguchi, K.; Sakamoto, K., "Photochemical and photocatalytic degradation of gaseous toluene using short-wavelength UV irradiation with TiO₂ catalyst: comparison of three UV sources", *Chemosphere*, **2004**, 57, 663-671.

Kaneko, M.; Okura, I., "Photocatalysis: Science and Technology", *Kodansha & Springer press*, **2002**.

Kim, S. B.; Hong, S. C., "Kinetic study for photocatalytic degradation of volatile organic compounds in air using thin film TiO₂ photocatalyst", *Appl. Catal. B: Environ.*, **2002**, 35, 305-315.

Lide, D. R., "Handbook of Chemistry and Physics", *CRC press*, 89th Ed., **2008**.

Ma, C. M.; Wang, W.; Ku, Y., Jeng, F. T., "Photocatalytic degradation of benzene in air streams in an optical fiber photoreactor", *Chem. Eng. Technol.*, **2007**, 30, 1083-1087.

Mahmoudkhani, F., "Simulation of a photochemical reactor for benzene elimination from waste gas," MSc Thesis, University of Calgary, Calgary, Alberta, **2012**.

Mohseni, M.; Zhao, J.L., "Coupling ultraviolet photolysis and biofiltration for enhanced degradation of aromatic air pollutants.", *J. Chem. Technol. Biotechnol.*, **2006**, 81, 146-151.

Parmon, V.; Emeline, A.V.; Serpone, N., "Glossary of Terms in Photocatalysis and Radiocatalysis", *Int. J. Photoenergy*, **2002**, 4, 91-129.

Peral, J.; Ollis, D., " Heterogeneous photocatalytic oxidation of gas-phase organics for air purification: acetone, 1-butanol, butyraldehyde, formaldehyde, and m-xylene oxidation", *J. Catal.*, **1992**, 136, 554-565.

Poling, B. E.; Prausnitz, J. M.; O'Connell, J. P., "The Properties of Gases and Liquids", 5th Ed., *McGraw-Hill, Inc.*, **2001**.

Robert, P.; Sung K. J.; Chul, A., Soon, Y. Y.; Demidyuk V., "Experimental Study of Toluene Decomposition by Combination of Barrier Discharge Plasma and UV Light.", *Air pollution XIV*, **2006**, 401-410.

Sanchez, L.; Peral, J.; Domenech, X., "Aniline degradation by combined photocatalysis and ozonation", *Appl. Catal. B: Environ.*, **1998**, 19, 59-65.

Sander S. P., Friedl R. R., Ravishankara A. R., Golden D. M., Kolb C. E., Kurylo M. S., Molina M. J., Moortgat G. K., Keller-Rudek H., Finlayson-Pitts B. J., Wine P. H., Huie R. E., Orkin V. L., “Chemical kinetics and photochemical data for use in atmospheric studies, evaluation number 15”, *NASA, Jet Propulsion Lab., Publication 06-2.*, **2006**.

Shindo, K.; Lipsky, S., “Photochemistry of benzene vapor at 1849 Å”, *J. Chem. Phys.*, **1966**, 45, 2292-2297.

Tsai, S. T.; Huang, C. L.; Lee, Y. T.; Ni, C. K., “Ring opening dissociation of d₆-benzene”, *J. Chem. Phys.*, **2001**, 115, 2449-2455.

Wang, J. H.; Ray M. B., “Application of ultraviolet photooxidation to remove organic pollutants in the gas phase”, *Separ. Purif. Technol.*, **2000**, 19, 11-20.

Wang, W.; Ku, Y., “Photocatalytic degradation of gaseous benzene in air streams by using an optical fiber photoreactor”, *J. Photochem. Photobiol. A: Chem.*, **2003**, 159, 47-59.

Wang, W.; Chiang, L.W.; Ku, Y., “Decomposition of benzene in air streams by UV/TiO₂ process”, *J. Hazard. Mat. B101*, **2003**, 133-146.

Yue, P., “Modeling, scale up and design of multiphasic photoreactors in photocatalytic purification and treatment of water and air”, *Int. J. Photoenergy*, **1993**, 14,495-510.

Zhang, P. Y.; Liu, J., “Photocatalytic degradation of trace hexane in the gas phase with and without ozone addition: kinetic study”, *J. Photochem. Photobiol. A: Chem.*, **2004**, 167, 87–94.

APPENDIX A:BLANK RUN FOR M-XYLENE

EXPERIMENTS

Date	Maximum intensity output, (mw/cm²)	Total flow rate, (L/min)	Relative humidity, %
May 6, 2011	48.8	1.087	88
May 9, 2011	48.5	1.133	87.1
May 10, 2011	48.2	1.127	86.85
May 11, 2011	47.9	1.037	93.41
May 16, 2011	48.1	1.002	93.65
May 17, 2011	47.7	1.095	91.97

APPENDIX B: DEVELOPED CODE

Data file:

```
length = 56;                %Rector length in cm
dz = 1;
zspan = 0:dz:length;
Nnodes = 19;                %Number of internal nodes in the grid
Ncomp = 47;                 %Number of compounds considered
P = 89000;                  %Pressure in Pa
T = 310;                    %Temprature in K
Ctot = P/1.38e-23/T;        %Concentration in molecules/m3
Ctot = Ctot/1e6;           %Concentration in molecules/cm3
MMbenz = 78;
Cmbenz = 1.2;               %Concentration in gr/m3
Cbenz = Cmbenz/MMbenz;     %Concentration in moles/m3
Cbenz = Cbenz*6.022e23/1e6;%Concentration in molecules/cm3
ybenz = Cbenz/Ctot;        %Benzene mole fraction
yH2O = 0.02;                %Water mole fraction
yO3 = 0.00;                 %Ozone mole fraction
yO2 = 0.21*(1-ybenz-yH2O-yO3); %oxygen mole fraction
yN2 = 0.79*(1-ybenz-yH2O-yO3); %nitrogen mole fraction
Cbenz = Ctot*ybenz;
CH2O = Ctot*yH2O;
CO2 = Ctot*yO2;
CN2 = Ctot*yN2;
CO3 = Ctot*yO3;

% Initial concentrations:
% y0(i+(j-1)*Ncomp) is initial concentration
% of compound j in node point i from the center
% j Compound
% -- -----
% 1 Benzene
% 2 O2
% 3 N2 + argon
% 4 H2O
% 5 O radical (O(3P))
% 6 OH radical
% 7 HO2 radical
% 8 O(1D) radical
% 9 O3
% 10 H2O2
% 11 Phenol
% 12 Glyoxal O=CHCH=O
% 13 Butenedial O=CHCH=CHCH=O
% 14 O=CHCH=CHCH=CHCH=O
% 15 O=CHCH=C(O)C=CHCH=O (epoxide)
% 16 cyclo-CH(O)CHCH(OH)COC=C
% 17 O=C=CHCH=O
```

```

% 18 O=C=CHCH=CHCH=O
% 19 CO
% 20 CO2
% 21 O=CHCH=C=O
% 22 Acrolein O=CHCH=CH2
% 23 1,2-benzenediol
% 24 O=CHC(OH)=O
% 25 p-benzoquinone
% 26 O=CHCH=CH(C=O)CH=O
% 27 1,2,3-benzenetriol
% 28 O=CHCH=CH(C=O)OH
% 29 1,2,3,4-benzenetetrol
% 30 O=CHCH2(C=O)(C=O)OH
% 31 1,2,3,4,5-benzenepentol
% 32 O=CH(C=O)CH(OH)(C=O)OH
% 33 O=CH(C=O)C(OH)=O
% 34 O=CHCH(OH)(C=O)OH
% 35 1,2,3,4,5,6-benzenehexol
% 36 Oxalic acid O=C(OH)C(OH)=O
% 37 O=C(OH)(C=O)CH(OH)C(OH)=O
% 38 O=CHCH=CHCH=O
% 39 Formaldehyde CH2O
% 40 O=CH(CO)CH=CH(CO)(COH)
% 41 O=CH(CO)CH=O
% 42 CO(OH)(CO)CH(OH)CO(OH)
% 43 O=CHCH(-O-)CHCH(OH)COCH=O
% 44 O=CHCH(-O-)CHCH=O
% 45 O=CHCOCH=CHCOCH=O
% 46 Ethylene dione O=C=C=O
% 47 C6H6O3 (Name??)

for i = 1:Nnodes
    y0(i) = Cbenz;
    y0(i+Nnodes) = CO2;
    y0(i+2*Nnodes) = CN2;
    y0(i+3*Nnodes) = CH2O;
    for j = 4:Ncomp-1
        y0(i+j*Nnodes) = 0;
    end
    y0(i+8*Nnodes) = CO3;
end
r0 = 1.25;           %Internal diameter, cm
r1 = 2.1;           %External diameter, cm
for j = 1:Ncomp
    for k = 1:2%k is spectral line (1 = 185 nm, 2 = 254 nm)
        sig(j,k)=0;
    end
end
sig(1,1) = 1.24e-17;
sig(1,2) = 30e-20;
sig(2,1) = 2e-21;
sig(4,1) = 5.5e-20;
sig(7,1) = 324.8e-20;
sig(7,2) = 29.9e-20;
sig(9,1) = 66.1e-20;

```

```

sig(9,2) = 1148.8e-20;
sig(10,1) = 80.1e-20;
sig(10,2) = 6.99e-20;
sig(11,1) = 3800e-20;
sig(11,2) = 2300e-20;
sig(12,2) = 1.596e-20;
sig(13,1) = 688e-20;
sig(13,2) = 36.2e-20;
power1 = 40*0.08;           %Emitted light at 185nm(W)
power2 = 40*0.30;           %Emitted light at 254nm(W)
nu1 = 299792458/185e-9;
nu2 = 299792458/254e-9;
photon1 = 6.626e-34*nu1;    %Photon energy at 185nm
photon2 = 6.626e-34*nu2;    %Photon energy at 254nm
E0(1) = power1/photon1/length/2/pi/r0;
E0(2) = power2/photon2/length/2/pi/r0;
                                %Photons per cm2 per s leaving lamp
                                %1= 185nm, 2=
D = 0.1;                       %Benzene diffusivity(cm2/s)
Q = 500/60;                     %Flow rate(cm3/s)
U = Q/pi/(r1*r1-r0*r0);         %Mean gas velocity(cm/s)
reflamp1 = 0.7;                 %Reflection at the lamp
reflamp2 = 0.7;                 %Fraction of the received light at the lamp
                                which is reflected
K=5e-16;                         %adsorption equilibrium constant of benzene
                                on TiO2 particle, cm3/molecule
                                %reaction rate constant, cm/molecule.s
                                %reaction order of applied UV light
                                intensity
k0=1.2e14;
n=0.5;

```

Function file:

```
function dydz =  
    Function(z,y,dz,Nnodes,Ncomp,r0,r1,sig,E0,D,U,P,T,reflamp,reflamp2,  
    K,K0,n,photon1,photon2)  
  
dydz = zeros(Nnodes*Ncomp,1);  
%j Compound  
%1 Benzene  
%2 O2  
%3 N2+argon  
%4 H2O  
%5 O radical (O(3P))  
%6 OH radical  
%7 HO2 radical  
%8 O(1D) radical  
%9 O3  
%10 H2O2  
%11 Phenol  
%12 Glyoxal      O=CHCH=O  
%13 Butenedial  O=CHCH=CHCH=O  
%14 O=CHCH=CHCH=CHCH=O  
%15 O=CHCH=C(O)C=CHCH=O      (episode)  
%16 cyclo-CH(O)CHCH(OH)COC=C  
%17 O=C=CHCH=O  
%18 O=C=CHCH=CHCH=O  
%19 CO  
%20 CO2  
%21 O=CHCH=C=O  
%22 Acroleine   O=CHCH=CH2  
%23 1,2-benzenediol  
%24 Acetic Acid O=CHC(OH)=O  
%25 p-benzoquinone  
%26 O=CHCH=CH(C=O)CH=O  
%27 1,2,3-benzenetriol  
%28 O=CHCH=CH(C=O)OH  
%29 1,2,3,4-benzenetetrol  
%30 O=CHCH2(C=O)(C=O)OH  
%31 1,2,3,4,5-benzenepentol  
%32 O=CH(C=O)CH(OH)(C=O)OH  
%33 O=CH(C=O)C(OH)=O  
%34 O=CHCH(OH)(C=O)OH  
%35 1,2,3,4,5,6-benzenehexol  
%36 Oxalic acid  O=C(OH)C(OH)=O  
%37 O=C(OH)(C=O)CH(OH)C(OH)=O  
%38 O=CHCH=CHCH=O  
%39 Formaldehyde CH2O  
%40 O=CH(CO)CH=CH(CO)(COH)  
%41 O=CH(CO)CH=O  
%42 CO(OH)(CO)CH(OH)CO(OH)  
%43 O=CHCH(-O-)CHCH(OH)COCH=O  
%44 O=CHCH=CHCOCH=O  
%45 O=CHCOCH=CHCOCH=O  
%46 Ethylene dione O=C=C=O
```

```

%47 C6H6O3 (Name??)
dr = (r1-r0)/(Nnodes+1); %Nodes distance
    %User-friendly notation of concentrations: i=node number
    %j= compound number

for j=1:Ncomp
    for i=1:Nnodes
        C(j,i+1)=y(i+Nnodes*(j-1));           %concentration of j in node
                                                i,molecules/cm3
    end
    C(j,1)=C(j,2)-(C(j,3)-C(j,2))/3; %boundary condition:zero radial flux
    C(j,Nnodes+2)=C(j,Nnodes+1)-(C(j,Nnodes)-C(j,Nnodes+1))/3;
end

%Calculate radiation fields
Eref(1,1)=E0(1)/reflamp; %Considering original radiation from the lamp
Eref(1,2)=E0(2)/reflamp; %Considering original radiation from the lamp
for k=1:2
    for i=1:Nnodes+1
        Etot(i+1,k)=0;
    end
    while (Eref(1,k)>0.01*E0(k))
        E(1,k)=reflamp*Eref(1,k);
        for i=1:Nnodes+1
            Ei=E(i,k);
            r=r0+dr*(i-0.5);
            alpha=0;
            for j=1:Ncomp
                Ci(j)=(C(j,i)+C(j,i+1))/2;
                alpha=alpha+Ci(j)*sig(j,k);
            end
            E(i+1,k)=(Ei/dr - alpha*Ei/2 - Ei/2/r)/(1/dr +alpha/2 +1/2/r);
            if E(i+1,k)<0
                E(i+1,k)=0;
            end
        end
        Eref(Nnodes+2,k)=0.01*E(Nnodes+2,k);
        %99 should be less with catalyst
        for i=Nnodes+1:-1:1
            Erefi=Eref(i+1,k);
            r=r0+dr*(i-.5);
            alpha=0;
            for j=1:Ncomp
                Ci(j)=(C(j,i)+C(j,i+1))/2;
                alpha=alpha+Ci(j)*sig(j,k);
            end
            Eref(i,k)=(Erefi/dr+Erefi/2/r-alpha*Erefi/2)/(1/dr-1/2/r+alpha/2);
            if Eref(i,k)<0
                Eref(i,k)=0;
            end
        end
        for i=1:Nnodes+2
            Etot(i,k)=Etot(i,k)+E(i,k)+Eref(i,k);
        end
    end
end

```

```

end
I=(Etot(Nnodes+2,1)*photon1+Etot(Nnodes+2,2)*photon2)*1;

A=K0*K*(I^n)/D;
C(1,Nnodes+2)=(-1-(2/3*A*dr)-(K*C(1,Nnodes)/3)+(4/3*K*C(1,Nnodes+1))+
((1+2/3*A*dr+C(1,Nnodes)/3*K-4/3*K*C(1,Nnodes+1))^2)-4/3*K*C(1,Nnodes)+
16/3*K*C(1,Nnodes+1)^(1/2))/(2*K);
value = C(1,Nnodes+2);
AA=K0*K*(I^(n-1))*value/(1+K*value)
difference1 = C(1,Nnodes+2)-C(1,Nnodes+1);
difference2 = C(1,Nnodes+2)-C(1,Nnodes);
%if z>27 & z<29
%z
%nu1=299792458/185e-9;
%nu2=299792458/254e-9;
%photon1=6.626e-34*nu1; %Photon energy at 185nm
%photon2=6.626e-34*nu2; %Photon energy at 254nm
%photon1*Etot(Nnodes+2,1)/2
%photon2*Etot(Nnodes+2,2)/2
%end

for i = Nnodes+1:-1:2
%Calculate reaction rates per reaction

%Photolytical reactions

const1 = 6.705;          % Parameters for quantum yield benzene photolysis
const2 = 340.06;

Pbenz = C(1,i)*1.38e-23*T*1e6;      % Benzene partial pressure, Pa
Pinert = (C(2,i)+C(3,i)+C(4,i))*1.38e-23*T*1e6;
phibenz = 1/(const1*(Pinert/1.01325e5 + const2*Pbenz/1.01325e5)+1);
rp1(i) = phibenz*C(1,i)*sig(1,1)*Etot(i,1);
rp2(i) = C(4,i)*sig(4,1)*Etot(i,1);
rp3(i) = C(9,i)*(sig(9,1)*Etot(i,1) + sig(9,2)*Etot(i,2));
rp4(i) = C(7,i)*(sig(7,1)*Etot(i,1) + sig(7,2)*Etot(i,2));
rp5(i) = C(10,i)*(sig(10,1)*Etot(i,1)*0.75 + sig(10,2)*Etot(i,2));
rp_5(i) = C(10,i)*sig(10,1)*Etot(i,1)*0.16;
rp6(i) = C(12,i)*sig(12,2)*Etot(i,2);
rp7(i) = C(13,i)*(0.55*sig(13,1)*Etot(i,1) + 0.12*sig(13,2)*Etot(i,2));
rp_7(i) = C(13,i)*(0.011*sig(13,1)*Etot(i,1) + 0.037*sig(13,2)*Etot(i,2));

% Oxygen atom reactions

ko1 = 2.3e-11*exp(110/T);
ko2 = 2.7e-11*exp(224/T);
ko3 = 1.4e-12*exp(-2000/T);
ko4 = 6e-34*(T/300)^(-2.8)*C(2,i) + 5.6e-34*(T/300)^(-2.8)*C(3,i);
ko5 = 2.7e-34*T^(-0.41)*(C(2,i)+C(3,i));
ko6 = 8e-12*exp(-2060/T);
ko7 = 7.9e-14*(T/298)^2.6*exp(945/T);
ko8 = 2.2e-10;
ko9 = 3.2e-11*exp(67/T);
ko10 = 1.8e-11*exp(107/T);

```

```

ro1(i) = ko1*C(5,i)*C(6,i);
ro2(i) = ko2*C(5,i)*C(7,i);
ro3(i) = ko3*C(5,i)*C(10,i);
ro4(i) = ko4*C(5,i)*C(2,i);
ro5(i) = ko5*C(5,i)*C(5,i);
ro6(i) = ko6*C(5,i)*C(9,i);
ro7(i) = ko7*C(6,i)*C(6,i);
ro8(i) = ko8*C(8,i)*C(4,i);
ro9(i) = ko9*C(8,i)*C(2,i);
ro10(i) = ko10*C(8,i)*C(3,i);

% Scavenging reactions

ks1 = 2.9e-12*exp(-160/T);
ks2 = 1.9e-12*exp(-1000/T);
ks3 = 1.4e-14*exp(-600/T);

rs1(i) = ks1*C(6,i)*C(10,i);
rs2(i) = ks2*C(6,i)*C(9,i);
rs3(i) = ks3*C(7,i)*C(9,i);

% Termination reactions

kt1 = 4.8e-11*exp(250/T);
kt2 = 2.2e-13*exp(600/T) + 1.9e-33*exp(980/T)*C(3,i) +
1.6e-33*exp(980/T)*C(2,i);
kt2 = kt2*(1 + 1.4e-21*exp(980/T)*C(4,i));
kt3zero = 6.9e-31*(T/300)^(-0.8)*C(3,i);
kt3inf = 2.6e-11;
kt3Fc = 0.5;
kt3F = 10^(log10(kt3Fc)/(1 + (log10(kt3zero/kt3inf))^2));
kt3 = kt3zero*kt3inf*kt3F/(kt3zero + kt3inf);

rt1(i) = kt1*C(6,i)*C(7,i);
rt2(i) = kt2*C(7,i)*C(7,i);
rt3(i) = kt3*C(6,i)*C(6,i);

% Degradation reactions

kd1 = 2.33e-12*exp(-193/T);
kd2 = 8.6e-12*exp(20/T);
phid2(i) = 5e-12*C(2,i)/(1e-11*C(2,i) + 1.4e-12*exp(-3160/T));
kd3 = kd2;
phid3(i) = 1 - phid2(i);
kd4 = 1.3e-13*(1 + 0.6*P/100000)*300/T;
kd5 = 2.63e-11;
kd6 = 10.4e-11;
kd7 = 20.5e-11;
kd8 = 20.5e-11;
kd9 = 20.5e-11;
kd10 = 20.5e-11;

```

```

rd1(i) = kd1*C(1,i)*C(6,i);
rd2(i) = kd2*C(12,i)*C(6,i)*phid2(i);
rd3(i) = kd3*C(12,1)*C(6,i)*phid3(i);
rd4(i) = kd4*C(19,i)*C(6,i);
rd5(i) = kd5*C(11,i)*C(6,i);
rd6(i) = kd6*C(23,i)*C(6,i);
rd7(i) = kd7*C(27,i)*C(6,i);
rd8(i) = kd8*C(29,i)*C(6,i);
rd9(i) = kd9*C(31,i)*C(6,i);
rd10(i) = kd10*C(35,i)*C(6,i);

```

```

% New reactions

```

```

kn1 = 60.2e-12;
kn2 = 16.41e-12;
kn3 = 39.07e-12;
kn4 = 0;
kn5 = 38.41e-12;
kn6 = 41.34e-12;
kn7 = 8.94e-12;
kn8 = 1.1e-11;
kn9 = 0.185e-12;
kn10 = 11.13e-12;
kn11 = 4.6e-12;
kn12 = 190.17e-12;
kn13 = 2.0e-11;
kn14 = 1.5e-11;
kn15 = 1.5e-11;
kn16 = 1.0e-11;
kn17 = 1.6e-12;
kn18 = 1.6e-12;
kn19 = 3.0e-11;
kn20 = 7.1e-12;
kn21 = 3.0e-11;
kn22 = 1.5e-11;
kn23 = 3.0e-11;
kn24 = 1.5e-11;
kn25 = 45e-12;
kn26 = 1.9e-11;

```

```

rn1(i) = kn1*C(38,i)*C(6,i);
rn2(i) = kn2*C(14,i)*C(6,i);
rn3(i) = kn3*C(15,i)*C(6,i);
rn4(i) = kn4*C(47,i)*C(6,i);
rn5(i) = kn5*C(17,i)*C(6,i);
rn6(i) = kn6*C(18,i)*C(6,i);
rn7(i) = kn7*C(22,i)*C(6,i);
rn8(i) = kn8*C(39,i)*C(6,i);
rn9(i) = kn9*C(24,i)*C(6,i);
rn10(i) = kn10*C(28,i)*C(6,i);
rn11(i) = kn11*C(25,i)*C(6,i);
rn12(i) = kn12*C(26,i)*C(6,i);
rn13(i) = kn13*C(30,i)*C(6,i);
rn14(i) = kn14*C(32,i)*C(6,i);

```

```

rn15(i) = kn15*C(33,i)*C(6,i);
rn16(i) = kn16*C(34,i)*C(6,i);
rn17(i) = kn17*C(36,i)*C(6,i);
rn18(i) = kn18*C(42,i)*C(6,i);
rn19(i) = kn19*C(43,i)*C(6,i);
rn20(i) = kn20*C(45,i)*C(6,i);
rn21(i) = kn21*C(41,i)*C(6,i);
rn22(i) = kn22*C(33,i)*C(6,i);
rn23(i) = kn23*C(44,i)*C(6,i);
rn24(i) = kn24*C(21,i)*C(6,i);
rn25(i) = kn25*C(46,i)*C(6,i);
rn26(i) = kn26*C(21,i)*C(6,i);

% Calculate reaction rates per species using stoichiometry

react(1,i) = -rp1(i) - rd1(i);
react(2,i) = -1.5*rd1(i) + ro1(i) + ro2(i) - ro4(i) + ro5(i) + 2*ro6(i);
react(2,i) = react(2,i) + rs2(i) + 2*rs3(i) + rt1(i) + rt2(i);
react(2,i) = react(2,i) - 3.75*rp1(i)
    -rp2(i) + rp3(i) - rp6(i)*(1.5*phid2(i)
+ 1*phid3(i)) - 2*rp7(i) - 1.5*rn1(i);
react(2,i) = react(2,i) - 1.5*rd2(i) - rd3(i)
- rd4(i) - 1.26*rd5(i) - 1.3*rd6(i) - 1.3*rd7(i)
- 1.3*rd8(i) - rd9(i) - 2.5*rd10(i) - 1.5*rn2(i) - 2*rn3(i) -
1.5*rn4(i) - 1.5*rn5(i) - 1.5*rn6(i)
- 1.5*rn7(i) - 1.5*rn9(i) - 1.5*rn10(i) - 1.5*rn11(i) - 1.5*rn12(i)
- 2*rn13(i) - 2*rn14(i) - 2*rn15(i)
- 1.5*rn16(i) - rn17(i) - 1.5*rn18(i) -
2*rn19(i) - 1.5*rn20(i) - 2*rn21(i)
- 2*rn22(i) - 2*rn23(i) - 2*rn24(i) - 1.5*rn25(i) - 1.5*rn26(i);
react(3,i) = 0;
react(4,i) = ro7(i) + rs1(i) + rt1(i)
- rp2(i) + rp_5(i) - ro8(i) + rd2(i) + rd3(i) + 0.1*rd5(i)
+ rn8(i) + rn9(i) + rn13(i) + rn14(i)
+ rn15(i) + rn16(i) + rn17(i) +rn18(i) +
rn19(i) + rn21(i) + rn22(i) + rn23(i) + rn24(i);
react(5,i) = -ro1(i) - ro2(i) - ro3(i) - ro4(i)
- 2*ro5(i) - ro6(i) + ro7(i) + 0.1*rp3(i)
+ rp4(i) + rp_5(i) + ro9(i) + ro10(i);
react(6,i) = -rd1(i) - ro1(i) + ro2(i)
+ ro3(i) - 2*ro7(i) - rs1(i) - rs2(i) +
rs3(i) - rt1(i) - 2*rt3(i) + rp2(i) + rp4(i) + 2*rp5(i);
react(6,i) = react(6,i) + 2*ro8(i) -
rd2(i) - rd3(i) - rd4(i) - rd5(i)
- rd6(i) - rd7(i) - rd8(i) - rd9(i) -
rd10(i) - rn1(i) - rn2(i) - rn3(i) + rn5(i) -
rn6(i) - rn7(i) - rn8(i) - rn9(i)
- rn10(i) - rn11(i) - rn12(i) - rn13(i) - rn14(i) - rn15(i) - rn16(i) -
rn17(i) - rn18(i) - rn19(i) - rn20(i) - rn21(i)
- rn22(i) - rn23(i) - rn24(i) - rn25(i) - rn26(i);
react(7,i) = rd1(i) + ro1(i) - ro2(i) + rs1(i) + rs2(i) - rs3(i)
- rt1(i) - 2*rt2(i) + 2*rp1(i) + rp2(i) - rp4(i)
+ 2*rp6(i) + 2*rp7(i) + rn2(i);

```

```

react(7,i) = react(7,i) + rd2(i)
+ rd3(i) + rd4(i) + rd5(i) + rd6(i) + rd7(i)
+ rd8(i) + rd9(i) + rd10(i) + rn1(i) + rn3(i) +
rn4(i) + rn5(i) + rn6(i) + rn7(i) + rn8(i) + rn9(i)
+ rn10(i) + rn12(i) + rn13(i) + rn14(i) + rn15(i) + rn16(i) + rn17(i) +
rn18(i) + rn19(i) + rn20(i) + rn21(i) +
rn22(i) + rn23(i) + rn24(i) + rn25(i) + rn26(i);
react(8,i) = 0.9*rp3(i) - ro8(i) - ro9(i) - ro10(i) - rn8(i);
react(9,i) = ro4(i) - ro6(i) - rs2(i) - rs3(i) - rp3(i);
react(10,i) = -ro3(i) - rs1(i) + rt2(i) + rt3(i) - rp5(i) - rp_5(i);
react(11,i) = 0.57*rd1(i) - rd5(i);
react(12,i) = - rp6(i) + 0.31*rd1(i)
- rd2(i) - rd3(i) + 2*rn1(i) + rn2(i)
+ rn3(i) + rn5(i) + rn6(i) + rn7(i) + rn10(i) + rn12(i) + rn26(i);
react(13,i) = - rp7(i) - rp_7(i) + 0.1*rd1(i) + 0.1*rd5(i) + rn2(i);
react(14,i) = 0.08*rd1(i) - rn2(i);
react(15,i) = 0.09*rd1(i) - rn3(i);
react(16,i) = 0.09*rd1(i);
react(17,i) = rp1(i) + rn3(i) - rn5(i) + rn6(i);
react(18,i) = 0.5*rp1(i) - rn6(i);
react(19,i) = 0.5*rp1(i) + rp6(i)*(phid2(i) + 2*phid3(i))
+ rp7(i) + rp_7(i) + rd2(i) + 2*rd3(i) - rd4(i)
+ 0.06*rd5(i) + rn8(i) + rn21(i);
react(20,i) = rp6(i)*phid2(i) +rd2(i) + rd4(i) +
rn3(i) + rn5(i) + 2*rn9(i) + rn13(i) + 2*rn14(i) +
3*rn15(i) + rn16(i) + 2*rn17(i) + 2*rn18(i) + 2*rn19(i)
+ 2*rn21(i) + 3*rn22(i) +
rn23(i) + rn24(i) + 2*rn25(i) + rn26(i);
react(21,i) = rp7(i) - rn24(i) - rn26(i);
react(22,i) = rp_7(i) - rn7(i);
react(23,i) = 0.8*rd5(i) - rd6(i);
react(24,i) = 0.1*rd5(i) + 0.2*rd6(i) +
0.2*rd7(i) + 0.1*rd8(i) + rn18(i)- rn9(i) - rn10(i) + rn14(i) + rn16(i);
react(25,i) = 0.04*rd5(i) - rn11(i);
react(26,i) = 0.06*rd5(i) - rn12(i);
react(27,i) = 0.8*rd6(i) - rd7(i);
react(28,i) = 0.2*rd6(i) - rn10(i);
react(29,i) = 0.8*rd7(i) - rd8(i);
react(30,i) = 0.2*rd7(i) - rn13(i);
react(31,i) = 0.8*rd8(i) - rd9(i);
react(32,i) = 0.1*rd8(i) - rn14(i);
react(33,i) = 0.1*rd8(i) + rn13(i) - rn15(i) - rn22(i);
react(34,i) = 0.1*rd8(i) - rn16(i);
react(35,i) = rd9(i) - rd10(i);
react(36,i) = rd10(i) - rn17(i);
react(37,i) = rd10(i);
react(38,i) = rn1(i);
react(39,i) = rn7(i) - rn8(i);
react(40,i) = rn11(i);
react(41,i) = rn12(i) - rn21(i);
react(42,i) = -rn18(i);
react(43,i) = rn4(i) - rn19(i);
react(44,i) = rn19(i) - rn23(i);
react(45,i) = -rn20(i);
react(46,i) = 2*rn20(i) + rn23(i) + rn24(i) - rn25(i);

```

```

react(47,i) = -rn4(i);

% Assume velocity not homogeneous; laminar flow

r(i) = r0 + dr*(i-1);
denom = 2*r1*r1 - (r1*r1-r0*r0)/log(r1/r0) - (r1*r1-r0*r0);
v(i) = 2*U*((r1*r1-r0*r0)*log(r(i)/r0)/log(r1/r0)
- (r(i)*r(i)-r0*r0))/denom;

% Build the differential equations
for j = 1:Ncomp
dcdr(j,i) = (C(j,i+1) - C(j,i-1))/2/dr;
d2cdr2(j,i) = (C(j,i-1) - 2*C(j,i) + C(j,i+1))/dr/dr;
dcdL(j,i) = (D*d2cdr2(j,i) + D/r(i)*dcdcr(j,i) + react(j,i))/v(i);
end
end

for j = 1:Ncomp
for i = 1:Nnodes
dydz(i+Nnodes*(j-1)) = dcdL(j,i+1);
end
end
%Calculation of concentrations in the intersections
for j = 1:Ncomp
Clamp(j) = (4*C(j,1)-C(j,2))/3;
% Concentrations on the lamp
(considering a parabolic equation for Conc.)

end

%Concentrations at intersections with horizontal lines
%theta = pi/40;
%for j = 1:Ncomp
%for n = 1:Nnodes+1
%xn = n*dr*cot(theta);
%if (xn/dz-floor(xn/dz))<0.5
% C_hor_intersec(n) = C(j,floor(xn/dz)+1);
%else
% C_hor_intersec(n) = C(j,floor((xn/dz)+2));
%end
%end

% Concentrations at intersections with vertical lines
%for m = 1:56/dz
%ym = m*dz*tan(theta);
%if (ym/dr-floor(ym/dr))<0.5
% C_ver_intersec(m) = C(j,floor(ym/dr)+1);
%else
%C_ver_intersec(m) = C(j,floor(ym/dr)+2);
%end
%end
%end
%end

```

Main File:

```
% main
clearall
clc
tic
formatlong
data
options = odeset('RelTol', 1e-6, 'ABsTol', 1e-8, 'InitialStep', 0.0001);
[Z,Y] = ode15s(@Function,zspan,y0,options,dz,Nnodes,Ncomp,
r0,r1,sig,E0,D,U,P,T,reflamp1,reflamp2,K,K0,n,photon1,photon2);
[s1,s2]=size(Z);
plot(Z,Y(1:s1,1:Nnodes))
figure
plot(Z,Y(1:s1,Nnodes+1:2*Nnodes))
jcomp=9;
figure
plot(Z,Y(1:s1,(jcomp-1)*Nnodes+1:jcomp*Nnodes))
Z
Y(1:s1,1:Nnodes)
toc%read the timer

dr=(r1-r0)/(Nnodes+1); %Node distance
for i=2:Nnodes+1
r(i)=r0+dr*(i-1);
denom=2*r1*r1-(r1*r1-r0*r0)/log(r1/r0)-(r1*r1-r0*r0);
v(i)=2*U*((r1*r1-r0*r0)*log(r(i)/r0)/log(r1/r0)-(r(i)*r(i)-r0*r0))/denom;
end
Ft0=0;
Ft=0;

for i = 1:(Nnodes-1)/2
Ft0=Ft0+2*pi*dr*(4*r(2*i)*v(2*i)*Y(1,2*i-1)+2*r(2*i+1)*v(2*i+1)*Y(1,2*i));
Ft=Ft+2*pi*dr*(4*r(2*i)*v(2*i)*Y(s1,2*i-1)+2*r(2*i+1)*v(2*i+1)*Y(s1,2*i));
end
s1
s2
Efficiency=(1-Ft/Ft0)*100
```